

2015

Development of Multifunctional Shape Memory Polymer and Shape Memory Polymer Composites

Sesha Spandana Pulla
University of Kentucky, spu224@uky.edu

[Right click to open a feedback form in a new tab to let us know how this document benefits you.](#)

Recommended Citation

Pulla, Sesha Spandana, "Development of Multifunctional Shape Memory Polymer and Shape Memory Polymer Composites" (2015). *Theses and Dissertations--Mechanical Engineering*. 74.
https://uknowledge.uky.edu/me_etds/74

This Doctoral Dissertation is brought to you for free and open access by the Mechanical Engineering at UKnowledge. It has been accepted for inclusion in Theses and Dissertations--Mechanical Engineering by an authorized administrator of UKnowledge. For more information, please contact UKnowledge@lsv.uky.edu.

STUDENT AGREEMENT:

I represent that my thesis or dissertation and abstract are my original work. Proper attribution has been given to all outside sources. I understand that I am solely responsible for obtaining any needed copyright permissions. I have obtained needed written permission statement(s) from the owner(s) of each third-party copyrighted matter to be included in my work, allowing electronic distribution (if such use is not permitted by the fair use doctrine) which will be submitted to UKnowledge as Additional File.

I hereby grant to The University of Kentucky and its agents the irrevocable, non-exclusive, and royalty-free license to archive and make accessible my work in whole or in part in all forms of media, now or hereafter known. I agree that the document mentioned above may be made available immediately for worldwide access unless an embargo applies.

I retain all other ownership rights to the copyright of my work. I also retain the right to use in future works (such as articles or books) all or part of my work. I understand that I am free to register the copyright to my work.

REVIEW, APPROVAL AND ACCEPTANCE

The document mentioned above has been reviewed and accepted by the student's advisor, on behalf of the advisory committee, and by the Director of Graduate Studies (DGS), on behalf of the program; we verify that this is the final, approved version of the student's thesis including all changes required by the advisory committee. The undersigned agree to abide by the statements above.

Sesha Spandana Pulla, Student

Dr. Y. Charles Lu, Major Professor

Dr. Haluk E. Karaca, Director of Graduate Studies

DEVELOPMENT OF
MULTIFUNCTIONAL SHAPE MEMORY POLYMER AND
SHAPE MEMORY POLYMER COMPOSITES

DISSERTATION

A dissertation submitted in partial fulfillment of the
Requirements for the degree of Doctor of Philosophy in the
College of Engineering
at the University of Kentucky

By
Sesha Spandana Pulla
Lexington, Kentucky

Director: Dr. Y. Charles Lu, Professor of Mechanical Engineering
Lexington, Kentucky
Co-Director: Dr. Haluk E. Karaca, Professor of Mechanical Engineering
Lexington, Kentucky

2015 Copyright © Sesha Spandana Pulla 2015

ABSTRACT OF THE DISSERTATION

Shape memory polymers (SMPs) are an emerging class of active polymers that can be used on a wide range of reconfigurable structures and actuation devices. The present study comprehensively examines the unconstrained shape recovery abilities of an epoxy-based SMP. In doing so, epoxy based SMP is synthesized and thermo-mechanically characterized. Results show that the present SMP exhibits excellent shape recoveries under unconstrained conditions, for a range of fixing strains and temperatures. Additionally, the stress-strain behavior of the SMP is determined to be nonlinear, finite deformation at all regions. The strain energy based models have been used to capture the complicate stress-strain behavior and shape recovery process of the SMPs.

Further SMP based composites are considered to obtain a smart material that is suitable for applications at both above and below the glass transition temperature of the polymer. A smart composite made of SMP and SMA would allow many design possibilities due to their controllable temperature-dependent mechanical properties. In this study, the shape memory composites (SMCs) are created by embedding SMA components (particles and fibers) into SMP matrices, which take advantage of the complementary properties of SMAs and SMPs. The SMA-particle and

SMA-fiber reinforced SMP composites are designed through numerical simulations for different weight fractions of the SMA fillers were varied from 0-50%. Addition of SMA fillers significantly increased modulus across the temperature regimes while maintaining the large actuation strain. In addition to the simulations, SMA-Particle + SMP composites are synthesized and tested using DMA in compression. The obtained modulus results from the simulations for SMA-Particle + SMP composite is comparable with the experimentally determined results. However, since SMP matrix is not conductive these composites often require external stimuli such as external heaters which limit their applications. To overcome this limitation, multi-functional Shape memory polymer based composites are thus fabricated in the present study by embedding CNT fibers and Ni particles in SMP matrix that resulted in electrically conductive and thermally stable SMP based composites.

Key Words: Shape memory polymer; Shape memory composite; Carbon nanotubes; Multi-functional composites; Finite Element modeling.

Sesha Spandana Pulla

Student's Signature

10/20/15

Date

DEVELOPMENT OF MULTIFUNCTIONAL SHAPE MEMORY
POLYMER AND SHAPE MEMORY
POLYMER COMPOSITES

By

Sesha Spandana Pulla

Y. Charles Lu

Director of Dissertation

Haluk E. Karaca

Co-Director of Dissertation

Haluk E. Karaca

Director of Graduate Studies

07/18/2015

This work is dedicated to my mother, father and brother

ACKNOWLEDGEMENTS

I would like to extend sincere gratitude to my advisor, Prof. Y.Charles Lu and Co-Advisor, Prof. Haluk E. Karaca for their constant support throughout my research. Their thoughtful guidance and encouragement to carry out this project has been highly valuable in conducting my project progressively. I would like to thank them for their patience and precious time spent in helping me guide through it and for giving their valuable suggestions from time to time that helped me complete this project successfully.

I would like to specifically thank Dr. Lu for placing his faith in my work right from my Master's Program and encouraging me to continue my higher studies when I expressed an interest to do so.

I would like to express my appreciation to my committee members, Dr.Babak Bazgari, Dr.Keith Rouch and Dr. Janet K. Lumpp for serving on my committee and for their valuable suggestions and comments.

I would also like to offer my special thanks to my lab-mates, Ali Sadi Turabi, Peizhen Li, Emre Acar, Irfan Kaya, Soheil Saedi, Sayed Saghalian, Mohammed Souri, Anil Erol and Hirobumi Tobe. Additionally, I would like to thank our lab technician Nick Cprek for his assistance with designing custom equipment used in the current project.

I would like to express my deepest gratitude towards my mother, father and brother for their patience, constant encouragement and immense moral support throughout my higher studies. Additionally, I would like to thank my friends Madhu Akasapu-Smith and Brian Hampton for their constant moral support as well.

Table of Contents	
List of Figures	vii
List of Tables	xvii
Chapter One	1
1 INTRODUCTION	1
1.1 BACKGROUND.....	1
1.2 OBJECTIVES OF THE DISSERTATION.....	3
1.3 ORGANIZATION OF THE DISSERTATION.....	3
Chapter Two.....	5
2 REVIEW OF LITERATURES.....	5
2.1 INTRODUCTION TO SHAPE MEMORY POLYMERS	5
2.2 TYPES OF SHAPE MEMORY POLYMERS	9
2.3 INTRODUCTION TO SHAPE MEMORY POLYMER COMPOSITES.....	15
2.3.1 Types of Shape Memory Polymer Composites	15
Chapter Three.....	37
3 SYSTHESIS AND CHARACTERIZATION OF SHAPE MEMORY POLYMERS	37
3.1 INTRODUCTION.....	37
3.2 EXPERIMENTAL	38
3.2.1 Materials and Sample Preparation	38
3.2.2 Transition Temperature.....	39
3.2.3 Thermo-Mechanical Testing.....	40
3.2.4 Coefficient of Thermal Expansion.....	40
3.2.5 Stress-Strain Tests.....	40
3.2.6 Shape Recovery Tests.....	41
3.3 RESULTS AND DISCUSSION	41
3.3.1 Transition Temperature.....	41
3.3.2 Thermo-Mechanical Behavior	42
3.3.3 Coefficient of Thermal Expansion.....	44
3.3.4 Mechanical Behavior	44
3.3.5 Shape Recoveries	45
3.4 CONCLUSIONS.....	49
Chapter Four	50

4	STRAIN ENERGY FUNCTION BASED MODELING OF SHAPE MEMORY POLYMERS	50
4.1	INTRODUCTION.....	50
4.2	STRAIN ENERGY FUNCTION BASED MODELING	51
4.2.1	Mooney-Rivlin Strain Energy Function.....	51
4.2.2	Yeoh Strain Energy Function.....	52
4.2.3	Ogden Strain Energy Function.....	53
4.2.4	Neo-Hooke Strain Energy Function.....	54
4.2.5	Arruda-Boyce Strain Energy Function	55
4.3	RESULTS AND DISCUSSION	56
4.3.1	Prediction of Mechanical Behavior of SMPs.....	56
4.3.2	Prediction of Shape Recovery of SMPs.....	63
4.4	CONCLUSIONS.....	66
	Chapter Five.....	67
5	DESIGN AND CHARACTERIZATION OF MULTIFUNCTIONAL SHAPE MEMORY COMPOSITES: SMA-SMP COMPOSITES.....	67
5.1	INTRODUCTION.....	67
5.2	SMA MODELING.....	68
5.2.1	Constitutive Model For the Thermo-Mechanical Response of NiTi SMA by Qidwai and Lagoudas	77
5.3	SMP MODELING.....	84
5.3.1	Ogden Strain Energy Function.....	85
5.4	DESIGN AND MODELING OF SMA-SMP COMPOSITES	87
5.4.1	Designing Of SMA-SMP Composites.....	87
5.4.2	Linking SMA Model and SMP Model in ABAQUS.....	96
5.4.3	Compiling and Linking User Subroutines with ABAQUS.....	99
5.5	SMA-SMP COMPOSITE	101
5.5.1	SMA Particle SMP Composite	102
5.5.2	SMA Fibre-SMP Composite.....	104
5.6	RESULTS AND DISCUSSION	105
5.6.1	Modeling of SMP and SMA	105
5.6.2	SMA Particle – SMP Composites.....	107
5.6.3	SMA Fibre – SMP Composites	121

5.6.4	Experimental Verification of SMA Particle – SMP Composite	134
5.7	CONCLUSIONS	139
Chapter Six	140
6	DESIGN AND CHARACTERIZATION OF MULTIFUNCTIONAL SHAPE MEMORY COMPOSITES: CNT – SMP COMPOSITES	140
6.1	INTRODUCTION	140
6.2	EXPERIMENTAL	141
6.2.1	CNT – SMP Composite Preparation	141
6.2.2	Ni – CNT – SMP Composite Preparation	142
6.2.3	Transition Temperature	144
6.2.4	Stress – Strain Tests	145
6.2.5	Electrical Measurements	146
6.3	RESULTS AND DISCUSSION	147
6.3.1	Thermal Behavior of CNT – SMP Composite	147
6.3.2	Mechanical Behavior of CNT – SMP Composite	149
6.3.3	Mechanical Behavior of Ni – CNT – SMP Composite	151
6.3.4	Electrical Behavior of CNT – SMP and Ni – CNT – SMP Composites ..	152
6.4	CONCLUSIONS	156
Chapter Seven	157
7	CONCLUSIONS AND FUTURE WORK	157
7.1	WORK TO DATE	157
7.2	FUTURE WORK	160
Appendix A	. Validation of Ogden Model with Additional SMP Material System.	162
Appendix B	. Stress – Strain responses of Ni Particle – SMP Composites	164
Appendix C	. Temperature Induced Phase Transformation of SMA + SMP Composite with Applied Stress.	166
REFERENCES	168
VITA	182

List of Figures

Figure 1.1 Diagrammatic representation of the thermo-mechanical cycle of an SMP.....	2
Figure 1.2 Spider plot representing the capabilities of a reconfigurable air vehicle [1].....	2
Figure 2.1 Diagram of thermo-mechanical cycle during free recovery for thermally induced SMP.....	7
Figure 2.2 Schematic illustrating a simple molecular mechanism of the thermally induced SMP [19].....	8
Figure 2.3 Definition of four types of shape-memory polymers with different shape-fixing and shape-recovery mechanisms depicted as a function of their dynamic mechanical behavior. Plotted is the tensile storage modulus vs. temperature as measured using a small oscillatory deformation at 1 Hz for: (I) chemically cross-linked glassy thermosets; (II) chemically cross-linked semi-crystalline rubbers; (III) physically cross-linked thermoplastics; and (IV) physically cross-linked block copolymers [7].	13
Figure 2.4 Various molecular structures of SMPs[20].	14
Figure 2.5 Figure shows storage modulus and tangent delta versus temperature of the pure SMP and SMPC [21].	17
Figure 2.6 Figure on left shows the storage modulus vs. temperature. Figure on the right shows the load displacement results from nano-indentation tests on Nanoclay-Polyurethane composites [22].....	18
Figure 2.7 Figure shows constrained bend recovery force as a function of temperature for reinforced and unreinforced SMP materials [23].....	19
Figure 2.8 Images show the shape recovery of magnetite reinforced SMP [28].....	21

Figure 2.9 The figure above shows the temperature induced shape memory effect of SMA [31].	23
Figure 2.10 Plots show the dependence of modulus and yield stress of SMA and SMP on temperature [15].	29
Figure 2.11 Stress–strain curves measured at T 363 K of the reinforced Al, and the TiNi Fibre: Al composite with and without pre-strain where two different volume fractions of Fibre are used; 4% and 9% vol [36].	30
Figure 2.12 Electro active shape recovery behavior of conductive PU-CNT shape memory composite [49].	32
Figure 2.13 The stress–strain curves in static tensile tests for four materials—SMP bulk, 1.7 wt. %, 3.3 wt. % and 5.0 wt. % at testing temperatures: (a) 25 °C, (b) 45 °C, and (c) 65 °C, respectively [51].	33
Figure 2.14 shows the stress–strain curves showing two stage yielding process in Cu-CNT nano-composite [52].	34
Figure 3.1 Shows the molecular structures of the chemicals used to make the shape memory polymer used in current project [102].	39
Figure 3.2 DSC results showing the glass transition temperature of the SMP.	42
Figure 3.3 DMA results showing the storage modulus as a function of temperature.	43
Figure 3.4 DMA results showing the phase angle as a function of temperature.	43
Figure 3.5 Thermal expansion strain as a function of temperature for the SMP.	44
Figure 3.6 Stress-strain responses of the SMP at various temperatures.	45
Figure 3.7a Strain-temperature profiles of unconstraint shape recoveries of the SMPs.	47
Figure 3.7b Shape recovery ratios of unconstraint shape recoveries of the SMPs.	47

Figure 3.8a Strain - temperature profiles of unconstraint shape recoveries of the SMP.....	48
Figure 3.8b Shape recovery ratios of unconstraint shape recoveries of the SMPs.....	49
Figure 4.1 Shows the unit-cell FE model and flowchart used for computing the stress and strain.....	56
Figure 4.2 Stress-strain responses of the SMP at 55°C.....	57
Figure 4.3 Stress-strain responses of the SMP at 50°C.....	57
Figure 4.4 Stress-strain responses of the SMP at 45°C.....	58
Figure 4.5 Stress-strain responses of the SMP at 35°C.....	59
Figure 4.6 Stress-strain responses of the SMP at 30°C.....	59
Figure 4.7 Variations of μ_i α_i in Ogden model.....	62
Figure 4.8 Comparisons of stress-strain responses of the SMP between experimental data and Ogden model.....	62
Figure 4.9 Strain-temperature profiles showing the shape recovery of the SMP.....	63
Figure 4.10 Contours of compressive strain (E22) showing the process of shape recovery of the SMP. (a) Original shape: heated up to 60°C, (b) Step1: compressed to a strain of 17.5%, (c) Step2: lowered temperature to 12°C (strain is seen to increase to 19.5% due to thermal contraction), (d) Step3: removed the compression, and (e) Step4: heated up to 60°C again (strain is seen to recover to ~ 0%).....	65
Figure 5.1 Shows the lattice parameters and their potential energy [69].....	69
Figure 5.2 Shows Bekker and Brinson's model to describe the SMA behavior when a complicated loading path is used [72].	71

Figure 5.3 Shows the Tension–compression tests (left part) and torsion tests (right part) under stress control with continuous line: $T = 285 \text{ K}$ (above $A_f = 248\text{K}$) without and with training [87].	75
Figure 5.4 Figure shows the schematic of an SMA uniaxial pseudo-elastic test [88].	83
Figure 5.5 Shows the schematic of the phase diagram [88].	84
Figure 5.6 Shows the tensile yield strength of polypropylene- CaCO_3 composite for different particle size at different volume fractions of CaCO_3 in PP matrix [91].	89
Figure 5.7 Shows the variation of young’s modulus in glass filled epoxy polymer composite with particle diameter for different volume fractions of particle from 10- 46% of glass fillers [91].	90
Figure 5.8 Shows the RVE of spherical SMA particle in SMP matrix.	92
Figure 5.9 Above shows the variation of elastic modulus of carbon-epoxy laminate composite when subjected to tensile loads with orientation of the fiber[94].	94
Figure 5.10 Above shows the fiber packing methods in place to obtain the maximum volume fraction of fiber that could be used in composite.	95
Figure 5.11 Above shows schematic of RVE of SMA-Wire in SMP composite.	96
Figure 5.12 The above flow chart shows different stages at which the subroutines are called in the general analysis in ABAQUS/Standard [95].	98
Figure 5.13 Shows the schematic of SMA (50% by weight) + SMP Particle composite FE model built in ABAQUS CAE.	104
Figure 5.14 Shows the schematic of SMA (50% by weight) + SMP Wire composite FE model built in ABAQUS CAE.	105

Figure 5.15 Shows the stress-strain response of (a) SMP matrix and (b) SMA reinforcement at different loading temperatures.....	106
Figure 5.16 Variations of elastic modulus with temperature of the present SMA and SMP.....	107
Figure 5.17 Shows the stress-strain response of NiTi 5% (by wt.) + SMP particle composite with different loading temperatures.....	108
Figure 5.18 Shows the stress-strain response of NiTi 15% (by wt.) + SMP particle composite with different loading temperatures.....	109
Figure 5.19 Shows the stress-strain response of NiTi 25% (by wt.) + SMP particle composite with different loading temperatures.....	109
Figure 5.20 Shows the stress-strain response of NiTi 35% (by wt.) + SMP particle composite with different loading temperatures.....	110
Figure 5.21 Shows the stress-strain response of NiTi 45% (by wt.) + SMP particle composite with different loading temperatures.....	110
Figure 5.22 Shows the stress-strain response of NiTi 50% (by wt.) + SMP particle composite with different loading temperatures.....	111
Figure 5.23 Shows the variation of modulus with temperature in NiTi 5% (by wt.) + SMP particle composite in comparison to that of SMP.....	111
Figure 5.24 Shows the variation of modulus with temperature in NiTi 15% (by wt.) + SMP particle composite in comparison to that of SMP.....	112
Figure 5.25 Shows the variation of modulus with temperature in NiTi 25% (by wt.) + SMP particle composite in comparison to that of SMP.....	112

Figure 5.26 Shows the variation of modulus with temperature in NiTi 35% (by wt.) + SMP particle composite in comparison to that of SMP.....	113
Figure 5.27 Shows the variation of modulus with temperature in NiTi 45% (by wt.) + SMP particle composite in comparison to that of SMP.....	113
Figure 5.28 Shows the variation of modulus with temperature in NiTi 50% (by wt.) + SMP particle composite in comparison to that of SMP.....	114
Figure 5.29 Variation of Modulus of SMA-Particle + SMP composite with SMA filler content with a loading temperature of 20°C.	115
Figure 5.30 Variation of Modulus of SMA-Particle + SMP composite with SMA filler content with a loading temperature of 60°C.	115
Figure 5.31 Change in Modulus of SMA+SMP particle composite with SMA filler content.....	116
Figure 5.32 Shows the variation of strength with temperature in NiTi 5% (by wt.) + SMP particle composite in comparison to that of SMP at 20% compressive strain.....	117
Figure 5.33 Shows the variation of strength with temperature in NiTi 15% (by wt.) + SMP particle composite in comparison to that of SMP at 20% compressive strain.....	117
Figure 5.34 Shows the variation of strength with temperature in NiTi 25% (by wt.) + SMP particle composite in comparison to that of SMP at 20% compressive strain.....	118
Figure 5.35 Shows the variation of strength with temperature in NiTi 35% (by wt.) + SMP particle composite in comparison to that of SMP at 20% compressive strain.....	119
Figure 5.36 Shows the variation of strength with temperature in NiTi 45% (by wt.) + SMP particle composite in comparison to that of SMP at 20% compressive strain.....	119

Figure 5.37 Shows the variation of strength with temperature in NiTi 50% (by wt.) + SMP particle composite in comparison to that of SMP at 20% compressive strain.....	120
Figure 5.38 Change in Strength of SMA+SMP particle composite with SMA filler content.....	120
Figure 5.39 Shows the stress-strain response of NiTi 5% (by wt.) + SMP fiber composite at various temperatures.	122
Figure 5.40 Shows the stress-strain response of NiTi 15% (by wt.) + SMP fiber composite at various temperatures.....	122
Figure 5.41 Shows the stress-strain response of NiTi 25% (by wt.) + SMP fiber composite at various temperatures.....	123
Figure 5.42 Shows the stress-strain response of NiTi 35% (by wt.) + SMP fiber composite at various temperatures.....	123
Figure 5.43 Shows the stress-strain response of NiTi 45% (by wt.) + SMP fiber composite at various temperatures.....	124
Figure 5.44 Shows the stress-strain response of NiTi 50% (by wt.) + SMP fiber composite at various temperatures.....	124
Figure 5.45 Shows the variation of modulus with temperature in NiTi 5% (by wt.) + SMP fiber composite in comparison to that of SMP.	125
Figure 5.46 Shows the variation of modulus with temperature in NiTi 15% (by wt.) + SMP fiber composite in comparison to that of SMP.	125
Figure 5.47 Shows the variation of modulus with temperature in NiTi 25% (by wt.) + SMP fiber composite in comparison to that of SMP.	126

Figure 5.48 Shows the variation of modulus with temperature in NiTi 35% (by wt.) + SMP fiber composite in comparison to that of SMP.	126
Figure 5.49 Shows the variation of modulus with temperature in NiTi 45% (by wt.) + SMP fiber composite in comparison to that of SMP.	127
Figure 5.50 Shows the variation of modulus with temperature in NiTi 50% (by wt.) + SMP fiber composite in comparison to that of SMP.	127
Figure 5.51 Variation of Modulus of SMA-Fiber + SMP composite with SMA filler content with a loading temperature of 20°C.	128
Figure 5.52 Variation of Modulus of SMA-Fiber + SMP composite with SMA filler content with a loading temperature of 60°C.	128
Figure 5.53 Change in Modulus of SMA+SMP fiber composite with SMA filler content at a loading temperature of 20°C.	129
Figure 5.54 Change in Modulus of SMA+SMP fiber composite with SMA filler content at a loading temperature of 60°C.	129
Figure 5.55 Shows the variation of strength with temperature in NiTi 5% (by wt.) + SMP fiber composite in comparison to that of SMP at 20% compressive strain.	130
Figure 5.56 Shows the variation of strength with temperature in NiTi 15% (by wt.) + SMP fiber composite in comparison to that of SMP at 20% compressive strain.	130
Figure 5.57 Shows the variation of strength with temperature in NiTi 25% (by wt.) + SMP fiber composite in comparison to that of SMP at 20% compressive strain.	131
Figure 5.58 Shows the variation of strength with temperature in NiTi 35% (by wt.) + SMP fiber composite in comparison to that of SMP at 20% compressive strain.	131

Figure 5.59 Shows the variation of strength with temperature in NiTi 45% (by wt.) + SMP fiber composite in comparison to that of SMP at 20% compressive strain.	132
Figure 5.60 Shows the variation of strength with temperature in NiTi 50% (by wt.) + SMP fiber composite in comparison to that of SMP at 20% compressive strain.	132
Figure 5.61 Shows the custom built mixer used to mix the NiTi SMA powder particles in the SMP matrix to obtain homogeneous dispersion of SMA particles.	135
Figure 5.62 Shows the stress-strain behavior of various SMA Particle SMP composites obtained from DMA test.	137
Figure 5.63 Shows the comparison of variation of modulus values obtained from experimental results and simulations for various SMA filler contents.	138
Figure 6.1 Above shows the aligned Ni chains along the radius and perpendicular to the radius of the CNT-SMP cylinder composite placed in magnetic field.	144
Figure 6.2 Schematic design of DMA under vertical load, showing the various possible test arrangements.	145
Figure 6.3 Shows the MTS setup used for testing mechanical behavior of CNT-SMP composites.	146
Figure 6.4 Shows the set up used to measure the electrical resistivity of CNT-Ni-SMP composites.	147
Figure 6.5 Shows the tan Delta Vs CNT filler content from thermal cycling on DMA.	147
Figure 6.6 Shows the variation of Tg of CNT-SMP composites with addition of CNT fillers.	148
Figure 6.7 shows the mechanical behavior of CNT-SMP obtained from DMA compressive test.	149

Figure 6.8 Change in Modulus of CNT+SMP particle composite with CNT filler content.	150
Figure 6.9 Change in strength of CNT+SMP particle composite with CNT filler content.	151
Figure 6.10 Shows the stress-strain curves of various CNT-SMP composites with Ni chains aligned in the direction parallel and perpendicular to the radius of compression specimen.	152
Figure 6.11 Variation of electrical resistivity of CNT fiber + SMP composites with addition of CNT filler content.....	153

List of Tables

Table 2.1 Table gives a comparison of properties of SMPs Vs SMAs [7]..... 25

Table 4.1 Comparisons of coefficients between Neo-Hooke model and Arruda-Boyce model.....60

Table 4.2 Summary of Ogden coefficients. 61

Table 5.1 Increase of Young’s modulus and tensile strength of a duromer matrix(polyester resin) by addition of glass fibers with a volume fraction of 65% to 70% [93].....93

Table 5.2 Summary of Ogden Coefficients for the SMP..... 101

Table 5.3 Summary of Material coefficients for the SMA [88]. 102

Table 6.1 Resistivity of CNT (0.5% by weight)-SMP composites measured perpendicular to the radius with (a) aligned Ni(25% by weight) chains and (b) No Ni chains.....154

Table 6.2 Resistivity of CNT (0.5% by weight)-SMP composites measured along the radius with (a) aligned Ni (25% by weight) chains and (b) No Ni chains..... 155

Table 6.3 Resistivity of CNT+Ni-SMP composites measured over a span of two years. 155

Chapter One

1 INTRODUCTION

1.1 BACKGROUND

Shape memory polymers (SMPs) are a class of shape memory materials (SMMs) that can recover their shape from a deformed state back to their permanent shape when exposed to the appropriate stimulus. Compared with other shape memory materials such as shape memory alloys, the SMPs can have much larger actuation strain (more than 200% recoverable elastic strain for most SMPs) and yet require relatively lower fixing forces. They also possess the advantages of low cost, low density and potential biocompatibility and biodegradability.

The shape memory effect in polymers comes from their unique molecular structures. A typical polymer is a mixture of many long, entangled molecular chains that are connected by characteristic net points created by either chemical cross-linking or physical cross-linking. At temperatures higher than the glass transition temperature (T_g), those polymer chains are relaxed and flexible. As a result, the polymer becomes soft and is characterized as the rubbery state. When an external force is applied, the polymer chains can be stretched or contracted to large extents and the net points may also be displaced. When the temperature is reduced below the transition temperature while maintaining the pre-deformed shape, some secondary cross-links can be formed among those deformed polymer chains. These secondary cross-links help fix the polymer at the temporary shape after the external force is removed. Upon re-heating the polymer above the transition temperature, those secondary cross-links are released and the original shape is recovered.

A schematic representation of the thermo-mechanical cycle for a typical SMP is shown in Figure 1.1

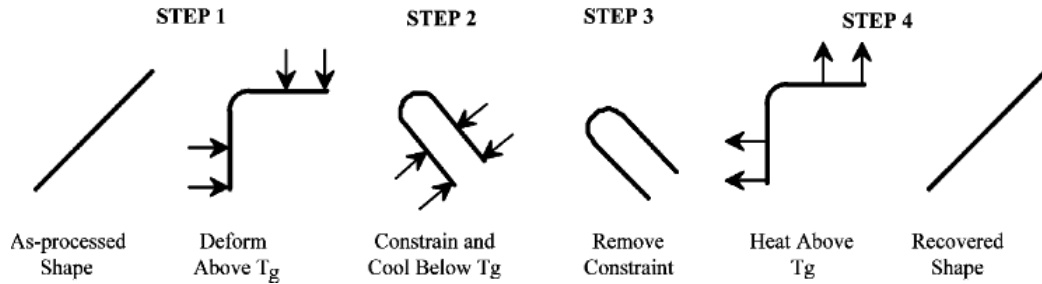


Figure 1.1 Diagrammatic representation of the thermo-mechanical cycle of an SMP.

Shape memory polymers have been considered for a variety of applications; the most significant application is probably in the aerospace field. For example, the ability to change wing geometry would allow a single air vehicle to be capable of meeting several performance parameters. A spider plot representing the proposed capability of an air vehicle with reconfigurable wings can be seen in Figure 1.2 [1].

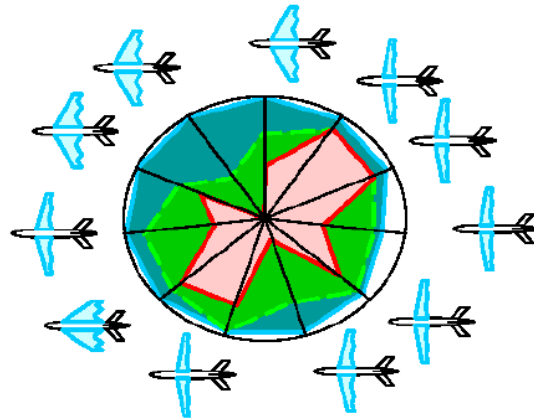


Figure 1.2 Spider plot representing the capabilities of a reconfigurable air vehicle [1].

1.2 OBJECTIVES OF THE DISSERTATION

Although SMPs can provide high actuation strain, are lightweight and inexpensive, they lack of strength, have low modulus at high temperatures and don't have the ability to perform reversible actuation [2-6]. In this project, shape memory composites (SMCs) will be created by embedding various reinforcement components into a shape memory polymer matrix. A composite is a hybrid of two or more constituent materials with significantly different physical or chemical properties and which remain discrete on a macroscopic level within the finished structure. A composite is designed to display a combination of the best characteristics of each of the constituent materials. Consequently, a composite's performance is superior to those of its constituents acting independently [7]. In this project, the reinforcement fillers include: (1) shape memory alloy particles, (2) shape memory alloy wires, (3) carbon nanotube fibers, and (4) nickel particles. The first two types of fillers (SMA particles and SMA wires) are aimed to improve the mechanical responses of the SMP; while the last two types of fillers (CNT fibers and Ni particles) are aimed to enhance the multifunctional performances of the SMP.

1.3 ORGANIZATION OF THE DISSERTATION

Chapter 2 of this dissertation presents a comprehensive review of literatures concerning the latest developments of SMPs and SMP composites. Chapter 3 shows the detailed synthesis of an epoxy-based shape memory polymer used in the project. The comprehensive characterization of the SMP is also presented in Chapter 3. Chapter 4 is concerned with the analytical modeling of the complicated SMP material: mechanical response and shape recovery process. Chapter 5 deals with the SMA reinforced SMP

composites. Chapter 6 deals with the CNT and Ni reinforced SMP composites. Chapter 7 presents a brief summary of overall work and possible future work.

Chapter Two

2 REVIEW OF LITERATURES

2.1 INTRODUCTION TO SHAPE MEMORY POLYMERS

Shape memory materials (SMMs) are a class of active materials that have dual-shape capability. The dual-shape capability or shape memory effect is characterized by the ability to recover a permanent shape from an initial level of pre-deformation when exposed to the appropriate external stimulus. Certain polymers, metal alloys, ceramics, and gels can be classified as SMMs [8]. Of all SMMs, shape memory alloys (SMAs) and shape memory polymers (SMPs) are by and large the most widely studied materials. The shape memory effect was seen in metal alloys as early as 1951, and the shape memory effect in polymers was reported a decade earlier. However, SMAs are more prominent and more widely used than SMPs [9]. Shape memory alloys and polymers vary in nearly every material aspect from the basic mechanism for the shape memory effect to the capability of tailoring specific material properties (i.e. modulus and transition temperature). Looking at the basic material characteristics of SMAs and SMPs it becomes very apparent that the properties of SMPs are more desirable. SMAs have been reported to have high stiffness, high cost, complicated processing demands, and very low recoverable strains, on average less than 8% [9]. In direct contrast SMPs are generally low cost, low density, and can recover strain levels of nearly 200% [9]. Another advantage of SMPs is the ability to specially adapt material properties for specific applications and SMPs do not require costly or complicated procedures of manufacturing. Furthermore, SMPs can be activated by several stimuli including heat, light, chemical, or perhaps a combination of these stimuli [109]. Additionally, most SMPs are

biocompatible and biodegradable [10]. Accordingly, all of these advantages lead to SMPs being widely adapted to applications in a variety of fields.

Thermally induced SMPs are the first polymers reported to show the shape memory effect, and consequently these SMPs are the most widely studied and used [11]. The thermo-mechanical cycles used to quantify the shape memory effect of SMPs have been well documented in the literature [8, 11-18]. Traditionally, there are two types of recoveries studied when considering shape recovery: constrained and free. Constrained recovery involves the measurement of the stress produced in the SMP when recovery is activated while the temporary deformation is constrained. This style of recovery would be useful when considering applications where the SMPs are used as actuators. Free recovery involves the recovery of the SMP while under zero constraint. Deployable applications are considered to be examples of free recovery situations. Figure 2.1 presents a graphic representation of the thermo-mechanical cycle of a SMP subjected to free recovery. The SMP is first activated at a deformation temperature, T_d , which should be above the SMP's glass transition temperature, T_g . Second, the constrained SMP is cooled to a storage temperature, T_s , which is less than T_g . Next the SMP is heated to a recovery temperature, T_r , to allow the free recovery. In general, a range of temperatures may be used for the recovery temperature to allow the SMP to recover its initial permanent shape through heating.

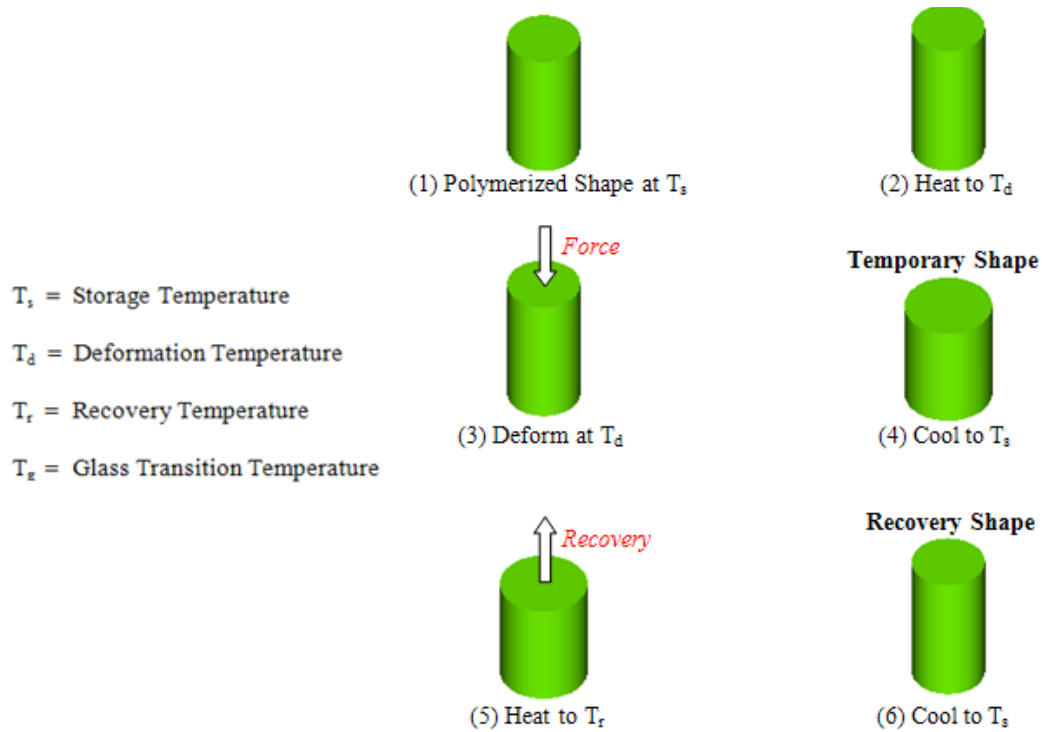


Figure 2.1 Diagram of thermo-mechanical cycle during free recovery for thermally induced SMP.

The shape memory effect is not a specific property of any single polymer; instead the shape memory effect results from a combination of polymer structure and polymer morphology together with applied processing and programming [8]. Although, most polymers present a degree of shape memory ability, cross-linking polymers can achieve a higher order of recoverability. Several studies [7, 8, 12] gave an in-depth discussion of the physical system that results in the thermally induced shape memory effect of SMP. The shape memory effect in thermal induced cross-linked polymers is a result of the transition from a state dominated by entropic energy (rubbery state) to state where internal energy dominates (glassy state) as temperature decreases. Figure 2.2 presents a schematic of the molecular mechanism for a thermally induced cross-linked SMP.

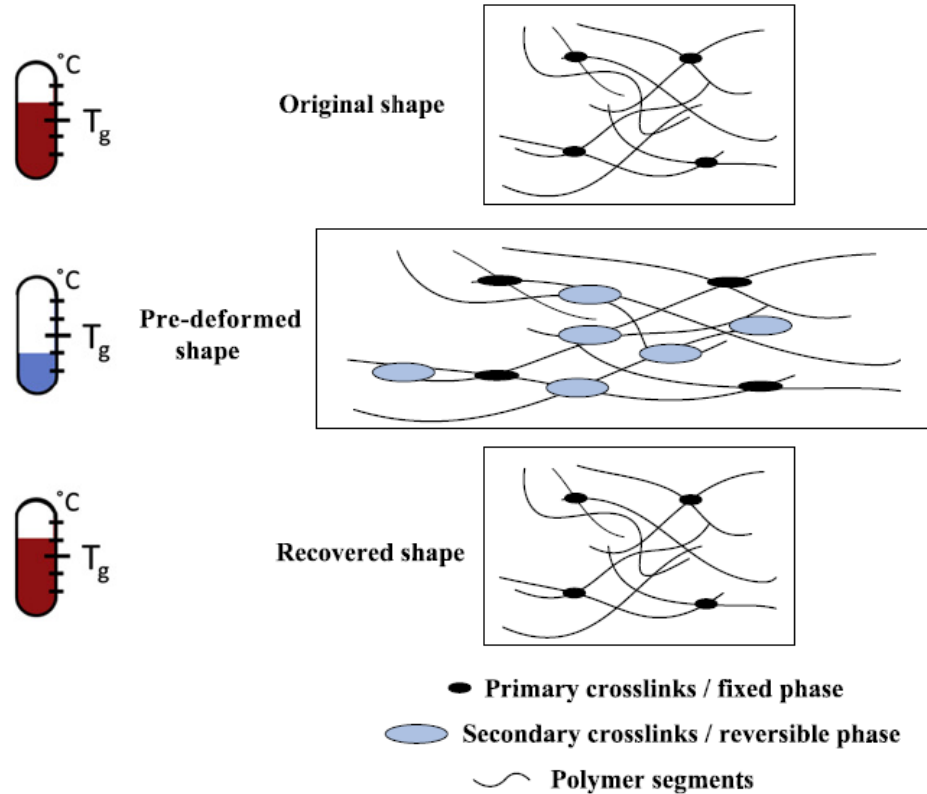


Figure 2.2 Schematic illustrating a simple molecular mechanism of the thermally induced SMP [19].

The permanent shape of a SMP is stabilized by cross-linking net points denoted by the black points in Figure 2.2. At temperatures above the glass transition temperature, T_g , the molecular chains are flexible and can slip off of each other. An entropy loss occurs as the polymer is deformed under these conditions, which corresponds to entropy elasticity. While in the rubbery state if the applied load is removed the polymer will tend to recover its permanent shape and thus recover the entropy lost. However, this recovery process can be interrupted by decreasing the temperature below T_g . Below T_g the molecular chains are frozen, but if the temperature is again increased above T_g the molecular chains will become flexible and return the original configuration based upon the cross-linking net points [8, 13].

2.2 TYPES OF SHAPE MEMORY POLYMERS

Shape memory polymers have several advantages over other smart materials such as shape memory alloys and as such, there were several studies carried out on this class of advanced materials to better understand and classify them based on different aspects since they were first recognized as important shape memory material in the 1960s. Some researchers like V.A. Beloshenko et al. have classified SMPs based on their microstructures: i.e. if the configuration fell into one of the following groups of glassy, crystalline, composites or gels [13]. They focused on how the thermal treatment would affect the physical response such as shape recovery rates. Although their study did not include how the chemistry of the materials would have an effect on SMP behavior. The shape memory effect observed in polymeric materials is similar to that observed in alloys. However, the driving mechanism to cause this shift back and forth from a temporary to a permanent shape is quite different from that seen in shape memory alloys. The shape memory effect in polymers is due to presence of elastic polymeric networks that are easily stretched at temperatures above the glass transition temperature specific to each polymer material. For this reason Liu et al. have studied the chemical bonding in polymers and used their findings to classify the shape memory polymers based on their driving mechanism for shape fixity. According to their study, shape memory polymers are broadly categorized into four groups as listed below [7].

Covalently cross-linked glassy thermoset networks as SMPs: These are the simplest type of polymers that exhibit shape memory behavior. These SMPs have a sharp glass transition temperature range. The characteristic of this class of polymers is that the shape memory behavior in these thermosets is triggered by their glass-transition

temperature. They have excellent modulus above the glass transition temperature due to the permanent cross-linking between the polymer segments giving it a three dimensional physical structure. This also helps in giving the polymer better shape recovery ability. This class of polymers has wide range of tunable glass transition temperature depending on the constituent monomer forming the polymer chain. Due to this property to have a variable modulus above the transition temperature and tunable transition temperature, they could be used for a specific application by changing the extent of cross-linking and there by changing the properties of the polymer. Hence glass transition temperature plays an important role in determining their end application. Some of the examples of shape memory polymers that belong to this category are Epoxy, Thermosetting poly urethane, Copolyester, Styrene copolymer. Although they have excellent shape recovery ability these polymers once processed are difficult to reshape. However, due to their broad range of T_g and tunable modulus gives these polymers advantages over the other classes discussed below.

Covalently cross-linked semi-crystalline networks as shape memory polymers: In this class of SMPs, in addition to the glass transition (T_g) temperature the melting temperature (T_m) of semi-crystalline networks could also be used to trigger shape recovery behavior. These polymers are easy to work with below their critical temperature (T_g and T_m). The shape recovery speeds are faster than those observed in glassy thermosets however, like the glassy thermoset polymers they are difficult to reshape once processed. Also, their stiffness depends on the degree of crystallinity and so indirectly on the extent of cross-linking. This gives the scope to have flexible modulus and fast shape recovery. This class of materials includes bulk polymers such as semi-crystalline rubbers

and liquid-crystal elastomers. Although they have faster shape recovery rates they lack in thermal stability which makes it challenging in specific applications that require long range of thermal stability. There has been some work done in this area to improve their thermal stability by cross-linking the amorphous fraction of the polymer instead of both amorphous and crystalline fractions by implementing special curing techniques. Such techniques become necessary and yet prove to be useful in biomedical applications where the polymer is required to have activation ability close to body temperature. One such classic material of this family of SMPs is chemically cross-linked trans-polyisoprene (TIP). Some other examples in this class of SMPs are Poly-caprolactone, EVA + nitrile rubber.

Physically cross-linked glassy copolymers as shape-memory polymers: Since processing the of SMPs has been a challenge from being used to their fullest potential, special methods were developed to make polymers that fall under this category of physically cross-linked glassy copolymers. In this SMP group, both soft and hard fractions in thermoplastics form physical cross-links that give the super elasticity and T_g that favor shape memory behavior. The shape memory effect is observed mainly in the form of phase-separated block copolymers. The characteristic of these materials in this class is that when they are subjected to a temperature above the glass transition (T_g) and melt temperature (T_m) of both the soft and hard segments, the polymer flows and at this stage is capable of being processed to a new shape. This is process ability is possible as they are only physically cross-linked. And they have stiffness similar to the cross-linked glassy thermosets. The example for this class shown in Figure 3 is that of a melt-

miscible blend of poly (vinyl acetate) (PVAc) and poly (lactic acid) (PLA). Some of the examples of this category of SMPs are PET-co-PEO, Aramid/PCL, and PE-co-Nylon 6.

Physically cross-linked semi-crystalline block copolymers as shape-memory polymers: The characteristic of this class of polymers involves using melt temperature (T_m) of the block copolymers to trigger the shape recovery. For these polymers the soft domain crystallizes so instead of their T_g , T_m could be used to activate the polymer and temporary shape is thus fixed when the soft segments crystallize. The example for this class, shown in Figure below, is that of a multi-block polyurethane featuring PEO as a soft segment. This material could be processed above its melting temperature and its rubbery properties could be tuned by varying the soft/hard segment ratio. Also, the transition temperature could be controlled by changing the soft segments. In addition these polymers are both bio-degradable and bio-compatible.

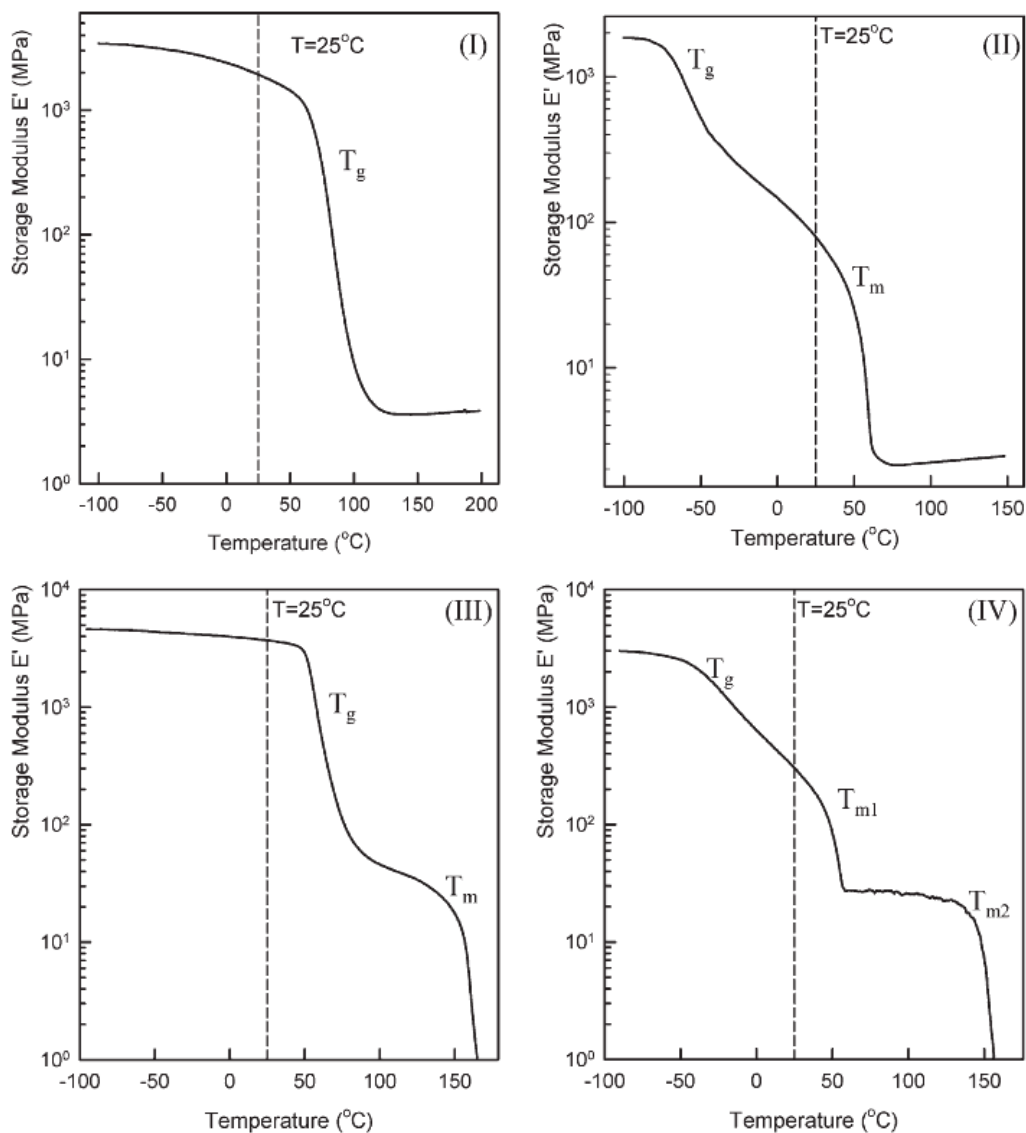


Figure 2.3 Definition of four types of shape-memory polymers with different shape-fixing and shape-recovery mechanisms depicted as a function of their dynamic mechanical behavior. Plotted is the tensile storage modulus vs. temperature as measured using a small oscillatory deformation at 1 Hz for: (I) chemically cross-linked glassy thermosets; (II) chemically cross-linked semi-crystalline rubbers; (III) physically cross-linked thermoplastics; and (IV) physically cross-linked block copolymers [7].

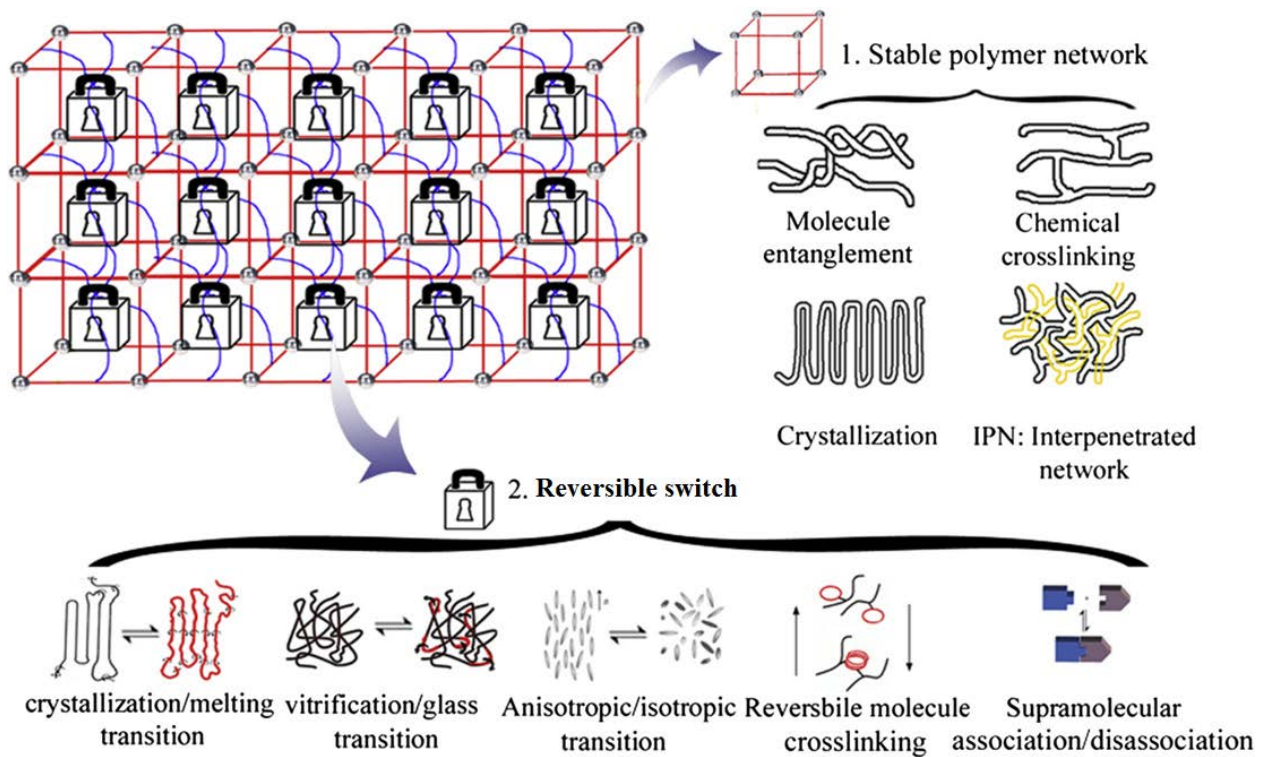


Figure 2.4 Various molecular structures of SMPs[20].

The figure 2.4 above shows the stable network and a reversible switch that are essential to observe shape memory effect in polymers. The stable network could be in the form molecular entanglement, chemical crosslinking, crystallization etc. as discussed earlier. And the reversible switch could be several different processes such as transition at melt temperature, transition at T_g and reversible molecule crosslinking.

Based on the above classification it is clear that shape memory polymers are easy to tailor to a specific application by devising special processing techniques and also by varying the cross linking soft and hard segments, cross-linking density and by controlling the extent of curing. By doing so a shape memory polymer that has favorable recovery rate, transition temperature and thermal stability along with flexible modulus at temperatures above the glass transition or melt temperature could be fabricated.

In this project an epoxy thermosetting shape memory polymer was synthesized that has a glass transition temperature of roughly 43°C. And as such the shape recovery process is triggered by the glass transition temperature and has a sharp transition and is capable of recovering fully. As the main objective is to develop multifunctional shape memory polymer based composites that have complex behavior, it is essential to use a matrix that has a T_g compatible with the reinforcing fibers and particles.

2.3 INTRODUCTION TO SHAPE MEMORY POLYMER COMPOSITES

Although shape memory polymers are advantageous and preferred material candidates for several high strain and low cost applications they are not electrically conductive and have lower stiffness compared to some other smart materials such as shape memory metal alloys, carbon nanotubes, Ni or iron oxide. In order to achieve the multifunctional ability and expand their applications in these fields, it is necessary to design better materials that have the above said properties in addition to having high recoverable strains and low cost of manufacturing.

2.3.1 Types of Shape Memory Polymer Composites

2.3.1.1 Conventional Fibre/Particle SMP Composite

Conventional reinforcements such as carbon Fibre, glass Fibre and Kevlar have been used to increase the mechanical strength of SMPs. These fillers could be designed in the several forms such as fabrics, mats or microfibers and embedded in the SMP matrix to make it stiffer based on their orientation. Depending on the mechanical loads that the composite material is subjected to, the fillers are aligned in the matrix. The fibers can bear higher loads in the direction parallel to their orientation. And since the mechanical strength is dependent on the fiber orientation, the properties such as modulus in the

direction perpendicular to the fiber alignment are not as much higher, hence the shape memory effect can be maintained in transverse direction which enhances the multifunctional abilities of the shape memory polymer based composites. These SMPCs have potential applications in self-deployable structures and vibration control structures.

1) Reinforcement by carbon fiber fillers: One such application of a shape memory polymer reinforced with carbon fiber fabrics to function as a hinge in deployable structures was built by Xin Lan et al [21]. The SMPC was reinforced with three-ply plain weaves of carbon fiber fabrics with standard fabrication techniques. The mechanical properties such as storage modulus of the composite increased compared to the SMP alone in the glassy phase prior transition [21]. And the results from their study are shown in the Figure 2.6 (below).

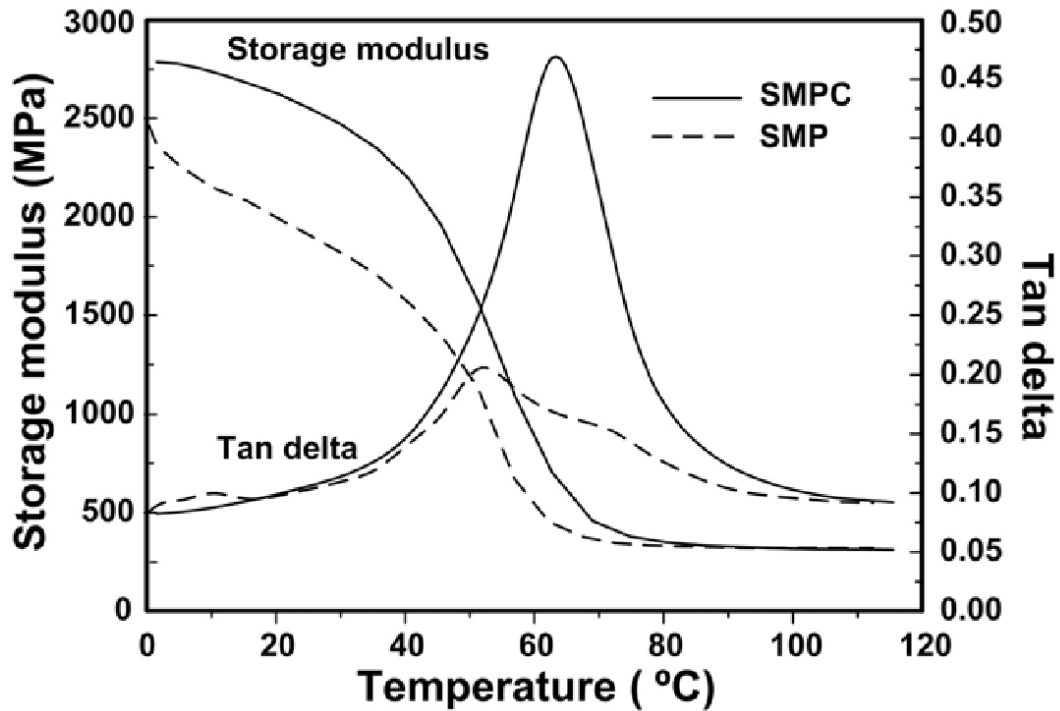


Figure 2.5 Figure shows storage modulus and tangent delta versus temperature of the pure SMP and SMPC [21].

2) Reinforcement by nano clay particulate fillers: Bin Xu et al. [22] have worked with nano size clay powder fillers in shape memory polymer matrix to study the improvements in thermo-mechanical properties of the shape memory polyurethane matrix. Addition of nano size clay fillers had significantly improved the storage modulus at ambient temperature. However, they also observed a steep drop in the modulus at transition temperature similar to the shape memory polyurethane matrix. Also, as the clay content was increased the shape memory effect of the polymer matrix was seen have decreased. The storage modulus change and the load-displacement curves for different clay content in polyurethane matrix in comparison to polyurethane alone are shown in the figures below.

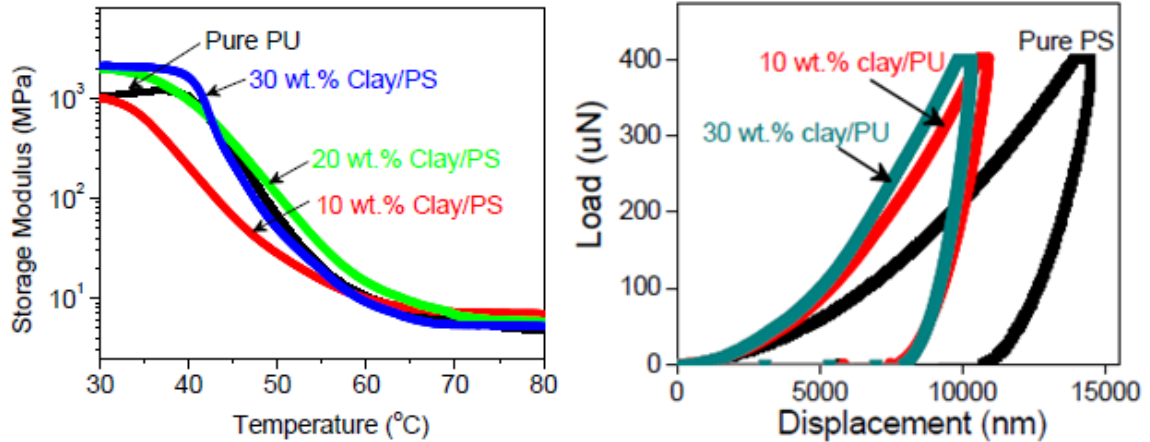


Figure 2.6 Figure on left shows the storage modulus vs. temperature. Figure on the right shows the load displacement results from nano-indentation tests on Nanoclay-Polyurethane composites [22].

From the figure above we can see that although the modulus has increased favourably with the addition of nano clay fillers to the shape memory polyurethane matrix, the strain recovery from the unloading curve reported from the results of direct test of nano-indentation is not complete. Hence it was concluded that although adding fillers to the matrix has certain advantages of improving the modulus and yield strength, it comes at a compromise of losing the shape recovery properties of the matrix. This is due to fillers that act as obstacle for easy deformation of polymer molecules causing incomplete recovery. For this reason, it becomes necessary to pick an appropriate filler content to strike a balance on mechanical performance and shape recoverability. And at times depending on specific applications striking a balance becomes very difficult. So, alternate, multifunctional fillers have been researched for in the recent times.

3) Reinforcement by SiC and SiO₂ fillers: Further from research work carried out on shape memory polymer composites in the early 90s included investigating the effects of

reinforcing SMP matrix with SiC and SiO₂. Ken Gall et al. [23]. In their study several weight fractions of SiC fillers ranging from 5% to 40% were used to reinforce an epoxy based shape memory polymer matrix. It was seen that the hardness and modulus values have increased considerably compared to the unreinforced base polymer matrix. However, the constrained recovery was affected with the addition of filler particles. The figure below shows the recovery stress change needed to cause the transition with temperature. It is clear that with the addition of SiC particles; more compressive recovery force is needed. It was also observed that the unconstrained recoverable strain limit was lowered with the addition of SiC particles. The reason for this was attributed to the inability of the SiC particles to exhibit shape memory characteristics.

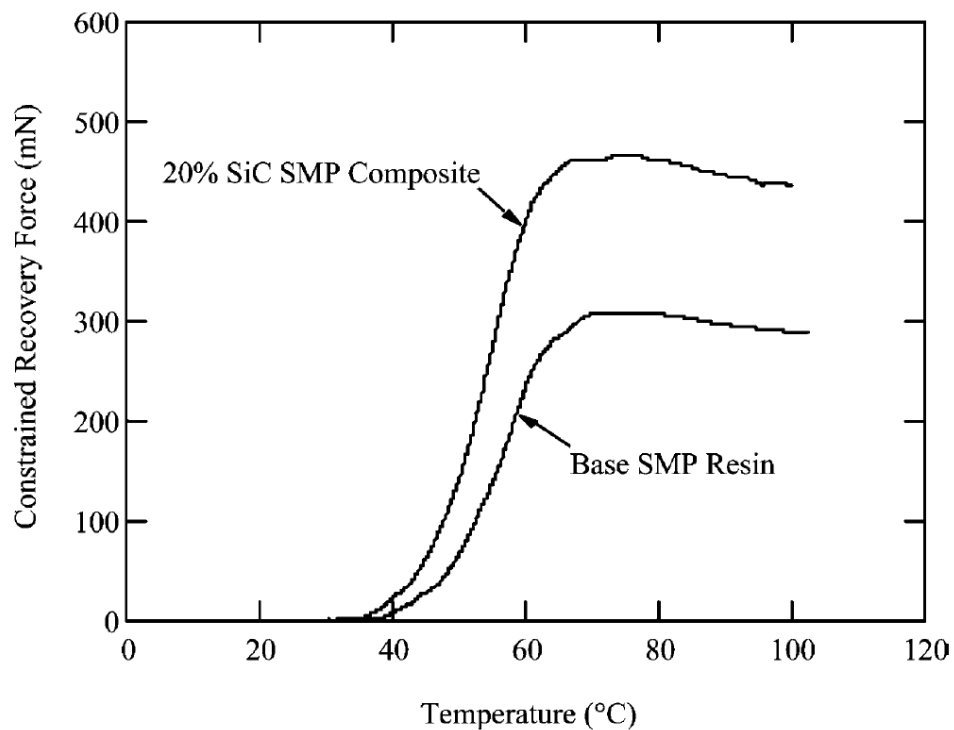


Figure 2.7 Figure shows constrained bend recovery force as a function of temperature for reinforced and unreinforced SMP materials [23].

This means that there is tradeoff between recoverable displacement and force which needs to be taken into account when using SiC nano particle reinforced shape memory composites for specific applications in deploying structures. For this reason other fillers such as SiO₂ were used as a cross linking agent to SiC in polymer matrix composites to see better mechanical performance without compromising the shape memory properties of the polymer matrix [24].

4) Reinforcement by conductive carbon black fillers: More recently, several studies focused on carbon black as filler material for fabricating conductive shape memory polymer composites [25, 26]. Since, carbon particles are conductive and when mixed with polymer matrix, they could be used as actuators for control surfaces such as elevators and rudders as suggested by Goo et al [27]. To replace a servomotor with a SMP actuator, as their first step they had reinforced shape memory polyurethane with conductive carbon black fillers. This increased the glass transition temperature of the composite and also made it polymer electrically conductive. Although, 30% by weight of carbon black was reported in their study as required filler content to make the polymer matrix sufficiently conductive. The conductivity then measured using four point probe method was $1 \times 10^{-1} \text{ S/cm}^{-1}$ [27].

Shape memory polymers are capable of being activated through several external stimuli. As discussed earlier, passing electric current is one such ways to activate the conductive fillers in the polymer matrix. Similarly, another stimulus is by magnetic energy by joule heating. For this the polymer is reinforced with electro-magnetic fillers such as magnetite nano particles (Fe₂O₃) that are capable of inductive heating. That

means they can transform electro-magnetic energy from external high frequency field to heat.

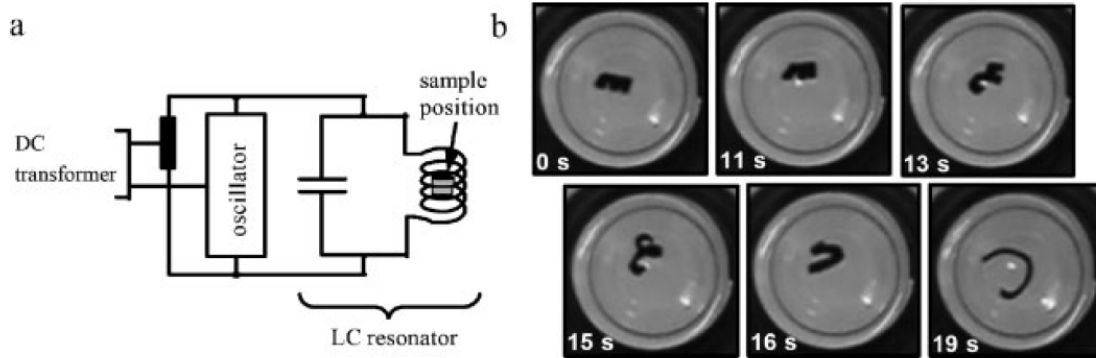


Figure 2.8 Images show the shape recovery of magnetite reinforced SMP [28].

Although high weight fraction of Fe_2O_3 around 40% are reported in study by Schmidt et al [28]. The figure above shows the transformation process of magnetite-polyurethane shape memory polymer composite. The composite is fixed in the temporary shape of a helix induced by high frequency electro-magnetic field. The shape transition was observed in the presence of AC field [28].

Although fillers like carbon black, magnetite and Ni micro and nano sized powders could be used to obtain multifunctional characteristics in a shape memory polymer composite, they are not the best suited filler materials since high weight fractions of carbon black and Ni, magnetite are necessary to make the polymer matrix conductive (from CB and Ni fillers) and obtain the shape recovery ability (from magnetite fillers).

Due to this reason to obtain better mechanical performance without compromising or having to tradeoff between the shape memory properties, and to obtain conductive,

self-activating shape memory polymer composites there has been special focus on multifunctional polymer composites with special fillers that are capable of keeping the shape memory behavior intact and at the same time have higher modulus and strength.

2.3.1.2 Multifunctional Fibre/Particle SMP Composite

Since using conventional filler particles was proving to be less optimal in terms of achieving a balance of mechanical performance and shape recovery ability and also to enhance the multifunctional characteristics of shape memory polymers, new Fibre and particle fillers were studied in the last decade. Some of these filler reinforcements include shape memory alloy fibers and particles, carbon nanotubes and Ni particles. To fully utilize the shape changing ability of the polymers it is necessary to embed reinforcements that have more than one function to carry out. They need to improve the thermal response when being used in applications that require activating the polymer at a specific temperature. For structural applications they need to be stronger and have higher modulus. And for applications that require self-activation without external stimuli it is necessary to reinforce the non-conductive shape memory polymer matrix with electrically conductive fillers. Using these multifunctional fillers instead of the conventional fillers could help in developing a stronger, thermally stable and electrically conductive shape memory polymer composites [29]. Recent studies have focused on reinforcing shape memory polymers with non-conventional fillers such as shape memory alloys and carbon-nanotubes [30].

1) **SMA-SMP composites:** Shape memory alloys have been studied for much longer than shape memory polymers. SMAs have similar controlled shape recovering ability as SMPs. However, both these smart material groups have very different physical,

mechanical, thermal and electrical properties as shown in the table below. The mechanism that causes the shape memory effect is quite different in SMAs compared to that of SMPs. The SME is due to the transformation of martensite phase (low temperature phase) when the martensite variants reorient themselves from twinned martensite to de-twinned martensite phase.

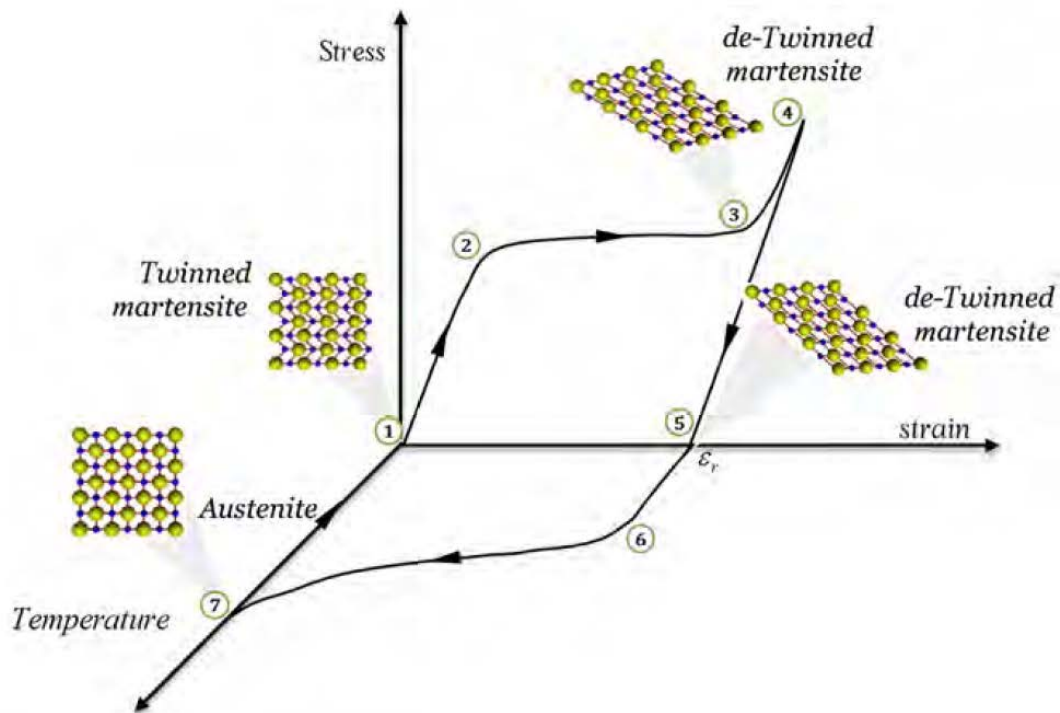


Figure 2.9 The figure above shows the temperature induced shape memory effect of SMA [31].

As the SME occurs at low temperatures, the material microstructure is initially composed of twinned martensite. Upon loading, the applied stress reaches the critical value for de-twinning (point 2) and the martensite reorientation starts, associated to a macroscopic deformation (plateau 2-3). At the end of the plateau, the martensite is completely de-twinned and after this plateau, when load is applied the de-twinned

martensite only deforms elastically to the new microstructure (slope 3-4). Upon unloading, the macroscopic deformation is retained as all variants of martensite are equally stable (point 5). When the material is heated above a critical temperature, the martensite to austenite phase transition starts, allowing it to recover the macroscopic deformation (points 6-7). Shape memory alloys are known to deform up to 8% [31].

Where as in shape memory polymers the mechanism that causes shape memory effect is due to the phase-segregated morphologies consisting of soft and hard domains. When the polymer is cooled under stress, crystallization or vitrification of soft domains can temporarily “fix” the material in an elastically strained state. These soft domains melt when heated above the glass transition or melt temperature and the loss of crystalline forces triggers a shape-memory transition, returning the material to its primary shape.

SMPs compared to shape memory alloys, exhibit high elastic deformation (more than 200%), high recoverable strain, low cost, low density, easy to process, broad range of tunable properties such as stiffness and transition temperature. Although SMPs have these advantages over SMAs, they have much lower modulus of 3 GPa below the transition temperature compared to that of SMAs which have higher modulus (83 GPa) [32] and also high recovery stress. And this modulus drops rather steeply as the polymer transitions to rubbery phase (soft domains). They are also incapable of reversible transformation as the shape memory alloys [33]. A comparison of their properties is shown in the table below.

Table 2.1 Table gives a comparison of properties of SMPs Vs SMAs [7].

	Shape-memory polymers	Shape-memory alloys
Density(g/cm ³)	0.9 – 1.1	6 – 8
Extent of deformation (%)	Up to 800%	<8%
Young's modulus at T < T _{tran} /GPa	0.01 – 3	83 (NiTi)
Young's modulus at T > T _{tran} /GPa	(0.1 – 10) × 10 ⁻³	28 – 41
Stress required for deformation/MPa	1 – 3	50 – 200
Stress generated during recovery/MPa	1 – 3	150 – 300
Critical temperatures /°C	-10–100	-10–100
Transition breath /°C	10 – 50	5 – 30
Recovery speeds	<1 s–several min.	<1 s
Thermal conductivity /W m ⁻¹ K ⁻¹	0.15–0.30	18 (NiTi)
Biocompatibility and biodegradability	Can be biocompatible and/or biodegradable	Some are biocompatible (i.e. Nitinol), not biodegradable
Processing conditions	<200 °C, low pressure	High temperature (>1000 °C) and high pressure required
Corrosion performance	Excellent	Excellent
Cost	<\$10 per lb	~ \$250 per lb

Also, these two types of smart materials have specific and different applications due to the intrinsic differences in their mechanical and visco-elastic properties. In order to obtain a multifunctional composite material, which includes self-deployable and smart actuator applications, it is necessary to reinforce the polymer matrix with shape memory alloys. These alloys could be embedded in the SMP matrix in the form of particles, short fibers or continuous fibers. In general, SMP composites filled with particles and short fibers are made to fulfill a specific function such as increase the electrical conductivity, improve the magnetic response and increase the stiffness of the matrix. Hence these materials could be classified as multifunctional materials. Whereas particle and short fibers are not suitable reinforcements for using these materials for structural applications and in such a situation, long continuous fibers could be used as reinforcements to improve the material's mechanical properties and strength [34].

Fiber reinforced shape memory composites are activated by thermo-mechanical loading. Their actuation depends on the coupled effect of thermal and mechanical loads. These materials are very sensitive to temperature changes. Most of the shape memory

composite (SMC) require coupling of temperature and stress during phase transition to cause the require output or change in properties of the SMC for a specific application. Two different mechanisms are the driving causes for this desirable change in properties of the SMC during the transition from martensite to austenite. These two mechanisms are discussed below:

Active property tuning: Through this mechanism, the shape memory composite could be made much stiffer by making use of the difference in stiffness of the two phases (SMA and SMP matrix). By active property tuning this difference is exploited to impart much higher stiffness to the composite material. However, there is no significant change observed in the shape recovery properties of the composite. Similarly, the recoverable strain levels also remain the same and are unaffected by this mechanism. To obtain significant changes in the stiffness, the composite needs to be reinforced with large quantities of SMAs as the ratio of modulus of the two participating materials is not large (ESMA/EMatrix is about 3 for NiTiInol).

Active strain energy tuning: By embedding restrained SMA wires in the matrix and making use of constrained recovery large recovery stresses could be produced at the SMA wire and matrix interface. When such composite will vibrate at resonance, the wires can be heated which will develop a recovery stress [35]. This produces a change in energy balance. In this mechanism constrained shape recovery could be used to develop large recovery stresses in the SMA, which will then affect the overall behavior of the smart structure made of SMCs.

Hence by making use of these two mechanisms, and SMC which combines the characteristics of both SMA and SMP could be developed. If the SMP is used as a matrix

in the SMC and SMA is used as a reinforcing material, a multifunctional composite could be fabricated. This is possible, since at high temperatures SMA has high recovery stress could be obtained and the residual strains that remain at low temperatures could be recovered by heating. Since the martensite transformation yield stress and elastic modulus of SMA is lower at higher temperatures, it cannot carry high loads at high temperatures. To help with this drawback, SMP matrix could be used to carry this load since SMP has high modulus at low temperature by cooling. SMP is soft at high temperature and recovers to original shape during unloading. So the SMP matrix could carry this load by keeping the temporary deformed shape. So, an SMC with the following characteristics could be obtained: large recovery stress could be obtained at high temperature, the deformed shape could be recovered and it could be held at low temperature, and a large load could be carried.

The characteristics of the SMC can be further understood by the figure 2.11 below that shows the dependence of elastic modulus and yield stress of the constituting materials with temperature. It can be seen that modulus and reverse transformation stress (σ_A) and stress induced martensite transformation stress (σ_M) are lower below A_s and higher at temperature above A_f . These properties increase with temperature. Due to the shape memory effect of SMA, when it is deformed below A_f there is some residual strain remaining after unloading but it is recovered when the SMA is heated above A_f under no load. Due to the super elastic behavior of SMA, when it is deformed above A_f , the strain is recovered during unloading. To obtain two way shape memory effect, SMA could be used to reinforce steel which has constant properties as shown in the figure 2.11.

The elastic modulus and yield stress are higher for SMP below the glass transition temperature as seen in the figure below and higher above T_g . So the SMP is soft at high temperatures and could be deformed above T_g and cooled below T_g under load and the SMP remains in this temporary deformed shape for as long it is below the transition temperature. This property of SMP is called shape fixity. And during the cooling process the SMP is capable of carrying large loads. And this deformation is recovered when it is heated above T_g . This property of SMP to revert to its original shape is called shape recovery. As such it can be seen that both SMA and SMP behave different at a given temperature. These attributes could be used to develop a smart composite that is stiffer at both low temperature and high temperatures as at high temperature rigidity of SMC combined with SMA becomes higher also generating high recovery stress at the same time. Similarly the rigidity of SMC becomes higher at low temperature as SMP matrix is much stiffer at low temperature. In this way multifunctional shape memory composites could be developed without compromising on the shape recovery properties or the mechanical properties as is the case when using conventional fillers as reinforcing material.

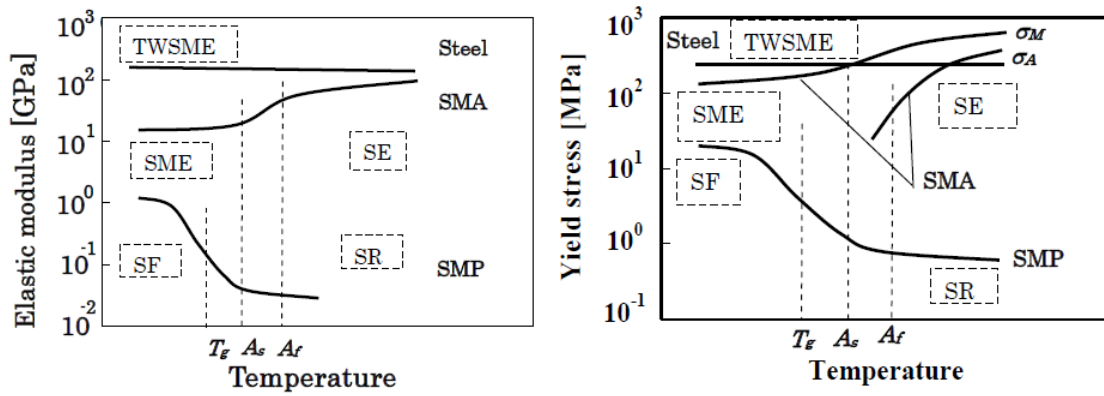


Figure 2.10 Plots show the dependence of modulus and yield stress of SMA and SMP on temperature [15].

Several potential applications can be met using the shape memory alloy fillers as reinforcing agents. One such application is in improving the mechanical performance of a conventional Aluminum matrix by embedding NiTi fibers in the matrix. When thermally activated (heating to above A_f) the SMA fibers create a compressive force and we can see that the mechanical properties improved and the modulus and yield strength increased with the addition of NiTi SMA fibers.

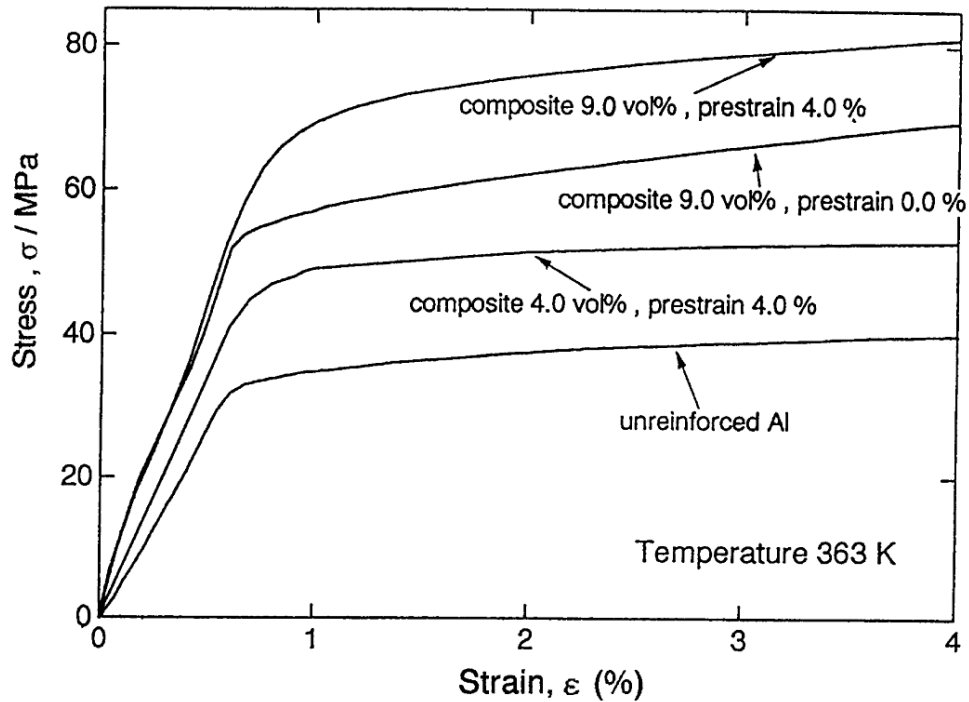


Figure 2.11 Stress–strain curves measured at $T = 363\text{ K}$ of the reinforced Al, and the TiNi Fibre: Al composite with and without pre-strain where two different volume fractions of Fibre are used; 4% and 9% vol [36].

Further mechanical properties of epoxy resin composites filled with SMA particles and short fibers were studied by Zhang et al [37]. They could see that addition of 3.5% of SMA fillers resulted in increment of storage modulus by 6 times as that of epoxy resin. In addition to the modulus flexural rigidity of the shape memory composite also increased [37].

The damping properties also improved with the addition of NiTi fillers. This could have applications to engine components where the materials becomes stronger at higher temperature because of the shape memory effect of NiTi SMA fibers and also lowers the noise due to its higher damping performance. Additionally, Lee and Lee had

carried out numerical analysis of buckling and post buckling behavior of laminated composites shells reinforced with SMA wires. In their analysis it was seen that activation of SMA wires had increased the value of critical buckling load [38]. In several studies carried out on SMA composites factors like the volume fraction of the SMA fillers, pre-strains of SMA wires, ply orientations in laminate composites had direct influence on the post buckling deflection and the natural frequencies of the laminate [39-41]. Hence it is possible to shift the natural frequency of a structure away from its exciting frequency and as such control the amplitude of its motion during vibration. Seismic performance of reinforced concrete (RF) joints is yet another field of potential application of SMA fillers composites. Youssef et al proposed to use SMA NiTi to reinforce RF instead of steel reinforcements. It was observed that SMA NiTi performed better due to its ability to recover post elastic strain [42]. Another application of SMA embedded composites is in creating self-healing structures where super-elastic embedded deformed wires create compressive stresses do not propagate crack growth and even promoting crack closure [43].

2) CNT-SMP composites: In addition to being light weight multi-walled carbon nanotubes have shown the ability to enhance the structural damping by 200% and an increase in bending stiffness by about 30% as shown by Koratkar et al. [44-48]. CNTs exhibit excellent mechanical, electrical, and magnetic properties as well as nano-meter scale diameter and high aspect ratio, which make them an ideal reinforcing agent for high strength polymer composites [49]. In their study shape memory polyurethane was reinforced with electrically conductive carbon nanotubes to obtain a conductive shape memory polymer composite. The idea was to electrically trigger the shape memory

behavior of the polymer. Since the polymer by itself is not conductive, carbon nanotubes fillers were added. They had further investigated the mechanical properties of PU SMP composites. Electric field triggered shape memory effect is shown in the figure below. A rectangular PU SMP composite with CNT fillers was bent into a round shape and electric field of 25V was applied to see the recovery. The composite recovered 96% of the original shape in 20 seconds.

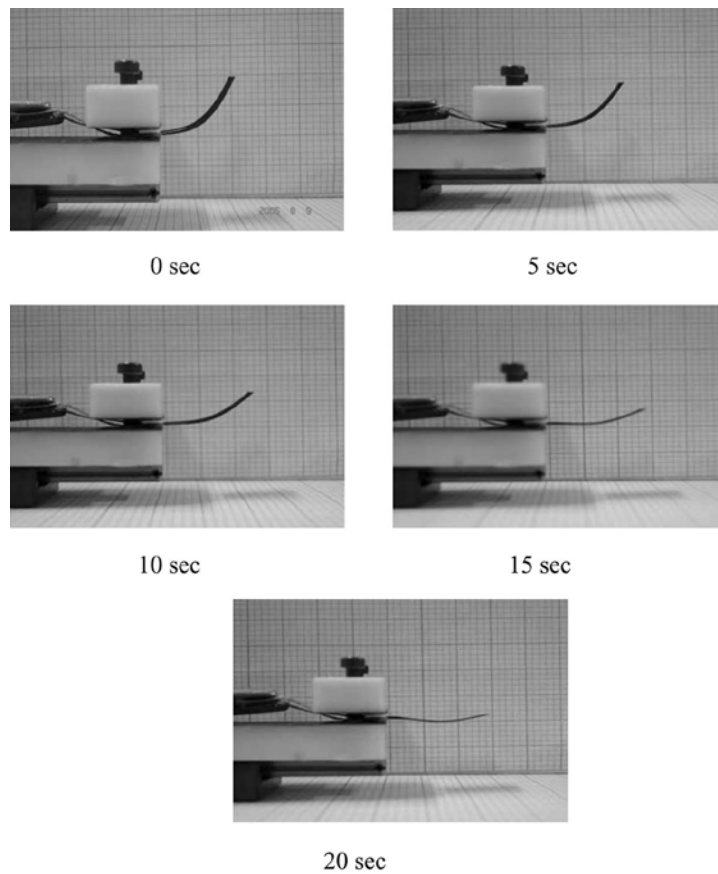


Figure 2.12 Electro active shape recovery behavior of conductive PU-CNT shape memory composite [49].

It was also observed that by addition of CNT fillers to the polymer matrix, a better thermal stability could be obtained as the glass transition temperature of polymer

increases considerably [50]. Due to these superior characteristics, CNTs have been commonly considered as potential filling material in polymeric nano-composites.

Further from the study carried out by Qing-Qing Ni et al on the shape memory effect and mechanical properties of CNT SMP nano-composites, it was observed that addition of small amount of CNT fillers to the SMP matrix had showed significant improvement in mechanical properties such as modulus [51]. The figure below shows the stress-strain curves of static tensile tests on four materials: SMP, 1.7wt. % CNT-SMP, 3.3 wt. % CNT-SMP and 5 wt. % CNT-SMP at different temperatures. It is clear that all temperatures addition of CNT fillers has improved the mechanical properties of SMP matrix.

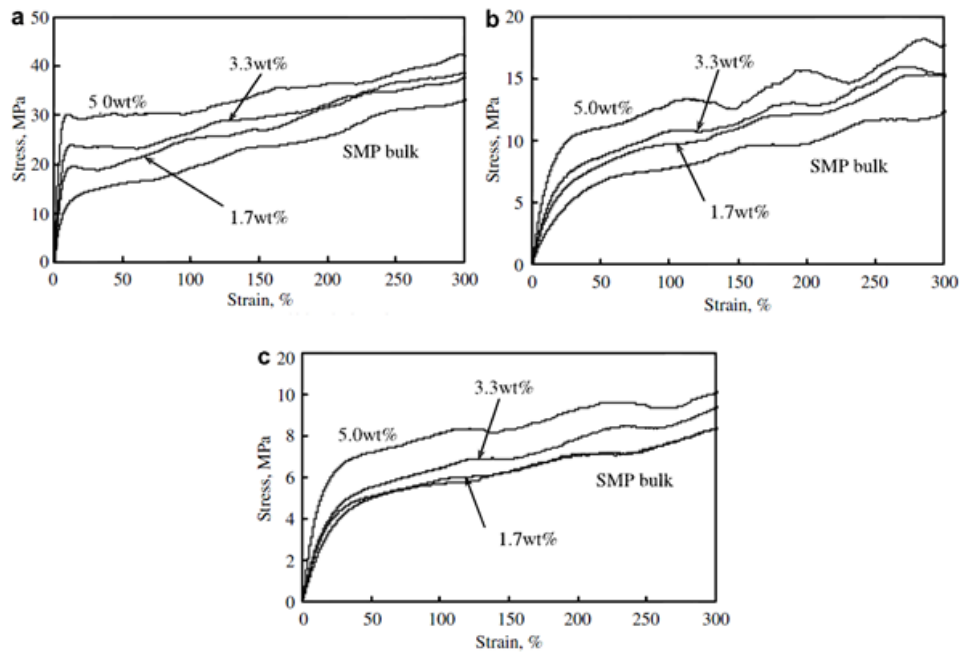


Figure 2.13 The stress–strain curves in static tensile tests for four materials—SMP bulk, 1.7 wt. %, 3.3 wt. % and 5.0 wt. % at testing temperatures: (a) 25 °C, (b) 45 °C, and (c) 65 °C, respectively [51].

Similar improvement in mechanical performance was observed in Cu-CNT nanocomposites studied by Bakshi et al. In addition to higher modulus, they observed a two stage yielding process in the composite, each one corresponding to the matrix yielding and CNT cluster yielding. And improvement in elastic modulus of the composite was due to the large tensile modulus of CNT fillers [52].

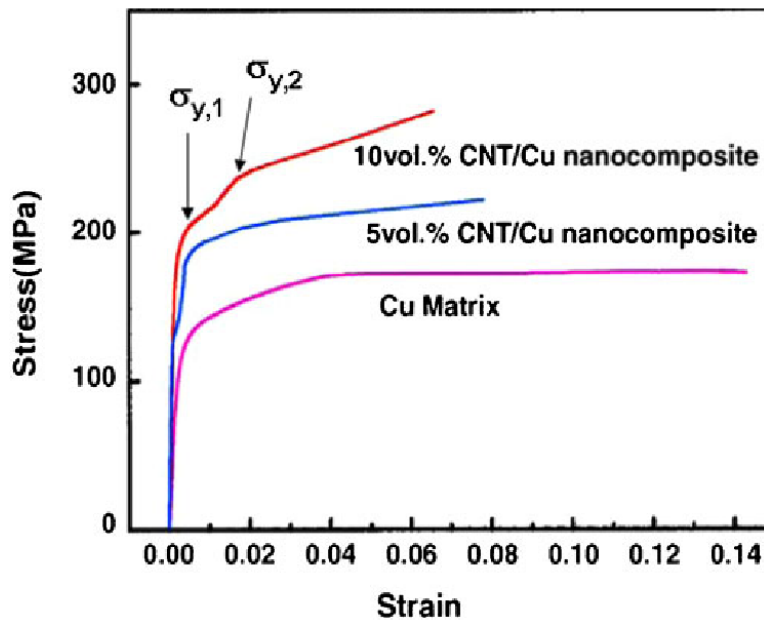


Figure 2.14 shows the stress–strain curves showing two stage yielding process in Cu-CNT nano-composite [52].

Earlier studies focused on adding carbon black as filler material to the polymer matrix to improve the electrical properties. However, higher concentrations of carbon black such as 15% to 20% is needed to obtain the desired electrical conductivity [53]. Hence by using small concentrations of carbon nanotube fillers of as minimum as 0.1% by weight, the electrical conductivity of the composite could be increased significantly without compromising the mechanical properties of the epoxy matrix. For this reason

several studies have been focusing on improving the electrical properties using carbon nanotube fillers. Although for this reason they are a more suitable choice in comparison to carbon black fillers, they do possess issues with uniform dispersion in the polymer matrix. This is because to avoid electrostatic charging of an insulating polymer matrix an electrical conductivity above $\sigma=10^{-6} \text{ Sm}^{-1}$ is needed as reported by [54]. At present, the most common practice to achieve this conductivity is to use conductive filler such as carbon black [55]. However by dispersing untreated catalytically grown carbon nanotubes in epoxy matrix and with intense stirring the required conductivity could be obtained with low filler volume fractions such as 0.1%.

In order to further reduce the electrical resistivity Ni powder particles could be added to the CNT-polymer composite. When Ni chains were formed in the CNT-polymer matrix in the presence of magnetic field, the electron transfer is easier as the Ni chain could act as bridges to fill the gaps between the dispersed CNT fillers in the matrix. This further helps reduce the electrical resistivity significantly. Moreover, this could prove to be cost effective as Ni powders and other metal fillers are less expensive compared to CNTs alone [56].

As discussed earlier similar to other shape memory materials, shape memory polymers can be activated by more than just by heat, such as light, electricity and magnetic field. Although so many efforts, focusing on stimuli-responsive SMPs and their composites, have been paid to date, still no convergent results were obtained. The demand to get rid of external heaters has led to conductive SMPs filled with fillers such as carbon nanotubes, carbon particles, conductive fiber and nickel, zinc, ferrite and ferromagnetic particles, etc. [57].

Hence in order to obtain the multifunctional ability of a shape memory material by avoiding the use of external stimuli for activation, incorporating CNT and Ni fillers in the shape memory polymer matrix is suggested. The shape memory actuator ability is maintained in tact in addition to attaining better mechanical, electrical and magnetic properties by addition of filler contents such as CNT fibers, Ni powders and iron oxide powder to the shape memory polymer matrix. For this reason in our current study we propose to fabricate multifunctional shape memory polymer based composite with addition of MWCNT fibers and Ni powders.

Chapter Three

3 SYNTHESIS AND CHARACTERIZATION OF SHAPE MEMORY

POLYMERS

3.1 INTRODUCTION

Shape memory polymers (SMPs) are a group of active materials that have been considered for the developments of reconfigurable structures and actuation devices [12, 13, 18, 58, 59]. Like conventional polymers, the shape memory polymers can also be grossly divided into two categories: thermosetting SMPs and thermoplastic SMPs. Thermosetting SMPs are formed through chemical cross-linking and therefore have excellent modulus above the glass transition temperature due to the permanent cross-linking between the polymer segments. This type of SMPs generally exhibits a sharp glass transition temperature (T_g). Depending on the applications, the transition temperature can be tuned by modifying the constituent monomers that form the polymer chain. The shape memory behaviors in these thermosetting SMPs are triggered by their glass-transition temperatures. There exist several thermosetting SMPs, including epoxy, polyurethane, polyester, and polystyrene.

The mechanical and shape recovery behaviors of the SMPs have been investigated before by utilizing various types of experiments [10, 14, 60, 61]. The first shape recovery ability test was conducted by Tobushi and co-workers in 1992 [15]. Tensile tests were performed on a polyurethane based SMP with a level of pre-strain up to 50%. The same research group also examined the shape fixity and recovery of a thin film SMP at different temperatures [16]. Atli et al. and Volk and Lagudas et al. have also used tensile tests to conduct thermo-mechanical characterizations of the SMPs [2, 62].

Liu et al. have performed uniaxial compression tests on shape memory polymers [63]. Fulcher et al have reported the use of nano indentation to evaluate the shape recovery of SMPs at small scales [64]. Baer et al. have examined the thermo-mechanics and shape-memory behavior for thermoset polyurethanes intended for medical applications as a function of curing temperature and deformation strain [65]. Diani et al. have recently developed a torsional testing apparatus to evaluate the shape recovery of the SMPs under torsional loads [66].

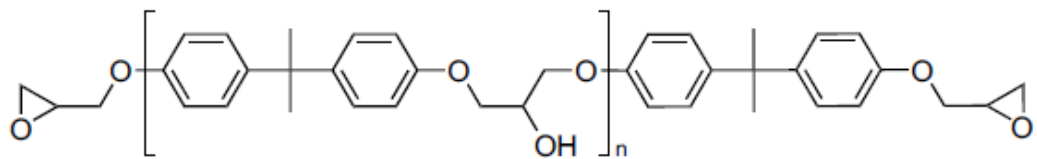
In this chapter, an epoxy based shape memory polymer will be synthesized and its thermal, mechanical, and shape memory behavior will be comprehensively examined.

3.2 EXPERIMENTAL

3.2.1 Materials and Sample Preparation

The epoxy based shape memory polymer was used in the present study. The polymer were composed of following substances: (1) diglycidyl ether of bisphenol, an epoxy monomer (EPON 826, available from Hexion), (2) curing agent poly (propylene glycol) bis (2-aminopropyl) ether (Jeffamine D230, available from Huntsman), and (3) neopentyl glycol diglycidyl ether (NGDE), manufactured by TCI America. The molecular structure of the chemicals is shown in the below Figure 3. 1. To synthesize the SMP, the EPON 826 was first placed in the furnace and heated to 80°C for 10 minutes to reduce its viscosity. The treated EPON 826 was then removed from the furnace and mixed with the other two ingredients. The solution was stirred for 15-30 seconds to ensure the proper mixing and then placed in vacuum at 20-in Hg for about 2 minutes to remove the bubbles that were developed during the mixing. The liquid SMP was subsequently poured into a cylindrical Teflon mold and placed in a furnace for curing at

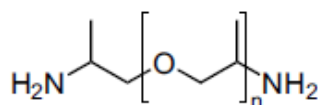
100°C for 1.5 hours. After cooled down, the samples were removed from the mold and polished to ensure the smooth surfaces.



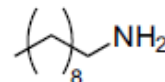
EPON 826, $n = 0.085$



Neopentyl glycol diglycidyl ether (NGDE)



Jeffamine D-230 ($n \sim 2.5$)



Decylamine

Figure 3.1 Shows the molecular structures of the chemicals used to make the shape memory polymer used in current project [102].

3.2.2 Transition Temperature

The transition temperature of the SMP was characterized with a Perkin Elmer Pyris1 Differential Scanning Calorimetry (DSC). DSC operates by recording the amount of heat required to increase the temperature of a material versus a change in temperature. Small sized samples, weighed ~ 5 mg, were used for the experiment. Sample was heated from 25°C to 70°C with a heating rate of 2°C/min.

3.2.3 Thermo-Mechanical Testing

The thermomechanical behavior of the SMP was established using a dynamic mechanical analyzer (DMA), a Perkin Elmer Pyris1 Dynamic Mechanical Analyzer. DMA yields information about the temperature-dependent mechanical properties and phase changes of a specimen by subjecting it to a small, sinusoidal, oscillating force. Cylindrical specimen of size 12 mm height by 6.25 mm diameter were tested in compression mode in the DMA. The specimens were heated from -20°C to 100°C at 2°C/min. The applied strain was 0.1% and oscillating frequency was 1 Hz.

3.2.4 Coefficient of Thermal Expansion

The coefficient of thermal expansion (CTE) of the SMP was measured by using the same Perkin Elmer Pyris1 Dynamic Mechanical Analyzer. Cylindrical specimen of size 12mm height by 6.25mm diameter were tested placed between two plates inside the DMA tester. A small compression force was applied and maintained to ensure the contact between the specimen and the plates during the entire test. To measure the CTE, the specimen was heated from -20°C to 100°C and then cooled down from 100°C to -20°C. The height change of the specimen during the tests were recorded and used to compute the strain change.

3.2.5 Stress-Strain Tests

The stress-strain behaviors of the SMP were obtained through uniaxial compressive tests conducted on the BOSE ElectroForce load frame system. The specimens were small cylinders with the nominal height of 11 mm and nominal diameter of 6.25 mm. The tests were performed under the force-control mode by applying a

compressive force of up to 2000 N at a rate of 2 N/sec. Tests were conducted at selected temperatures from 30°C to 60°C.

3.2.6 Shape Recovery Tests

The shape recovery tests were conducted by using cylindrical shaped specimens, the same size specimens as used in compressive tests. The fixations of the SMPs were carried out in a servo-hydraulic MTS LandMark testing system equipped with a custom built cooling-heating system. Omega CN8200 temperature controller was used to control the temperature of the sample. The temperature was measured by a K-type thermocouple attached to the sample and compression grips. The shape recoveries of the SMPs were carried out in a DMA (Dynamic Mechanical Analyzer) by following standard shape recovery cycle. First, the specimens were heated up to a temperature above its glass transition (T_g). After equilibrium, the specimens were fixed, cooled, and then heated up again for recovery (unconstraint recovery). The rate of heating or cooling used in the experiment was kept constant, i.e., 2°C/min.

3.3 RESULTS AND DISCUSSION

3.3.1 Transition Temperature

Figure 3.2 depicts the heat flow versus temperature response of the present SMP measured by the DSC. The glass transition temperature of the SMP is determined as the temperature corresponding to the maximum heat flow: $T_g \approx 43^\circ\text{C}$. The transition region started at about 39°C and ended at about 46°C. The SMP can be classified as the glassy state below 39°C and the rubbery state above 46°C.

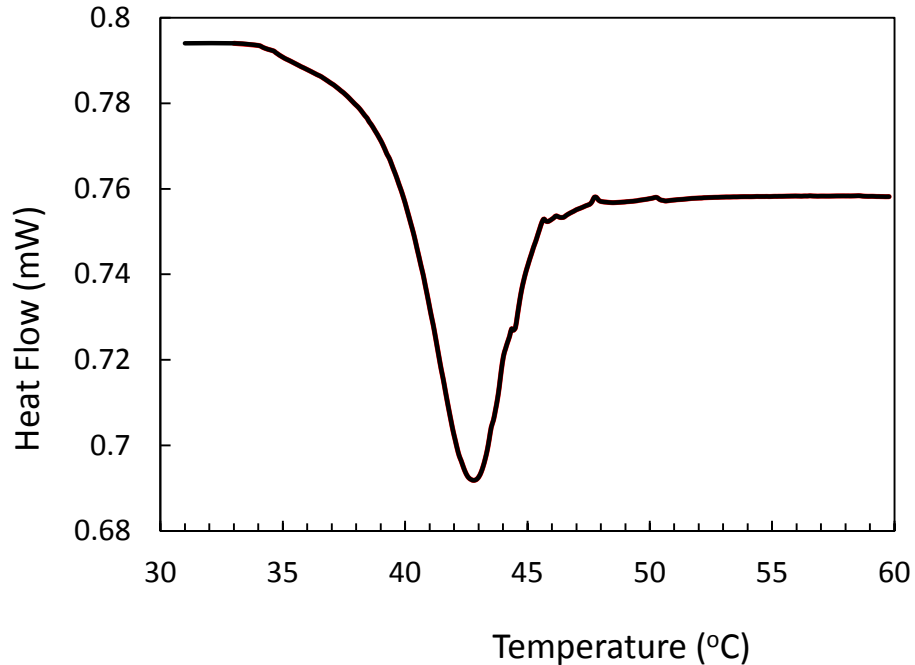


Figure 3.2 DSC results showing the glass transition temperature of the SMP.

3.3.2 Thermo-Mechanical Behavior

The thermo-mechanical behavior of the SMP was characterized with a dynamic mechanical analyzer (DMA). Figure 3.3 depicts the storage modulus (E') and phase angle $\text{Tan}(\delta)$ curves of the SMP as a function of temperature. The modulus-temperature plot (Figure 3.3a) shows clearly that the two states of the SMP material: the glassy state and the rubbery state. At the glassy state ($T < 35^\circ\text{C}$), the material behaves as a rigid glass. At the rubbery state ($T > 60^\circ\text{C}$), the material behaves like a soft rubber. From the phase angle plot (Figure 3.3b); the glass transition temperature (T_g) of the SMP can be determined, as the peak of the $\text{Tan}(\delta)$ curve. It is seen that the transition temperature of the original SMP occurs at $\sim 45^\circ\text{C}$, which is consistent with the result obtained from the DSC (Figure 3.2).

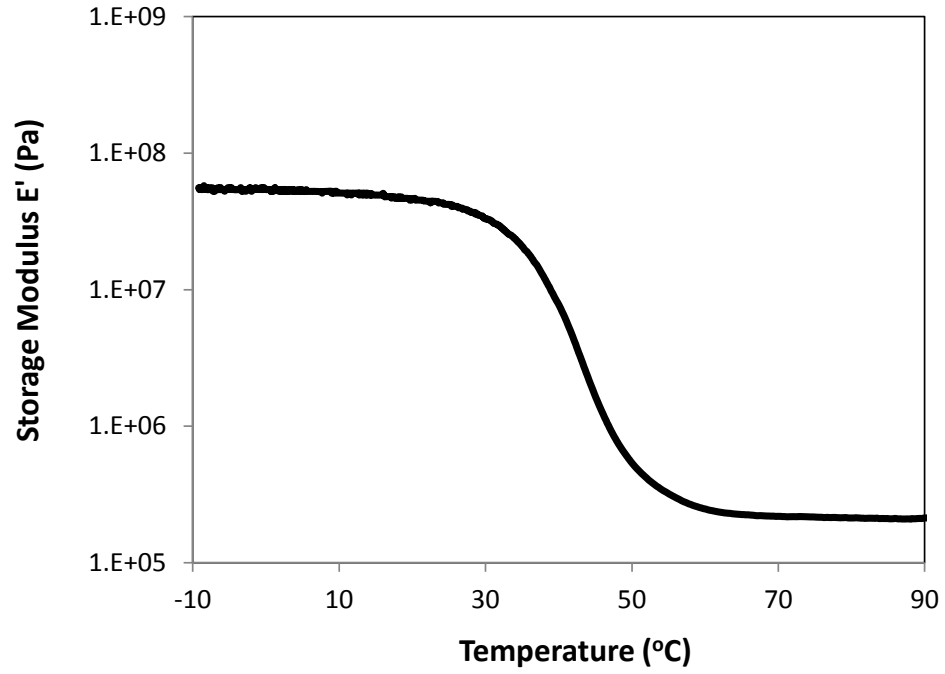


Figure 3.3 DMA results showing the storage modulus as a function of temperature.

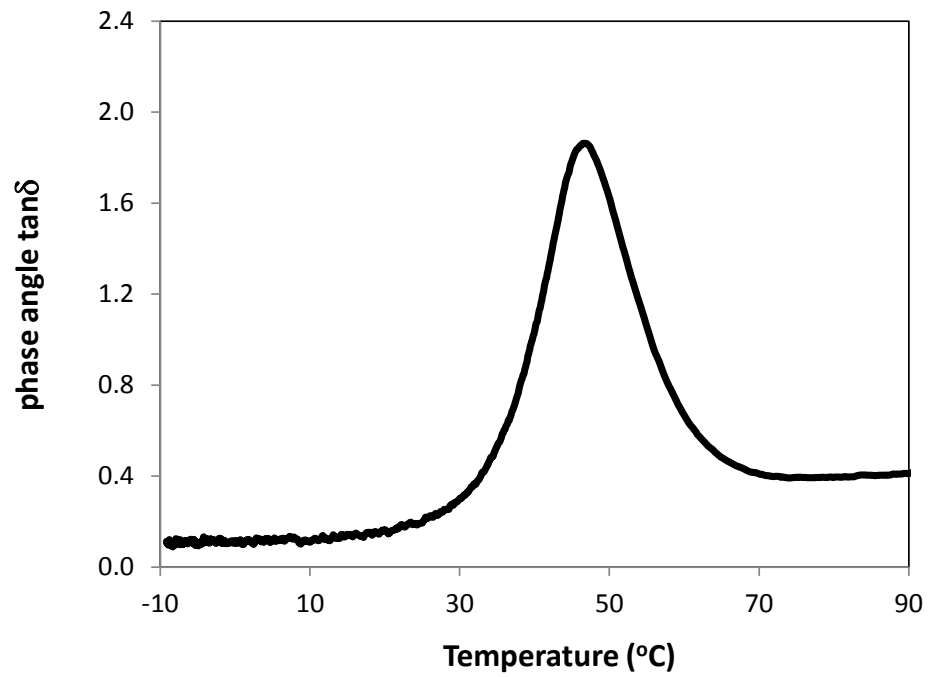


Figure 3.4 DMA results showing the phase angle as a function of temperature.

3.3.3 Coefficient of Thermal Expansion

The coefficient of thermal expansion (CTE) of the SMP was measured by using the Perkin Elmer Pyris1 Dynamic Mechanical Analyzer. Figure 3.5 shows the thermal expansion strain versus the temperature during the heating from -20°C to 100°C . The portions below and above the T_g are used to obtain the slopes, which are the CTEs of the SMP at glassy and rubbery states. From Figure 3.5, the CTEs were measured as $\alpha_1=1.15 \times 10^{-4}$ for temperature below the T_g and $\alpha_2=2.10 \times 10^{-4}$ for temperature above the T_g .

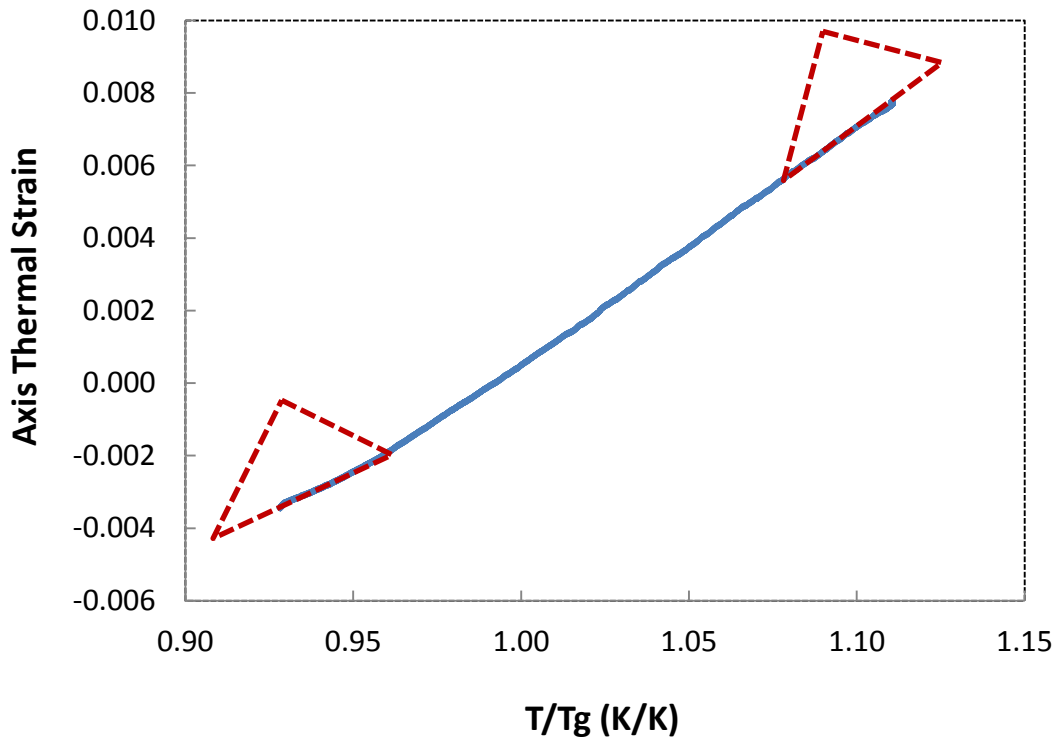


Figure 3.5 Thermal expansion strain as a function of temperature for the SMP.

3.3.4 Mechanical Behavior

The mechanical responses of the present SMP were examined in compression mode at temperatures spanning all three regions of the polymer: glassy region (30°C , 35°C), glassy-to-rubbery transition region (45°C), and rubbery region (50°C , and 55°C).

Figure 3.6 shows the isothermal compressive stress-strain curves of the SMP at various temperatures.

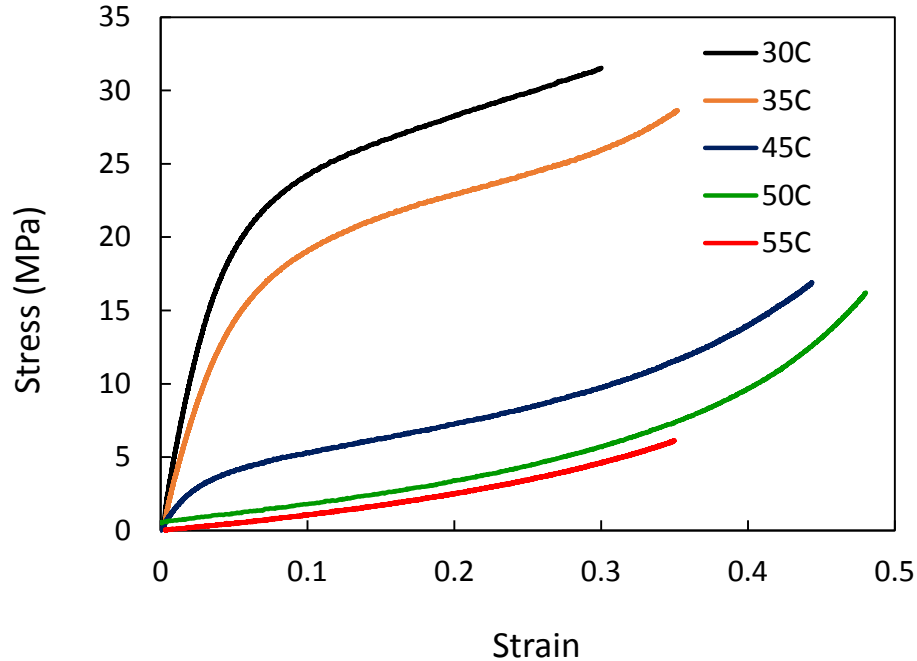


Figure 3.6 Stress-strain responses of the SMP at various temperatures.

The material is seen to display typical hyperplastic behavior in the rubbery regions above T_g . At temperatures below T_g , the material shows inelastic behavior. With the increase of strain, the material starts to stress softening. As the temperature changes from glassy state to rubbery state, the amounts of stress required achieving the same level of strain has been dramatically decreased. For example, the stress required to configure the SMP at 30% strain at glassy state is 32 MPa while the stress to configure the SMP at the same strain at rubbery state is only 4.5 MPa, corresponding to a drop of 86%.

3.3.5 Shape Recoveries

Shape recovery is important to the SMPs because it is the indication of the materials' ability to return to their original shapes after fixing. The unconstrained shape

recovery tests were conducted by fixing the specimens at various prescribed strains of 6%, 15%, 25%, and 30% at room temperature. The fixed specimens were then placed in the DMA and heated to an elevated temperature, 80°C, with the rate of 5°C/min. The changes in compressive strain for each specimen are shown in Figure 3.7(a) and the shape recovery ratio (R) is shown in Figure 3.7(b).

The linear shape recovery ratio, R, is a ratio of the recovered compression at a specified recovery temperature to the original specimen height. Evaluation of the linear shape recovery ratio provides a better quantitative assessment.

$$R_{ur} = (1 - h_f / h_i) * 100 \quad (3.1)$$

where h_f is the final compression corresponding to each recovery temperature and h_i is the initial specimen height.

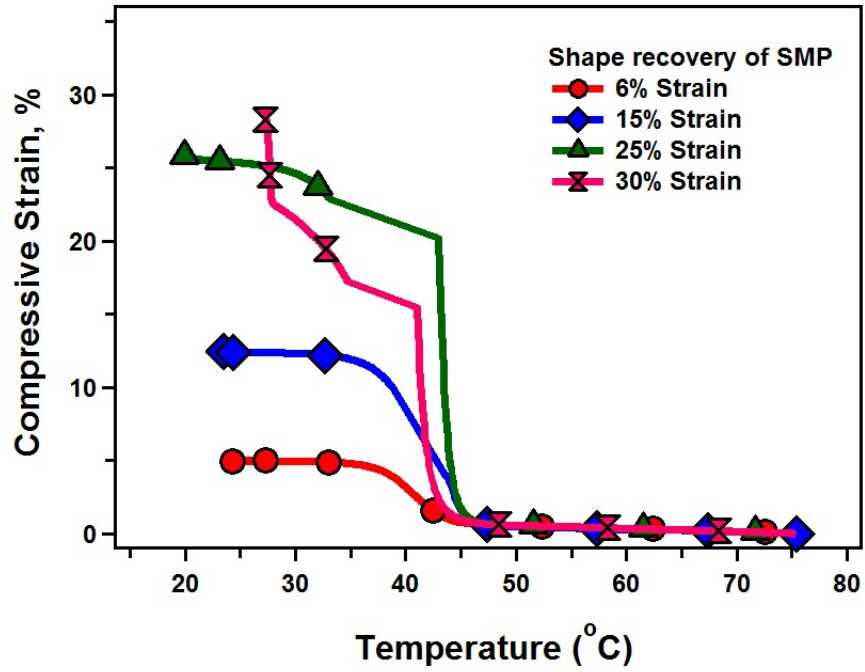


Figure 3.7a Strain-temperature profiles of unconstraint shape recoveries of the SMPs.

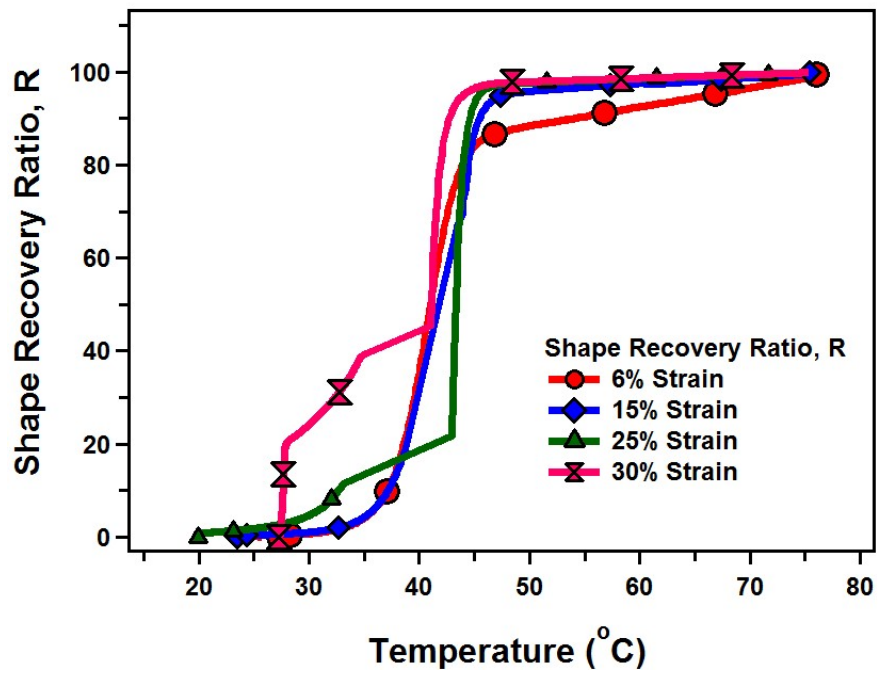


Figure 3.7b Shape recovery ratios of unconstraint shape recoveries of the SMPs.

It is observed that all specimens have fully recovered their original shapes. The shape recovery ratio result also reveal that the transition temperature for this SMP can be determined as $T_g \approx 43^\circ\text{C}$, which is consistent with that obtained from the DSC (Figure 3.2).

To comprehensively characterize the shape memory effect, the present SMPs were also fixed to a 30% strain at selected temperatures: 30°C , 35°C , 40°C , 45°C and 50°C . The amount of force required to achieve this same level of 30% has been dramatically decreased. The fixed specimens were then placed in the DMA and heated to 80°C to observe their recoveries. The compressive strain profiles and shape recovery ratios are shown in Figure.3.8 (a) and Figure 3.8 (b), respectively. In all cases the prescribed strains have been fully recovered.

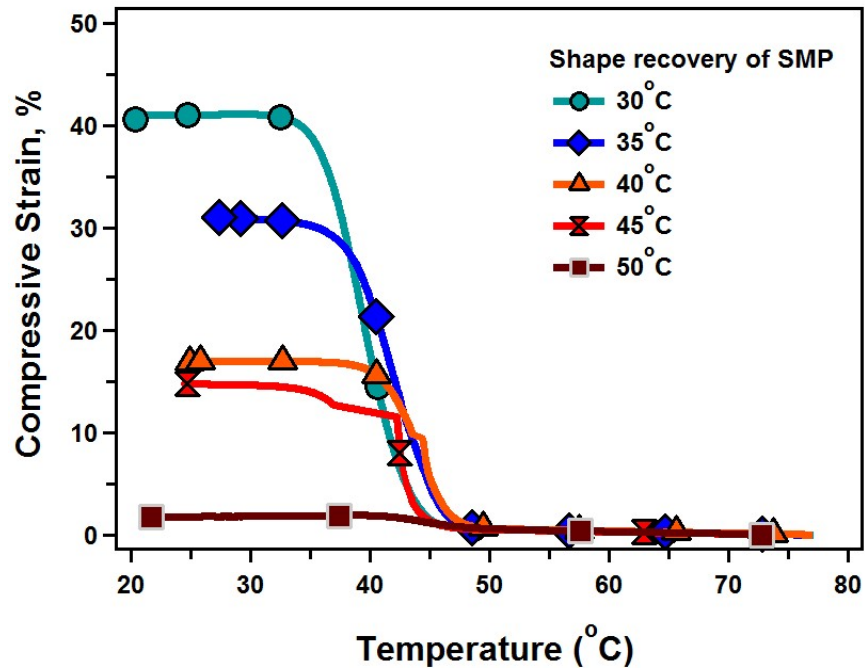


Figure 3.8a Strain - temperature profiles of unconstrained shape recoveries of the SMPs.

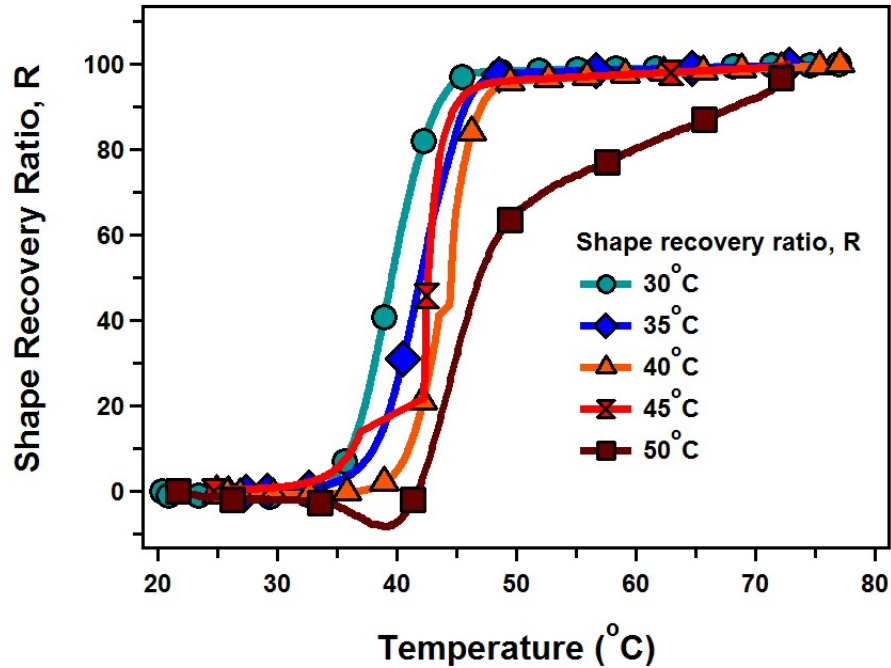


Figure 3.8b Shape recovery ratios of unconstrained shape recoveries of the SMPs.

3.4 CONCLUSIONS

An epoxy-based shape memory polymer (SMP) has been fabricated as a candidate material for reconfigurable structures and devices. The material behaves as a two-phase material, exhibiting distinct mechanical behaviors at glassy and rubber states. The glass transition temperature of the present SMP was determined as: $T_g \approx 45^\circ\text{C}$, from both DSC and DMA. The coefficient of thermal expansion at the rubbery state is 2.1×10^{-4} , about twice of the CTE at glassy state. The shape recovery behavior of the SMP has been systematically examined and analyzed. Under unconstrained condition, the SMP has demonstrated remarkable shape recovery abilities at various fixing strains and fixing temperatures.

Chapter Four

4 STRAIN ENERGY FUNCTION BASED MODELING OF SHAPE MEMORY POLYMERS

4.1 INTRODUCTION

The design of SMP-based structures and devices requires thorough characterization and constitutive modelling of the thermo-mechanical behavior of the materials. Many phenomenological and micromechanics based constitutive models are available for the SMPs, although most of them have focused on small deformations (<10% nominal strain for compression or tension). Tobushi has developed a spring-dashpot system to model the behavior of the SMP for small deformations [67]. The model has been later improved by incorporating the thermal expansion and some nonlinear elastic terms [63]. Srinivasa and Gosh have subsequently developed a rheological-based model by also using the spring-dashpot analogy [103]. A phenomenological based model has been developed by Liu et al., in which the SMP is treated as a material consisting of two-phase: the frozen phase and the active phase. The material becomes “frozen” at low temperatures and then “active” upon heating, which allow the stored deformation returning to the original shape [63]. Following the framework of Liu et al., Chen and Lagudas have developed the three-dimensional constitutive model for the SMP [104, 105]

The existing models often have a large number of material parameters, for instance, more than 17 in Qi et al. [106], 18 in Hong et al. [107], and up to 45 in Srivastava et al [103]. To accurately acquire such a large number of material parameter would require specific experiments and complex calibration processes. Therefore,

although some models are very comprehensive and capable of capturing the complex behaviors of the SMPs, they are difficult to use in practices and none of these models have been implemented in commercial analysis codes.

In this chapter, the strain energy functions, commonly used for modelling the large deformation of elastomeric materials, are used to model the stress-strain and shape recovery responses of the SMP.

4.2 STRAIN ENERGY FUNCTION BASED MODELING

For isotropic, incompressible materials that are subjected to uniaxial tension or compression, Rivlin has shown that

$$\frac{\sigma}{(\lambda - \lambda^{-2})} = 2 \left[\frac{\partial W}{\partial I_1} + \frac{1}{\lambda} \frac{\partial W}{\partial I_2} \right] \quad (4.1)$$

where σ is the engineering stress and λ the stretch ratio. W represents the strain energy function, $W = f(I_1, I_2, I_3)$ where I_1, I_2, I_3 are the three invariants given in terms of the principal stretch ratios $\lambda_1, \lambda_2, \lambda_3$.

4.2.1 Mooney-Rivlin Strain Energy Function

There exist various strain energy functions for modelling materials that undergo finite deformation. By assuming incompressibility ($I_3=1$), Rivlin has proposed that the strain energy function be expressed in the power series

$$W = \sum_{i+j=1}^{\infty} C_{ij}(I_1 - 3)^i(I_2 - 3)^j \quad (4.2)$$

Taking only the first two terms ($i=j=1$) in Equation (2) results in the Mooney-Rivlin strain energy function:

$$W = \sum_{i+j=1}^{\infty} C_{ij}(I_1 - 3)^i(I_2 - 3)^j = C_{10}(I_1 - 3) + C_{01}(I_2 - 3) \quad (4.3)$$

Substituting Equation (4.3) into Equation (4.1) yields

$$\frac{\sigma}{(\lambda - \lambda^{-2})} = 2C_{10} + \frac{1}{\lambda} 2C_{01} \quad (4.4)$$

By plotting $\sigma/(\lambda - \lambda^{-2})$ vs $1/\lambda$, the constants C_{10} and C_{01} can be estimated.

4.2.2 Yeoh Strain Energy Function

Based on the experimental observations, Yeoh has noticed that $\partial W/\partial I_1$ is much greater than $\partial W/\partial I_2$. Therefore, Yeoh has proposed to neglect the second term in generalized strain energy function as shown in Equation (4.2), which has resulted in the Yeoh's model.

$$W = \sum_{i=1}^{\infty} C_i(I_1 - 3)^i = C_{10}(I_1 - 3) + C_{20}(I_1 - 3)^2 + C_{30}(I_1 - 3)^3 \quad (4.5)$$

Substituting Equation (4.5) into Equation (4.1) yields

$$\frac{\sigma}{(\lambda - \lambda^{-2})} = 2C_{10} + 4C_{20}(I_1 - 3) + 6C_{30}(I_1 - 3)^2 \quad (4.6)$$

By plotting $\sigma/(\lambda - \lambda^{-2})$ vs $(I_1 - 3)$, the constants C_{10} , C_{20} and C_{30} can be estimated.

4.2.3 Ogden Strain Energy Function

In contrast with the invariant-based strain energy function, Ogden has proposed to derive W in terms of stretch ratios, which results in a stretch-based strain energy function

$$W = \sum_{i=1}^n \frac{\mu_n}{\alpha_n} (\lambda_1^{\alpha_n} + \lambda_2^{\alpha_n} + \lambda_3^{\alpha_n} - 3) \quad (4.7)$$

In simple tension or compression, we have $\lambda_1 = \lambda$, $\lambda_2 = \lambda_3 = \lambda^{-1/2}$. Taking the first two terms,

Equation (7) reduces to

$$W = \frac{\mu_1}{\alpha_1} (\lambda^{\alpha_1} + 2\lambda^{-\frac{\alpha_1}{2}} - 3) + \frac{\mu_2}{\alpha_2} (\lambda^{\alpha_2} + 2\lambda^{-\frac{\alpha_2}{2}} - 3) \quad (4.8)$$

Substituting Equation (4.8) into Equation (4.1) yields

$$\sigma = \mu_1 \left(\lambda^{\alpha_1 - 1} - \lambda^{-\frac{\alpha_1 - 1}{2}} \right) + \mu_2 \left(\lambda^{\alpha_2 - 1} - \lambda^{-\frac{\alpha_2 - 1}{2}} \right) \quad (4.9)$$

By curve fitting, the constants $\mu_1, \alpha_1, \mu_2, \alpha_2$, can be estimated.

4.2.4 Neo-Hooke Strain Energy Function

Based on the physics of polymer chain networks, a few micromechanical based strain energy function have been developed. The simplest one among those types of functions is the neo-Hookean model

$$W = C_{10}(I_1 - 3) \quad (4.10)$$

where $C_{10} = \frac{1}{2}nkT$, in which n is the chain density per unit of volume, k is the Boltzmann constant and T is the absolute temperature. The only material parameter C_{10} denotes the initial shear modulus: $\mu = 2C_{10}$.

Substituting Equation (4.10) into Equation (4.1) yields

$$\frac{\sigma}{(\lambda - \lambda^{-2})} = 2C_{10} \quad (4.11)$$

By plotting σ vs $(\lambda - \lambda^{-2})$, the constant C_{10} can be estimated.

4.2.5 Arruda-Boyce Strain Energy Function

Arruda and Boyce have recently developed a new micromechanics-based strain energy function

$$W = \mu \sum_{i=1}^5 \frac{C_i}{N^{i-1}} (I_1^i - 3^i), \quad [C_1, C_2, C_3, C_4, C_5] = \left[\frac{1}{2}, \frac{1}{20}, \frac{11}{1050}, \frac{19}{7000}, \frac{519}{673750} \right] \quad (4.12)$$

where μ the initial shear modulus and N the number of Kuhn segments per polymer chain.

By solving Equation (4.12), the stress-stretch relation in simple tension or compression can be obtained

$$\frac{\sigma}{(\lambda - \lambda^{-2})} = \sum_{i=1}^5 \frac{2\mu C_i}{N^{i-1}} (I_1^{i-1}) \quad (4.13)$$

By curve fitting, the constants μ and N can be estimated. In the present study, the coefficients of various strain energy functions were determined by using the curve-fitting utility in commercial finite element program, ABAQUS. A unit-cell element was built in a Cartesian coordinate system with axes x_1 , x_2 , and x_3 as shown in the below Figure 4.1. To conduct compressive testing, a displacement was assigned to a node at the top of the specimen to allow it deforming in the longitudinal axis (x_2 direction). The specimen was free to extend or contract in x_1 and x_3 directions. Experimental stress-strain data were entered into program to compute the coefficients of strain energy functions.

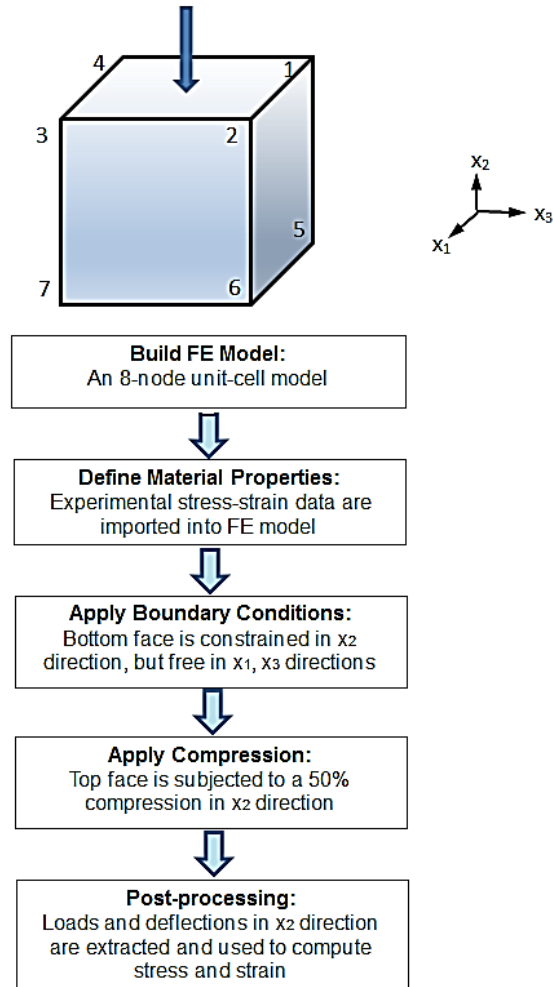


Figure 4.1 Shows the unit-cell FE model and flowchart used for computing the stress and strain.

4.3 RESULTS AND DISCUSSION

4.3.1 Prediction of Mechanical Behavior of SMPs

The stress-strain responses of the SMP have been modelled with commonly used strain energy functions (Mooney-Rivlin, Yeoh, Neo-Hooke, Arruda-Boyce, and Ogden).

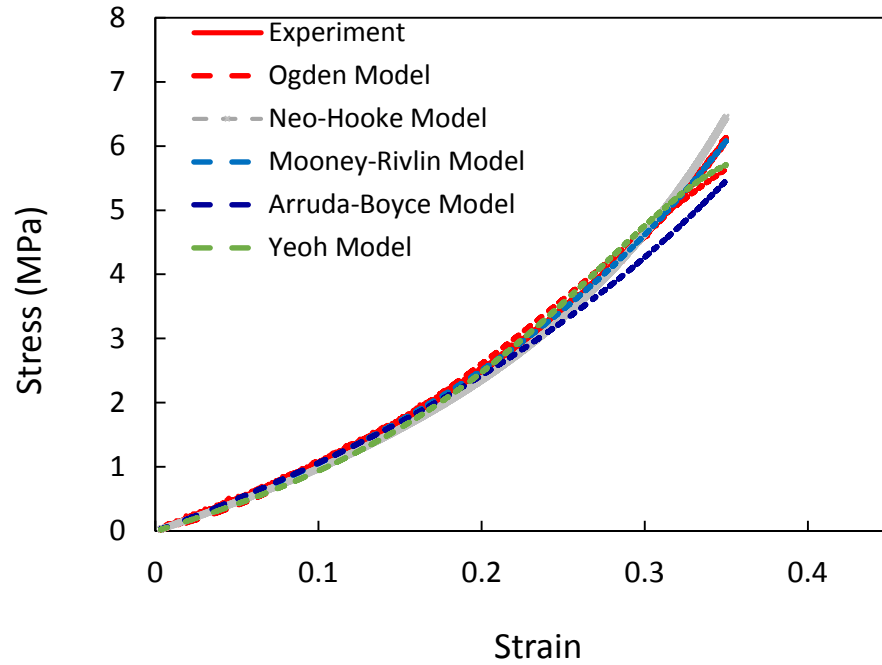


Figure 4.2 Stress-strain responses of the SMP at 55°C.

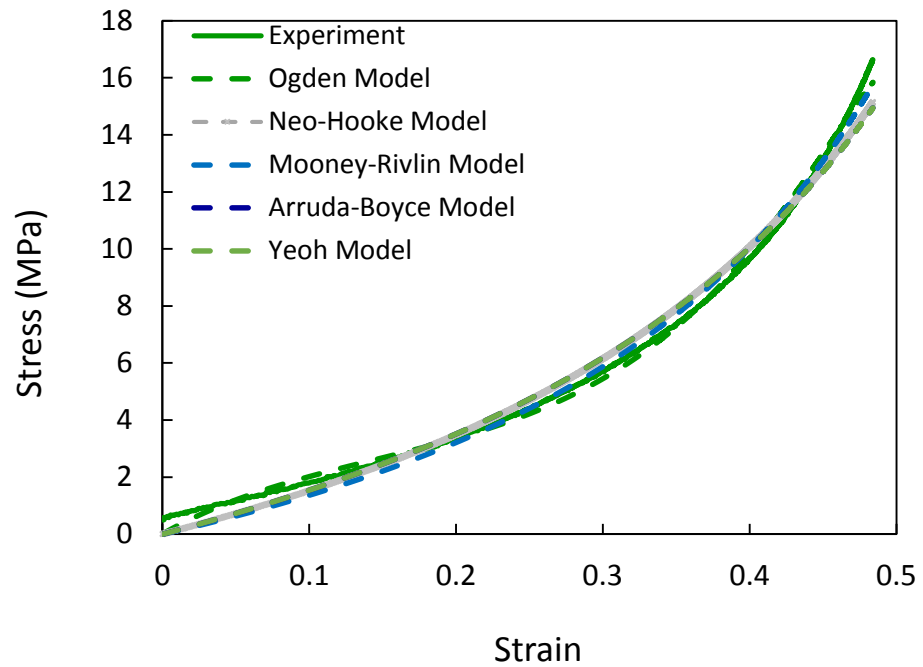


Figure 4.3 Stress-strain responses of the SMP at 50°C.

Figures 4.2- 4.6 show the predicted results at various temperatures. Figures 4.2 and 4.3 show the stress-strain responses of the SMP above the T_g (50°C and 55°C) predicted from various strain energy functions. In the rubbery state, the SMP behaves like a typical unfilled rubber. The stresses are seen to increase slowly with the increase of strain, without any sudden “upturns” or “downturns”. Most strain energy functions can successfully predict the responses of the SMP at this state.

As the material moves to the transitional state (45°C , Figure 4.4) and the glassy state (35°C and 30°C , Figures 4.5 and 4.6), the stress-strain curves display some sudden changes, noticeable the stress-softening after the yield points. In those cases, some strain energy functions have failed to properly capture the responses.

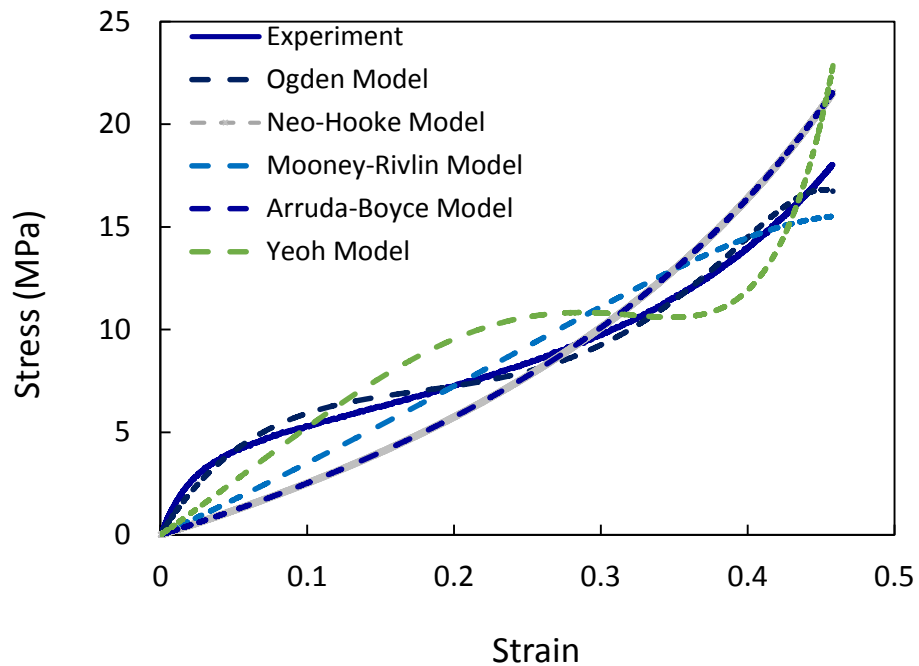


Figure 4.4 Stress-strain responses of the SMP at 45°C .

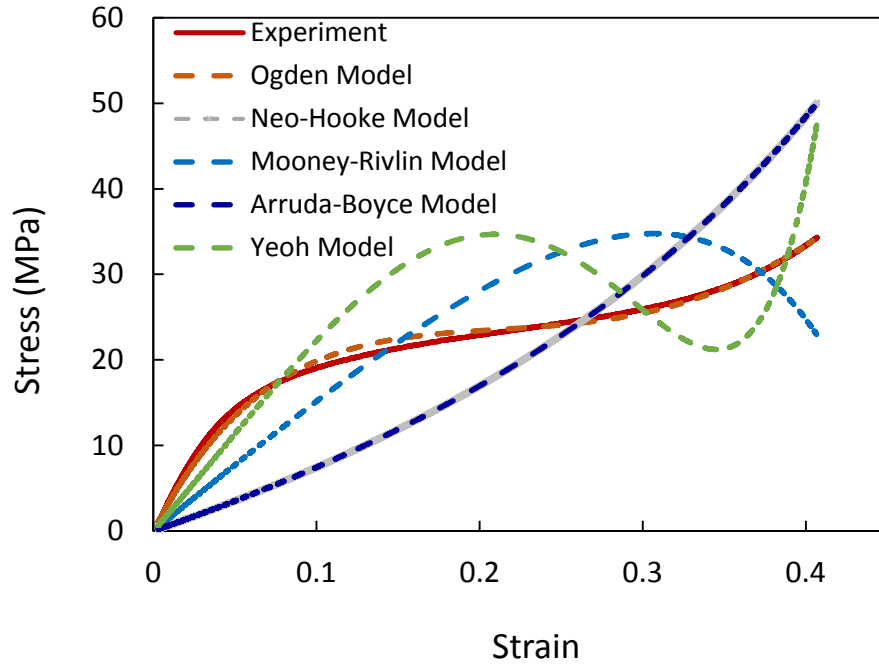


Figure 4.5 Stress-strain responses of the SMP at 35°C.

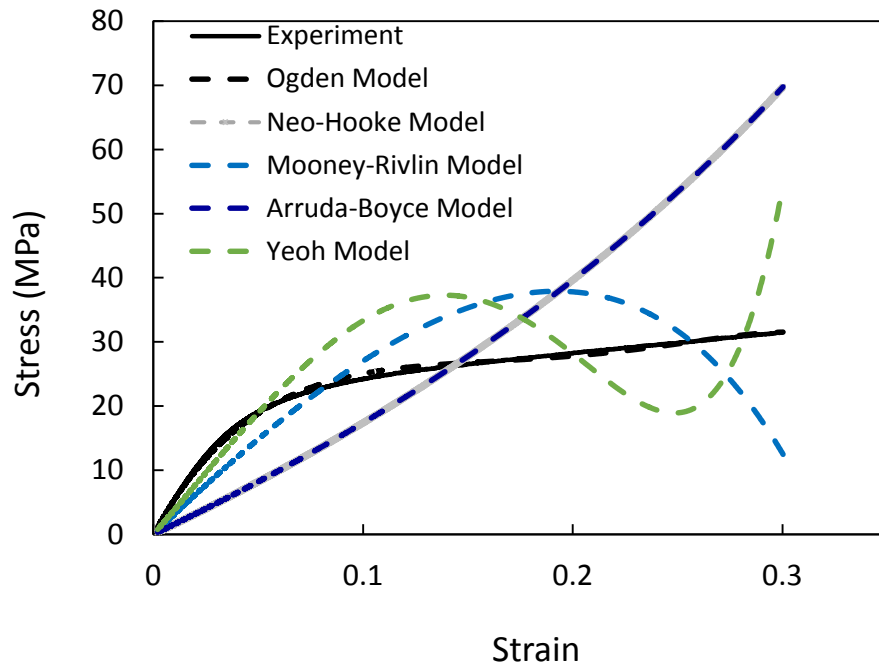


Figure 4.6 Stress-strain responses of the SMP at 30°C.

The micromechanical-based models, Neo-Hooke and Arruda-Boyce, are derived from molecular chain statistics. The stress-strain responses are mostly predicted by the initial shear modulus of the molecular chain stretching, $2C_{10}$ in neo-Hookean model and μ in Arruda-Boyce model. As presented in Table 4.1, the initial shear modulus predicted from these two models are exactly the same. Since only uniaxial data was used in the present study, the second term (N) in Arruda-Boyce model does not seem to have played any significant role. Therefore, the stress-strain curves predicted from Arruda-Boyce model overlap with those from Neo-Hookean model.

Table 4.1 Comparisons of coefficients between Neo-Hooke model and Arruda-Boyce model.

Temperature	Neo-Hooke	Arruda-Boyce	
	C_{10}	μ	N
30°C	25.979	51.958	1159.214
35°C	11.121	22.243	1577.362
45°C	3.763	7.526	1836.209
50°C	2.307	4.548	3.114
55°C	1.590	2.859	1.037

Overall, the predictions from micromechanics-based models are deviated from experimental data due to some significant “turns” that are presented.

Some phenomenological based models, such as Mooney-Rivlin and Yeoh, can capture the initial responses of the material but become unstable at large strains. In all

cases, the Ogden models seem to have provided excellent fits to the experimental data. The coefficients of the Ogden models for the present SMP are summarized in Table 4.2.

Table 4.2 Summary of Ogden coefficients.

Temperature	μ_1	α_1	μ_2	α_2
30°C	380.920	18.333	-182.824	-9.277
35°C	241.345	13.313	-117.241	-6.701
45°C	73.8194	14.690	-35.211	-7.425
50°C	16.5839	11.603	-6.782	-6.084
55°C	2.25313	2.064	-0.820	-2.152

In Ogden model, the free energy density is formulated as a finite sum of scaled powers of the principal stretches λ_i (Equation 4.8). There are $2i$ material constants in the model, the shear modulus like μ_i and the dimensionless exponents α_i , and the sum of these two constant is the classical shear modulus of the

modulus, $\sum_{i=1}^n \mu_i \alpha_i = 2\mu$. For the model to be stable, $\mu_i \alpha_i > 0$ has to be satisfied.

Examining the values of $\mu_i \alpha_i$ shown in Figure 4.7, we can see that the conditions for stabilities have been met in all cases. The comparisons in stress-strain curves between Ogden models and experimental data for all temperatures are depicted in Figure 4.8.

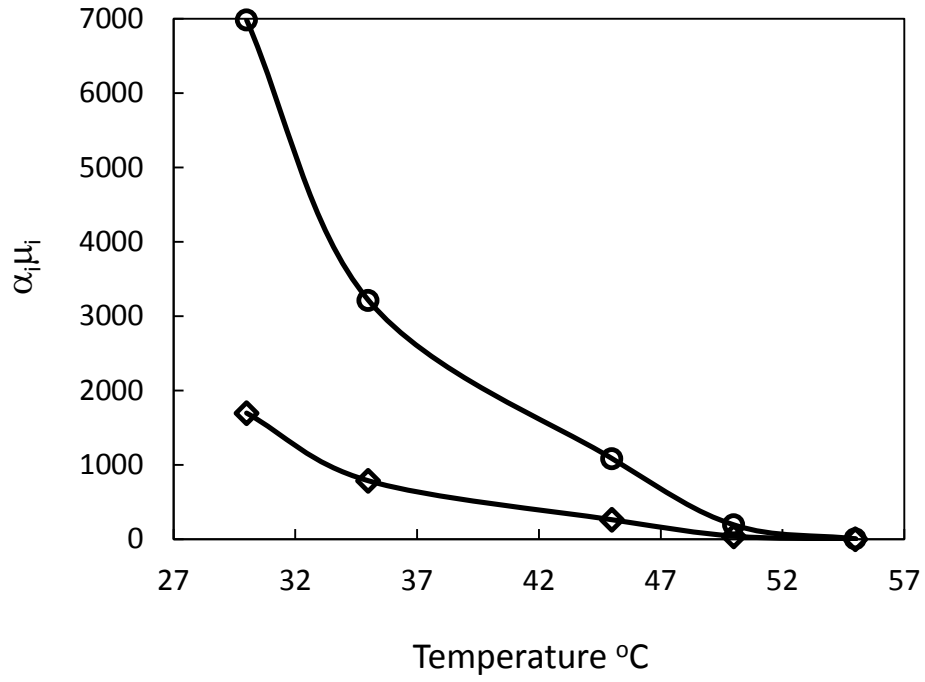


Figure 4.7 Variations of $\mu_i \alpha_i$ in Ogden model.

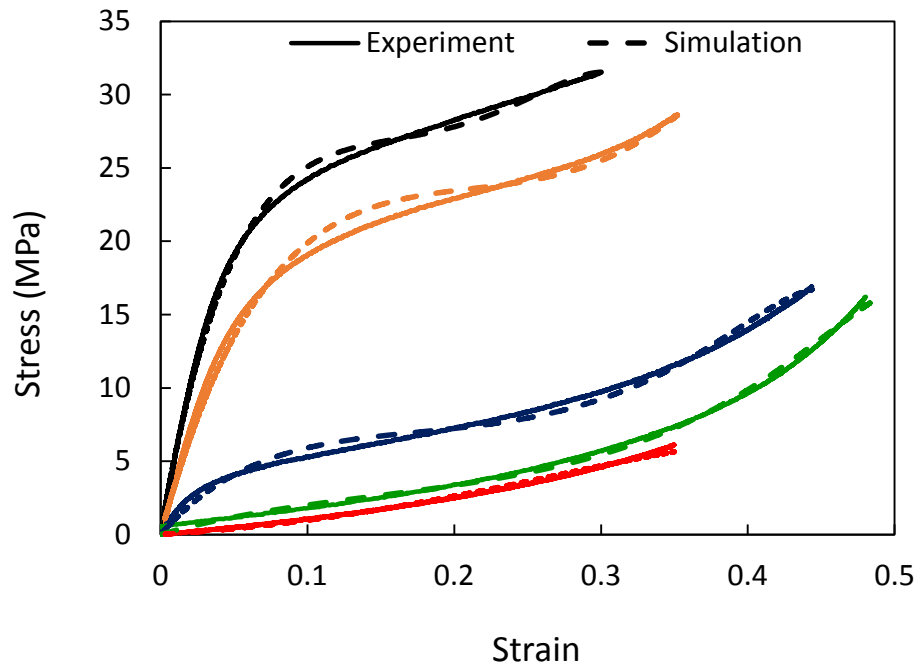


Figure 4.8 Comparisons of stress-strain responses of the SMP between experimental data and Ogden model.

The Ogden model has been further tested by using additional SMP material systems available in the literature: an epoxy based SMP [108]. Detailed information about the material and the predictions are given in Appendix A. Overall, the Ogden model has provided good predictions to the stress-strain responses of the materials.

4.3.2 Prediction of Shape Recovery of SMPs

Shape recovery ability is important to the SMPs because it is the indication of the materials' ability to return to their original shapes upon programming. The unconstrained shape recovery tests were conducted by following the standard thermo-mechanical cycle.

Figure 4.9 shows a breakdown of the complete shape-memory cycle.

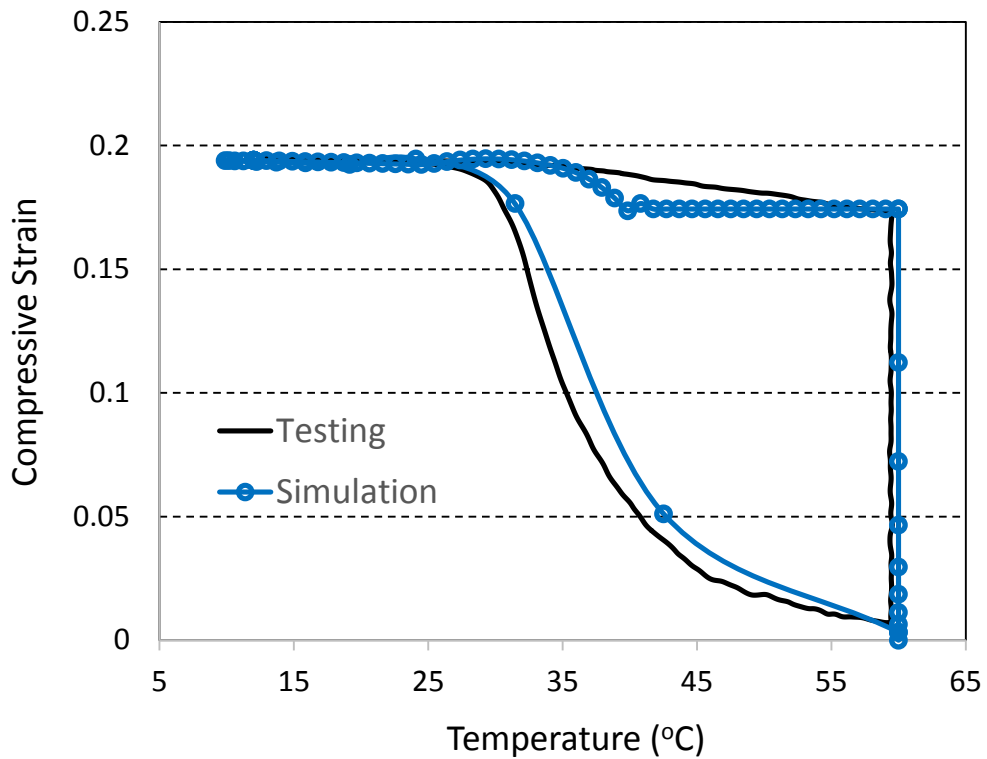


Figure 4.9 Strain-temperature profiles showing the shape recovery of the SMP.

The material was first heated to a temperature above its glass transition, 60°C. After temperature had reached equilibrium, the sample was deformed to a compressive strain of approximately 17.5% (Step 1). The deformed material was then cooled a temperature below its glass transition, 12°C (Step 2). After cooling the constraint was released and a permanent shape was fixed at the sample (Step 3). This step also shows the material's shape fixity which is its ability to hold a shape after it has been deformed. The level of fixing strain was approximately 19.5% now, a slight increase from original (17.5%) due to thermal contraction of the polymer as the temperature dropped from 60°C to 12°C. Finally, the material was reheated to the starting temperature of the thermo-mechanical cycle, 60°C, to recover its shape freely (Step 4). The SMP's recovery characteristics can be illustrated by producing a shape-memory plot of strain vs. temperature. From this plot, the linear shape recovery ratio, R , can be estimated:

$$R = \left(1 - \frac{\varepsilon_f}{\varepsilon_i}\right) \cdot 100, \text{ where } \varepsilon_i \text{ and } \varepsilon_f \text{ are the initial and final strain of the cylindrical specimens, respectively.}$$

It is seen that after the final step, the SMP has returned completely to its original position and the estimated linear shape recovery ratio (R) is 100%.

The shape recovery process under unconstraint condition can be simulated through the finite element method by using the Ogden strain energy functions. The commercial nonlinear finite element (FE) code ABAQUS was used. The actual cylinder shaped specimen was modeled with axisymmetric, hybrid elements and the compression platen was modeled with rigid surface. The contact between specimen and indenter was treated as frictionless. The base of the specimen was constrained in the vertical direction while the nodes along the center line constrained in the horizontal direction. The

displacements of the rigid surface were controlled through a “reference node”, and the reactant force of the reference node was calculated. The modeling of the shape configuration process of the specimen followed the same four steps as used in the experiment (described above). The shape recovery results obtained from the simulation is plotted on the same chart obtained from the experiment (Figure 4.10). It is seen that the finite element prediction from the Ogden model agrees very well with the experimental measurements.

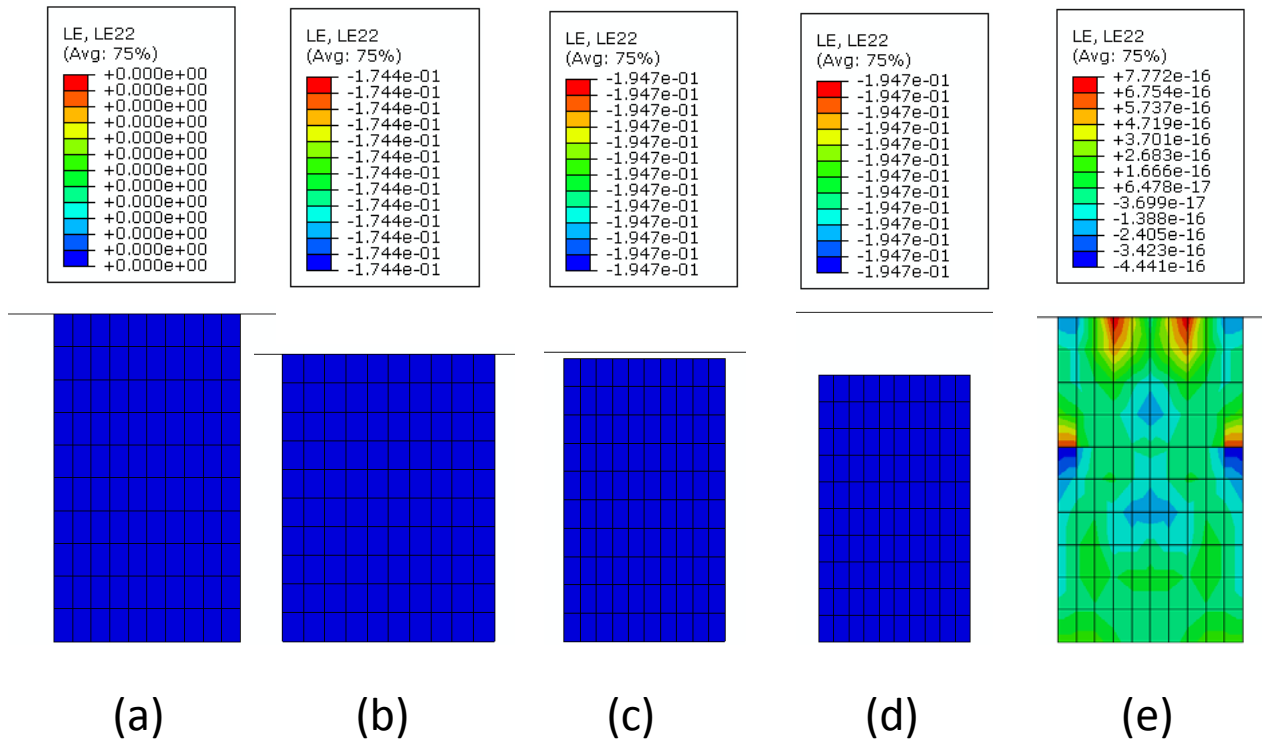


Figure 4.10 Contours of compressive strain (E_{22}) showing the process of shape recovery of the SMP. (a) Original shape: heated up to 60°C , (b) Step1: compressed to a strain of 17.5%, (c) Step2: lowered temperature to 12°C (strain is seen to increase to 19.5% due to thermal contraction), (d) Step3: removed the compression, and (e) Step4: heated up to 60°C again (strain is seen to recover to $\sim 0\%$).

4.4 CONCLUSIONS

An epoxy-based shape memory polymer (SMP) has been fabricated as a candidate material for reconfigurable structures and devices. The stress-strain behaviors of the SMP have been characterized through compressive tests at various temperatures. Overall, the SMP is seen to exhibit nonlinear, finite deformation at all regions. To capture the complicate stress-strain responses across various temperature regimes, the strain energy based modeling has been used. Along all models, the stretch-based Ogden model has provided the best fit to the stress-strain response. The shape recovery ability of the SMP has also been examined by following standard programing cycle. Results show that the SMP can fully recover its original shape under unconstraint condition. The shape recovery process can be well simulated by using the Ogden model.

Chapter Five

5 DESIGN AND CHARACTERIZATION OF MULTIFUNCTIONAL SHAPE MEMORY COMPOSITES: SMA-SMP COMPOSITES

5.1 INTRODUCTION

As we have seen earlier, shape memory composites are a special class of composites that have the multifunctional characteristics that have potential applications in science, engineering and medical fields. These characteristics depend on the type of reinforcements used and the polymer matrix to support the reinforcements. Hence to fully understand the complex material response of multifunctional shape memory composites, it is necessary that we characterize them thoroughly. Several researchers as would be discussed in detail in the following sections have focused their research onto either SMA behavior or SMP behavior separately. And some others have modeled the shape memory effect and super-elasticity of SMA composites where the matrix does not have the shape memory abilities. In such cases, the shape memory properties of SMAs are not fully utilized to their maximum potential. Due to this reason, we have modeled a smart composite material system that makes use of the shape memory abilities for both the matrix and reinforcement. This enables the proper transfer of loads between the SMA fillers and SMP matrix and at the same time improves the mechanical properties of the composite as a whole. Further details on the same aspect are discussed in the following sections. We start by studying several existing constitutive models for SMAs. The SMA constitutive model used in our current project is based on the unified thermo-mechanical constitutive model developed by Qidwai and Lagoudas and as such we have given its detailed description. Then we considered the constitutive model developed for SMP in

the previous chapter of Strain energy based modeling of SMPs. We have used Ogden's strain energy model to describe the non-linear behavior of the SMP in our current project and as such a brief description is provided for this model. Then followed by sections on design of shape memory composites in detail for both particle and fiber fillers used in the SMP matrix are provided. The finite element model developed in the commercial finite element software ABAQUS is also detailed in this section. Details on the use of Lagoudas' subroutine for constitutive model of SMA are given in this section with special attention given on linking the SMA user subroutine to ABAQUS. Further the results of the analysis are presented that predict the mechanical behavior of the shape memory composite. Finally based on the strain-strain response of different SMA-SMP composites with varying volume fractions of SMA fillers in the shape memory polymer matrix conclusion and remarks are presented on the mechanical behavior of the multifunctional shape memory composite.

5.2 SMA MODELING

Ever since the first discovery of NiTiInol in the US naval laboratory in 1962, there has been special focus on its applications not only in engineering field but also in medical field. And as such, there are several constitutive models in place to understand the shape memory behavior of Nickel and Titanium alloy. The first uniaxial thermomechanical behavior of NiTi alloys was proposed by Tanaka et al in 1986 [68]. Their approach is based on deriving the thermo-mechanical constitutive equations and kinetics of the transformation based on Clausius-Duhem inequality which is a way to express the second law of thermodynamics in continuum mechanics. However, their model had the limitations of not considering the changes to the crystal structure during transformation

[68]. Achenbach proposed a model with three phases consisting of austenite, martensite in compression and martensite in tension. He used the idea of potential wells to study the occurrence of phase transformation. At the natural state, the lattice particles are thought to be arranged in layers and the layers stacked on top of the other to represent the body in martensite phase at low temperature as shown in the Figure 5.1 below. In this state the M_+ and M_- are alternating to form the configuration of the alloy.

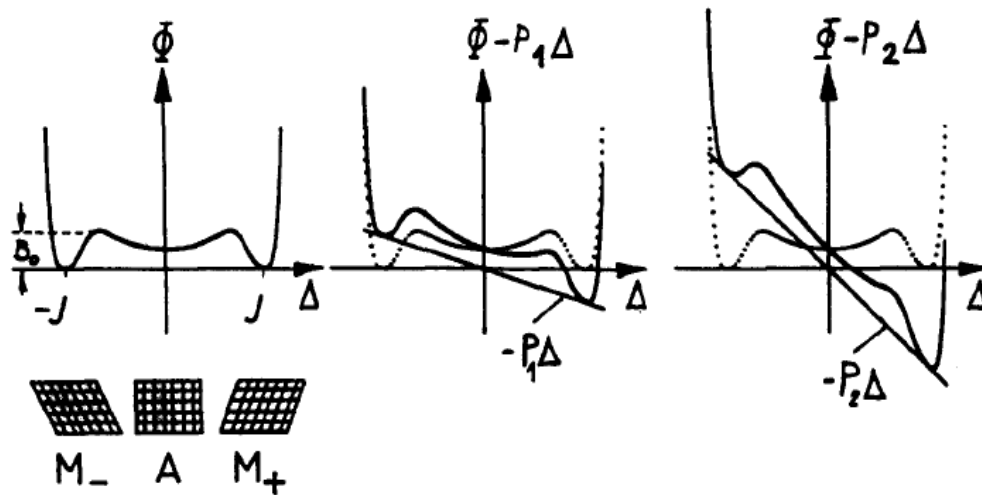


Figure 5.1 Shows the lattice parameters and their potential energy [69].

When slight load is applied in the vertical direction M_- layers become steeper and M_+ layers become flatter as the layers are subjected to shear stresses. And when the load reaches beyond the critical load all the M_- flip and we can see a residual deformation. This causes the change in potential energy which is used to probabilistically figure out when the phase transformation occurs [69]. Liang and Rogers proposed to use martensite fraction as internal variable. The generation of the martensite fraction was determined by phase kinetic laws. They made use of cosine functions to for the evolution of martensite fraction to get a closer fit to the experimental data [70]. They also considered material

properties to be constant during phase transformation like Tanaka et al. Later on Abeyaratne et al. pointed out since phase transitions are greatly influenced by the temperature, a constitutive model that is purely based on mechanical behavior is not sufficient to understand the shape memory behavior of a material [71]. Hence they made use of Helmholtz free energy density, kinetic relations which govern the speed of phase boundaries, nucleation criterion that indicates the beginning of a phase transition to describe both the effect of thermal as well as mechanical behavior to develop their constitutive one dimension thermo-mechanical model. Brinson (9) used two internal variables which were described by cosine hardening law that included a variable elastic stiffness during the phase transformation. Again in 1997, Bekker and Brinson together developed a mathematical model to describe the macroscale SMA kinetic law that used the geometry of loading path on the experimentally defined stress-temperature phase diagram. This model enabled the clear prediction of 1D SMA material behavior to any complicated or arbitrary stress-temperature loading [72]. Figure 5.2 below shows the idealized phase diagram with a complicated loading path. It can be seen that such complicated loading paths could be modeled using Bekker and Brinson's model. Later Govindjee and Kasper introduced a model to describe martensite variants in both tension and compression. They made use of the stress-temperature space (referred to as the phase space in their work) to address the constitutive modeling of 1D SMAs to obtain the super-elastic and shape memory effects. In doing so they had made use of constant stiffness and coefficient of thermal expansion [73]. Similarly Auricchio and Sacco developed a 1D constitutive model for SMA on the basis of phase-diagram and beam finite theory. They made use of one internal variable for single-variant volume fraction

with the governing equations for the evolution of this internal volume fraction were considered to be functions of stress and temperature [74]. Rajagopal and Srinivasa developed their constitutive equations to model the pseudo-elasticity and shape memory effects using Helmholtz potential and dissipation mechanisms [75]. Marfia et al. proposed a model for SMA in applications as reinforcement material in beams [76]. Ikeda et al. proposed a constitutive model for SMA under unidirectional loading case derived from microscopic aspects that included the shape memory effects of deformation history [77].

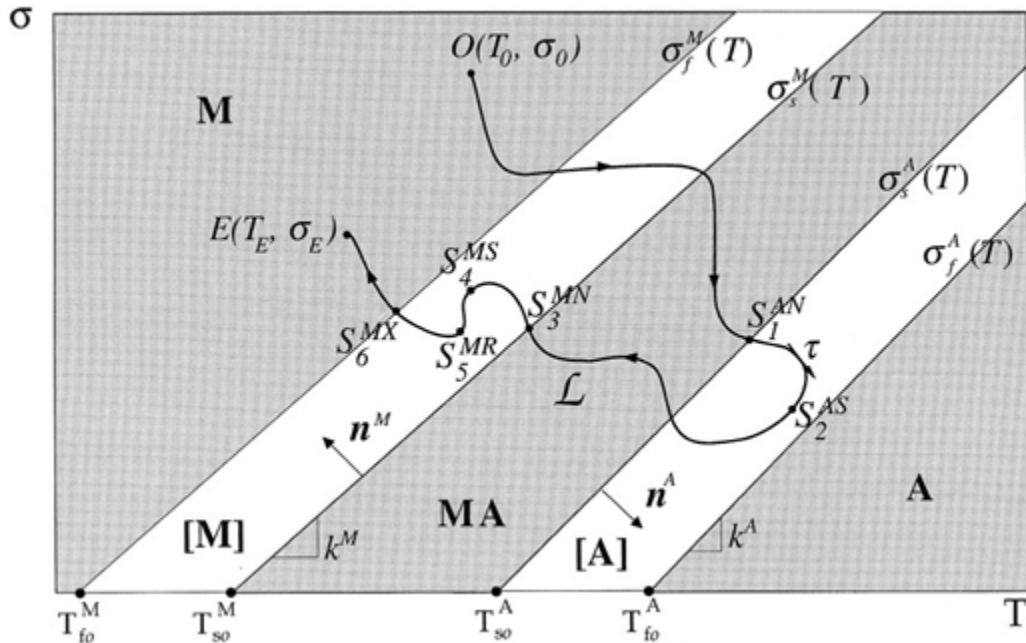


Figure 5.2 Shows Bekker and Brinson's model to describe the SMA behavior when a complicated loading path is used [72].

A different approach was used by Paiva et al. and Savi and Paiva in developing their constitutive model [78, 79]. The free energy of SMA was proposed to be a combination of the free energies of the four different phases namely: tensile, compressive

martensite, austenite and multivariant martensite. Burravalla and Khandelwal proposed a 1D constitutive model that emphasized on the importance of certain memory properties such as the distance of a point on the loading path from the finish boundary in the transformation zone and the effect of this distance on the extent of transformation [80]. Evangelista et al. came up with a new beam finite element method by making use of a thorough time integration algorithm to develop the basis of finite element method [81]. This method was used in the 1D formulation of the SMA model and also gave a clear understanding and mechanical significance of the material parameters that are responsible for the constitutive model. Nallathambi et al. used the effect of mechanical dissipation inequality coming from the second law of thermodynamics to come up with the main equations of their constitutive model in a uniaxial setup comprising of three phases namely: austenite, plus martensite and minus martensite [82]. Rizzoni et al developed their constitutive model for a commercial NiTi SMA strip using theoretical and experimental results as the strip is bent and the deformation recovered from uniform bending [83]. They had used twinned and de-twinned martensite as the internal variables to obtain the solution for the distribution of martensite fraction and stress in the SMA strip.

Many researchers shifted their focus on to the cyclic response of the SMA as interesting behavior was observed in shape memory properties when the SMAs were subjected to cyclic loading-unloading. Mainly two effects were seen due to the cyclic loads on SMAs [84-86]:

- 1) Due to the cyclic loading there is a decrease in the critical stresses in both forward (austenite to martensite) transformation and reverse transformation (from martensite to austenite).
- 2) Due to the cyclic loading there is an increase in the plastic deformation or plastic strain that could be recovered by heating the SMA above the austenite finish temperature.

The second aspect of sustaining a permanent deformation due to cyclic loading or training could lead to reversible automatic shape change during heating and cooling without any externally applied load. This is due to the presence of residual martensite variants and this process gives rise to two way shape memory effect (TWSME). This phenomenon led to whole new potential applications of SMAs as temperature sensitive actuators, reversible medical implants and reversible fasteners. Following which several studies were carried out to develop constitutive models to understand the TWSME for these potential applications. Among these a few such studies are mentioned in this section. Tanaka et al. have extended their 1D model to further study the cyclic training effects on SMA by using three internal variables that include the residual stress and strain and residual martensite fraction that result from training [84]. LExcellent and Bourbon later developed a 1D SMA model for SMA in cyclic tensile loading which used instantaneous residual martensite volume fraction as a new internal variable. Here they assumed that the residual strain obtained was solely due to the unrecovered martensite from the cyclic loads. Their model was accurate for several cycles [85]. Bo and Lagoudas were the first researchers to come up with a model that worked for both plastic strain and transformation strain that are generated at the same time during both forward and reverse

transformation. This model was able to explain the minor hysteresis loops by taking plastic strain and TWSME into consideration [86]. Likewise there are several studies that used different internal variables for both types of constitutive models (twinned and detwinned martensite configurations). All of the work discussed so far was done for one dimensional constitutive model as they were thought of satisfactorily describing the pseudo-elastic and shape memory effects as a 3D model would in addition to needing lesser variables compared to 3D models. Although as the industry applications of SMA grew in the recent years, such as their applications in bio-medical field, aero-space and automotive actuators, earthquake energy dissipation devices etc., the need for a more comprehensive model that could simulate the behavior of the SMA when there are multi-axial forces acting also became significant. For this reason, 3D constitutive models were developed to study the complicated behavior in multi-axial loading on the pseudo-elastic and shape memory effects of SMA.

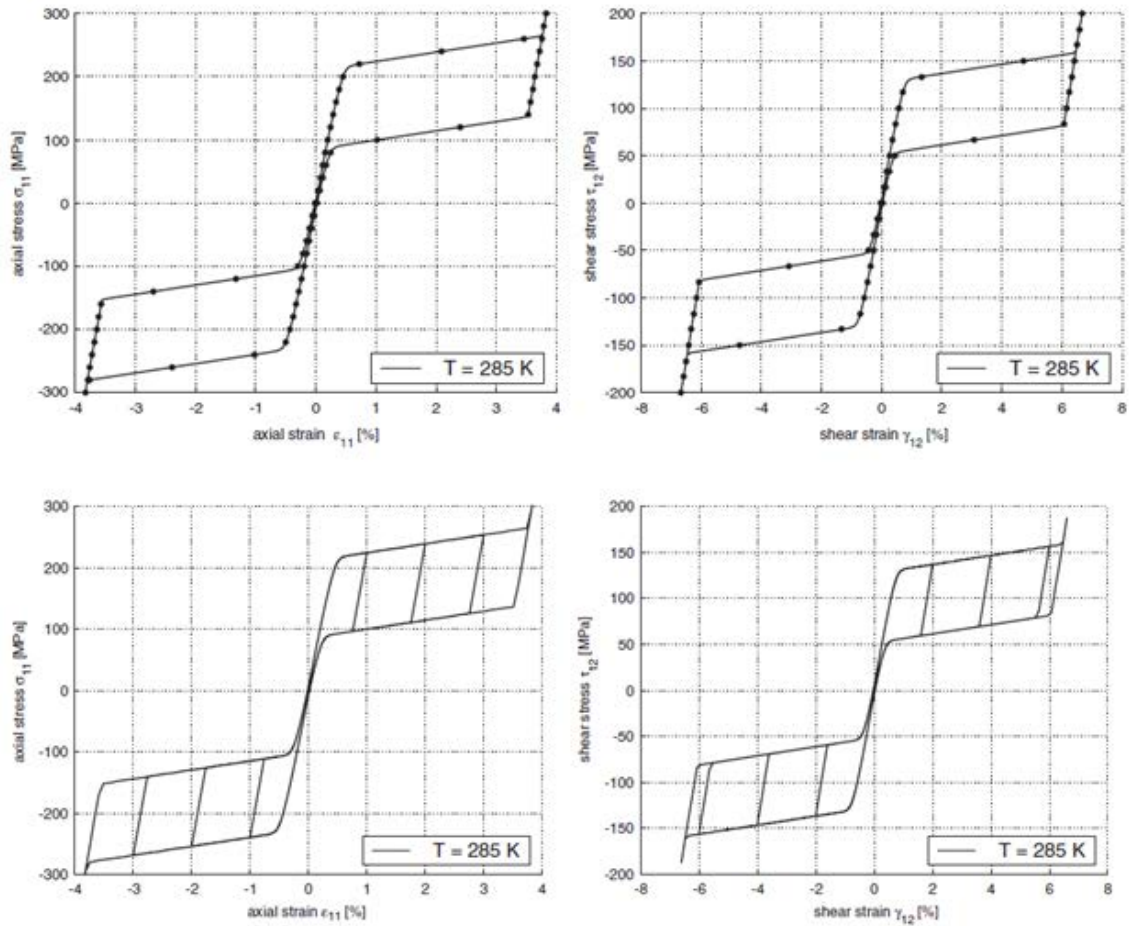


Figure 5.3 Shows the Tension–compression tests (left part) and torsion tests (right part) under stress control with continuous line: $T = 285\text{ K}$ (above $A_f = 248\text{ K}$) without and with training [87].

Aurichio et al. proposed a 3D constitutive model to comprehend the significant macroscopic features of SMAs such as SME, pseudo-elastic effect, asymmetric tension-compression response and thermo-mechanical coupling. They developed an integration algorithm which could be used in the commercial finite element code eventually [87]. To check the algorithm they had developed, two different testing modes were considered: uniaxial tension-compression and shear tests under stress control and the same under

strain control. They could see that the model predicted the SMA behavior for these testing modes and under training as well. Figure 5.3 shows the results of the tension-compression and torsion tests under each stress and strain control methods. It can be seen that the algorithm was able to predict the stress-strain response in both cases.

Zhang et al. studied the effects of indentation on the shape recovery properties of SMA. To do so, they simulated the indentation response of 3D model with spherical indentation and observed that shallow indents are fully recovered whereas deeper indents result in plastic deformation [44].

As we can see in all the models mentioned so far, there a special attention to a particular case be it specific loading type, martensite configuration (single or multi variant martensite) or one dimensional model and three dimensional models. Also, the phase transformations are seen to be highly dependent on the loading paths, and both thermal and mechanical responses. Due to this dependency of phase transitions on coupled thermo-mechanical conditions and loading path, constitutive models need internal state variables such martensite volume fraction, transformation strain residual stresses due to transformation. In addition, there has been increasing demand for use of SMAs in aero-space, biomedical and structural applications. Designing such devices that incorporate the use of SMAs in these applications requires numerical methods that can support the design process. Finite element method (FEM) is one such numerical method can support the constitutive models for complex material behavior such as SMAs. Hence, it is necessary to implement a constitutive model in a commercial finite element software (such as ABAQUS) to be able to simulate the response of a shape memory alloy when it is subjected

to multi-axial complex thermo-mechanical loads to design and analyze the use of SMAs in the earlier mentioned applications.

Since our main objective is to obtain the thermo-mechanical/mechanical response of SMA reinforced SMP composite, we had further looked at a generalized and unified constitutive model proposed by Qidwai and Lagoudas. In the next section we present a detailed description of some of the important equations of the constitutive model.

5.2.1 Constitutive Model For the Thermo-Mechanical Response of NiTi SMA by Qidwai and Lagoudas

Qidwai and Lagoudas developed constitutive models for shape memory materials based on first principles of thermodynamics. The basis of their model was to express the second law of thermodynamics in terms of Gibbs free energy [88].

$$G(\sigma, T, \xi, \varepsilon^t) = -\frac{1}{2\rho} \sigma : S : \sigma - \frac{1}{\rho} \sigma : [\alpha(T - T_0) + \varepsilon^t] + c \left[(T - T_0) - T \ln \left(\frac{T}{T_0} \right) \right] - s_0 T + u_0 + \frac{1}{\rho} f(\xi) \quad (5.1)$$

where G is specific Gibbs free energy, σ represents Cauchy stress tensor, T is temperature tensor, ξ is martensite volume fraction, ε^t is uniaxial transformation strain, ρ represent mass density, α is thermal expansion coefficient, T_0 is reference temperature, c is specific heat capacity, s_0 and u_0 represent specific entropy and specific internal energy at reference point respectively, and $f(\xi)$ is the transformation hardening function. The reason for using this functional form for martensite volume fraction is to be able to apply this constitutive model to different SMAs that have different hardening functions. For example, Liang and Rogers used a cosine hardening function to define the interactions between the two phases [70]. Similarly Tanaka et al. used an exponential function to

obtain the recovery in their model [89]. Later as the rest of the steps in the current model are presented we obtain the hardening function used by Boyd Lagoudas. Hence it is clear that the hardening function can take any form suitable for a particular constitutive model and thus making it comprehensive and more versatile in its applications.

The material constants used in the above equation are obtained from the rule of mixtures as shown below:

$$S = S^A + \xi(S^M - S^A), \quad \alpha = \alpha^A + \xi(\alpha^M - \alpha^A), \quad (5.2a)$$

$$c = c^A + \xi(c^M - c^A), \quad s_0 = s_0^A + \xi(s_0^M - s_0^A), \quad u_0 = u_0^A + \xi(u_0^M - u_0^A) \quad (5.2b)$$

where, the superscripts A and M specify the values of material properties in austenite and martensite phases. And S, α, ρ, c, s_0 and u_0 are effective compliance tensor, effective thermal expansion tensor, density, effective specific heat, effective entropy at reference state and effective internal energy at the reference state.

Further, the thermodynamic force conjugate of ξ was obtained as shown below.

$$\pi(\sigma, T, \xi) = \sigma : \Lambda + \frac{1}{2} \sigma : \Delta S : \sigma + \sigma : \Delta \alpha (T - T_0) - \rho \Delta c \left[(T - T_0) - T \ln \left(\frac{T}{T_0} \right) \right] + \rho \Delta s_0 T - \rho \Delta u_0 - \frac{\partial f}{\partial \xi} \quad (5.3)$$

where π is thermodynamic force conjugated to ξ , Λ is transformation tensor and S represents the compliance tensor. Generally, conjugate of state variables obtained from Legendre's transforms are used in most cases that involve experimental data. By using conjugate of state variable extensive properties that depend on the physical dimensions of the system in consideration are replaced by their conjugate which is the partial derivative of the original state variable with respect to the original state variable. This way, the new function or the new state variable becomes an intensive variable which can be more easily

controlled in a physical experiment. Hence we have the thermodynamic force conjugate as given above. Here, Λ is the transformation tensor which gives the direction of transformation and is given by the following set of equations:

$$\Lambda = \begin{cases} \frac{3}{2}H \frac{\sigma'}{\bar{\sigma}}, \dot{\xi} > 0 \\ H \frac{\varepsilon^{t-r}}{\bar{\varepsilon}^{t-r}}, \dot{\xi} < 0 \end{cases} \quad (5.4)$$

Where H is the maximum uniaxial transformation strain, ε^{t-r} is the transformation strain at the reversal of the transformation. Depending on the loading type, the transformation tensor could be picked. The above shown equations are for uniaxial loading case.

In the above thermodynamic conjugate equation, Δ gives the difference of a quantity in between martensite and austenite phases.

From Clausius-Planck inequality we obtain the following:

$$\left(\sigma : \Lambda - \rho \frac{\partial G}{\partial \xi} \right) \dot{\xi} = \pi \dot{\xi} \geq 0 \quad (5.5)$$

From here we can determine the criterion for forward and reverse martensite phase transformation, as given below:

1. In forward transformation, since austenite is transforming to martensite, $\dot{\xi}$ is positive. Now for the above inequality to be satisfied π has to be positive. Hence, the force conjugate of ξ will be of the form $\pi = Y$.
2. In reverse transformation, since martensite is transforming to austenite, $\dot{\xi}$ will be negative. Now for the above inequality to be satisfied π has to be negative. Hence, the force conjugate of ξ will be of the form $\pi = -Y$.

3. In the absence of a phase transformation the value of ξ shall remain constant and as such $\dot{\xi}$ will be equal to zero. In this case, the Clausius-Planck inequality is always satisfied as $\pi = 0$.

The above conditions are called Kuhn-Tucker conditions and are summarized below for the all the above explained cases:

$$\dot{\xi} \geq 0; \Phi(\sigma, T, \xi) = \pi - Y \leq 0; \Phi \dot{\xi} = 0; \quad (5.6)$$

$$\dot{\xi} \leq 0; \Phi(\sigma, T, \xi) = -\pi - Y \leq 0; \Phi \dot{\xi} = 0; \quad (5.7)$$

where Φ is the transformation function and Y is the critical value of thermodynamic force to cause the transformation.

Finally, the appropriate hardening function is considered which defines the interactions between martensite and austenite phases and also between the martensite variants. The hardening function used in the current constitutive model by Lagoudas is given below:

$$f(\xi) = \begin{cases} \frac{1}{2} \rho b^M \xi^2 + (\mu_1 + \mu_2) \xi; & \dot{\xi} > 0 \\ \frac{1}{2} \rho b^A \xi^2 + (\mu_1 - \mu_2) \xi; & \dot{\xi} < 0 \end{cases} \quad (5.8)$$

where ρ , b^M , b^A , μ_1 , and μ_2 are material constants determined from thermo-mechanical experiments. And M, A represent martensite phase and austenite phase respectively.

In summary the following five conditions are to be considered in modeling the SMA using Qidwai and Lagoudas constitutive model.

1. Beginning of forward phase transformation at zero stress:

$$\pi(\sigma, T, \xi) = Y \quad \text{at} \quad \sigma = 0, \quad T = M_s, \quad \xi = 0$$

2. Ending of forward phase transformation at zero stress:

$$\pi(\sigma, T, \xi) = Y \quad \text{at} \quad \sigma = 0, \quad T = M_f, \quad \xi = 1$$

3. Beginning of reverse phase transformation at zero stress:

$$\pi(\sigma, T, \xi) = -Y \quad \text{at} \quad \sigma = 0, \quad T = A_s, \quad \xi = 1$$

4. Ending of reverse phase transformation at zero stress:

$$\pi(\sigma, T, \xi) = -Y \quad \text{at} \quad \sigma = 0, \quad T = A_f, \quad \xi = 0$$

5. Continuity of Gibbs free energy:

$$\pi(\sigma, T, \xi) = -Y \quad \text{at} \quad \sigma = 0, \quad T = A_f, \quad \xi = 0$$

Model parameters for the quadratic polynomial hardening function model are defined as below:

$$Y = \frac{1}{4} \rho \Delta s_0 (M_s + M_f - A_f - A_s)$$

$$b^A = -\Delta s_0 (A_f - A_s)$$

$$b^M = -\Delta s_0 (M_s - M_f)$$

$$\mu_1 = \frac{1}{2} \rho \Delta s_0 (M_s + A_f) - \rho \Delta u_0$$

$$\mu_2 = \frac{1}{4} \rho \Delta s_0 (A_s - A_f - M_f + M_s)$$

This constitutive model was then implemented into a finite element code. A subroutine was compiled with the above mentioned criteria for evolution parameters to obtain the pseudo-elasticity and shape memory effect of the SMA. The constitutive model requires experimentally determined materials constants, which is discussed in the following section.

5.2.1.1 Experimentally Determined Material Constants Used In The User Subroutine

The Young's moduli of elasticity of both the phases: austenite (E^A) and martensite (E^M), which were obtained from pseudo-elastic test. Thermal expansion coefficients for martensite (α^M) and for austenite (α^A). These properties were obtained from standard test for martensite at low temperature and for austenite at high temperature. The transformation temperatures: martensite start M^{0s} and finish M^{0f} , austenite start A^{0s} and finish A^{0f} at zero stress state were obtained by a standard DSC test. The maximum transformation strain was calculated from the pseudo-elastic test as shown in the Figure 5.4 shown below. The stress influence coefficients were calculated from the phase diagram and pseudo-elastic test (Figure 5.5).

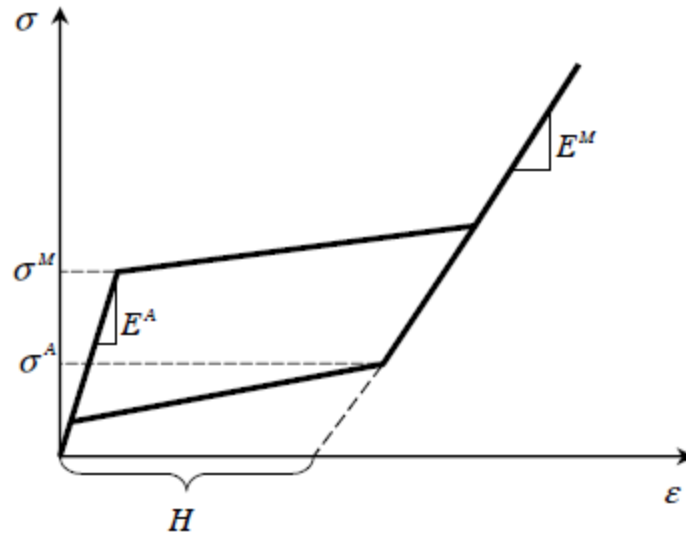


Figure 5.4 Figure shows the schematic of an SMA uniaxial pseudo-elastic test [88].

The transformation strain is obtained from the pseudoelastic test indicated in the figure while stress influence coefficients are obtained from the following equations:

$$\rho\Delta S^A = -\frac{\sigma^A}{T_{test} - A^{0s}}H,$$

$$\rho\Delta S^M = -\frac{\sigma^M}{T_{test} - M^{0s}}H,$$

where, T_{test} is the temperature at which the pseudo-elastic test was performed. σ^A and σ^M were obtained from the Figure 5.4 shown above.

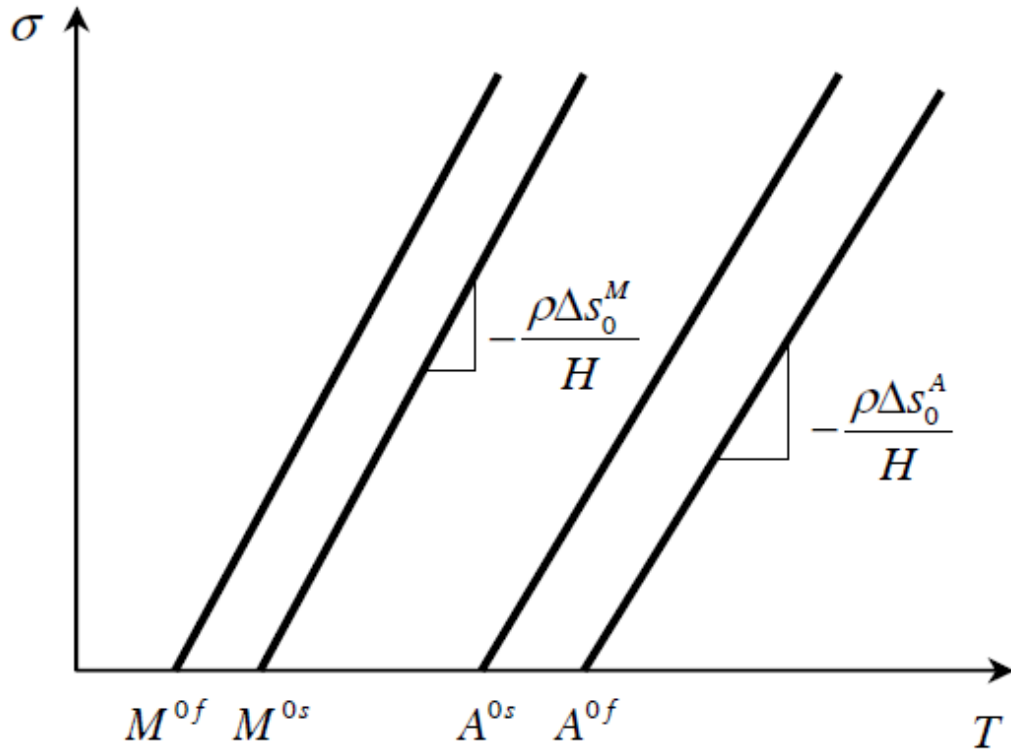


Figure 5.5 Shows the schematic of the phase diagram [88].

5.3 SMP MODELING

Several constitutive models exist for the shape memory polymers and to describe them thoroughly most models use large number of material parameters. As discussed in the previous chapter, it becomes a complex calibration process to experimentally determine these parameters although these models are highly comprehensive in simulating the shape memory behavior of SMPs. And for this reason some of the strain energy density based functions such as Mooney-Rivlin, Neo-Hookean, Yeoh, Ogden and Arruda-Boyce (discussed in chapter 4) were used to model the shape recovery behavior of SMP. In addition to this there are several other strain energy density based functions that could be used to model rubber like hyper-elastic materials. It is necessary to choose the model appropriately by ensuring that the model is being used in its valid range of

loading conditions and applied strains. Most models are suitable for strain less than 10%. For small strains like this Neo-Hookean model would be a suitable choice. Whereas for larger strains (>10%) Ogden model provides a better fit to the experimental data as pointed out by Marckmann and Verron in their comparison of various hyper elastic models. According to their findings and suggestions, a model that uses lesser number of material parameters are need experimental results to obtain is ranked higher and considered a better choice compared to those that require a large number of parameters to be determined experimentally. Additionally, a model that best fits the experimental results is ranked higher. Although Ogden model uses 6 parameters higher than Neo-Hook and Yeoh, these models are used for lower strains below 10% as mentioned before. Also it was seen that there was a better fit for the stress-strain curves obtained from Ogden's hyper-elastic model with the experimental results. Hence, SMP in the current research was modeled using Ogden's coefficients obtain from the simulation of shape recovery tests in the commercially available finite element software: ABAQUS. It is recommended to refer Chapter 4: "Strain energy function based modeling of SMPs" of this thesis for further details on the hyper-elastic modeling of SMPs. As such, in this section we briefly present the Ogden's model to study the shape memory behavior of SMP.

5.3.1 Ogden Strain Energy Function

From Rivlin's findings for isotropic, incompressible materials subjected to uniaxial tension or compression we can obtain the following relation for Strain energy function in terms of the engineering stress, stretch ratio and strain invariants.

$$\frac{\sigma}{(\lambda - \lambda^{-2})} = 2 \left[\frac{\partial W}{\partial I_1} + \frac{1}{\lambda} \frac{\partial W}{\partial I_2} \right] \quad (5.9)$$

where σ is the engineering stress and λ the stretch ratio. W represents the strain energy function, $W = f(I_1, I_2, I_3)$ where I_1, I_2, I_3 are the three invariants given in terms of the principal stretch ratios $\lambda_1, \lambda_2, \lambda_3$.

Typically the rest of the strain energy density function based approaches derive W in terms of the invariants (I_1, I_2, I_3). However, in Ogden model W is obtained from stretch ratios as shown below:

$$W = \sum_{i=1}^n \frac{\mu_n}{\alpha_n} (\lambda_1^{\alpha_n} + \lambda_2^{\alpha_n} + \lambda_3^{\alpha_n} - 3) \quad (5.10)$$

In simple tension or compression, we have $\lambda_1 = \lambda, \lambda_2 = \lambda_3 = \lambda^{-1/2}$. Taking the first two terms, Equation (7) reduces to

$$W = \frac{\mu_1}{\alpha_1} (\lambda^{\alpha_1} + 2\lambda^{-\frac{\alpha_1}{2}} - 3) + \frac{\mu_2}{\alpha_2} (\lambda^{\alpha_2} + 2\lambda^{-\frac{\alpha_2}{2}} - 3) \quad (5.11)$$

Substituting Equation (5.8) into Equation (5.1) yields

$$\sigma = \mu_1 (\lambda^{\alpha_1 - 1} - \lambda^{-\frac{\alpha_1}{2} - 1}) + \mu_2 (\lambda^{\alpha_2 - 1} - \lambda^{-\frac{\alpha_2}{2} - 1}) \quad (5.12)$$

By curve fitting, the constants $\mu_1, \alpha_1, \mu_2, \alpha_2$, can be estimated.

In the present study, the coefficients of Ogden's strain energy function were determined by using the curve-fitting utility in commercial finite element program, ABAQUS. Experimental stress-strain data were entered into program to compute the coefficients of strain energy functions.

In order to obtain a stable solution the following criteria should be satisfied by the SMP. For a stable model that does not give arbitrary deformations in the presence of load $\mu_i \alpha_i > 0$ must hold true. This ensures that physically meaningful stress-strain curves are obtained for the material. For this reason, the SMP in our current study was checked for this criterion with the material model involving Ogden coefficients and it was seen that the material is stable.

5.4 DESIGN AND MODELING OF SMA-SMP COMPOSITES

Design of SMA-SMP composites is a new area of research that is gaining attention in the recent years. As such there are very few studies and constitutive models that incorporate the multifunctional properties of SMAs and SMPs in medical, structural and aero-space applications.

5.4.1 Designing Of SMA-SMP Composites

As in any engineering applications, the design of SMA-SMP composites is focused on specific application. Based on their applications, an appropriate constitutive model for SMA and SMP are taken into consideration. Although the response of our specific material system of this smart composite is new, its design for improved

mechanical properties is similar to that of a typical composite material. Another notable aspect in designing SMA-SMP composite is the dependence of its performance based on the type of SMA fillers. In the current project, two types of SMA fillers were examined, namely, particle and fiber fillers. The shape of SMA reinforcements that is compatible with the SMP matrix or in other words, the reinforcements need to bond well with the matrix in order to transfer the loads between each other. Therefore, we have investigated the effect of SMA spherical particles and SMA wires on the mechanical properties of the smart composite. The design parameters for particle fillers are quite different from that of fiber filler. And as such the design considerations for the both types are dealt separately.

5.4.1.1 Design of SMA Particle – SMP Composites

- a) ***Volume fraction of SMA particles:*** The volume fraction of SMA-particle reinforcements affects the performance of the composite. When volume fraction of the reinforcements is close to 50% of that of the matrix there is a lack of proper adhesion between the two and this would result in poor stress transfer and consequently affecting the mechanical properties of the composite as a whole. This is especially true for particle reinforcements.
- b) ***Particle size:*** The size of the reinforcement (diameter of SMA particles and aspect ratio of wires) is another design parameter that needs to be taken into consideration before setting up either the physical experiment or the numerical model. Although it is true that adding particle and fiber reinforcements improves the mechanical properties of the matrix by increasing its strength, it does not ensure that this is true for all sizes of particles. Usually micro and nano sizes for diameter are considered suitable reinforcements for polymer matrices. Again as

the size of the particles increases, the interfacial bonding is poor and as state earlier, the stresses are not transferred effectively between the matrix and the reinforcements. For this reason, surface modification techniques are in place when bigger size reinforcements are to be used.

- c) ***Homogeneous distribution:*** Lastly, uniform distribution of the particles is essential to obtain accurate mechanical properties. When the particles are not distributed uniformly, they form clusters or agglomerations that cause poor interaction between the matrix and the reinforcements.

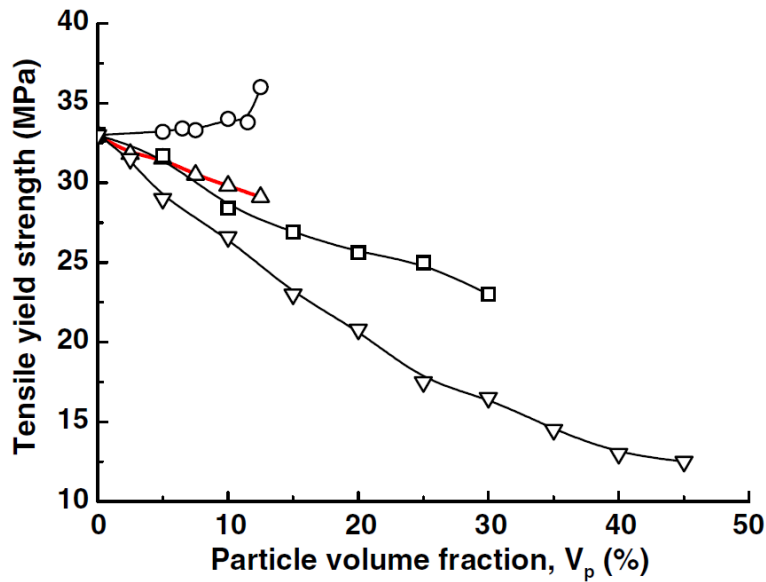


Figure 5.6 Shows the tensile yield strength of polypropylene- CaCO_3 composite for different particle size at different volume fractions of CaCO_3 in PP matrix [91].

From the studies conducted by Fu et al. [90], on the effects of particle size and volume fractions on the mechanical performance of the particulate-polymer composites, it was observed that although there is not much change in the young's modulus of the composite the yield strength decreased with increase in of the particles. Figure 5.6 below

shows the tensile yield strength of polypropylene embedded with CaCO_3 particles for different particle sizes at different volume fractions of the particle in the polymer matrix [91].

And in the Figure 5.7 below we can see that the young's modulus of glass bead filled epoxy composite is not affected by the change in particle size of the fillers. The reason for this as proposed by Fu et al, is that, since the modulus is measured at the initial stages of the loading, there is not much interfacial de-bonding between the matrix and the filler and as such the stresses are transferred well within the composite material between the matrix and the filler. Although, at lower volume fractions (up to 18%) the modulus of the composite remains constant and as the volume fraction increases for higher values such as 30%, 40% and 46% as shown in the figure below, there is a slight drop in the modulus as the particle size increases.

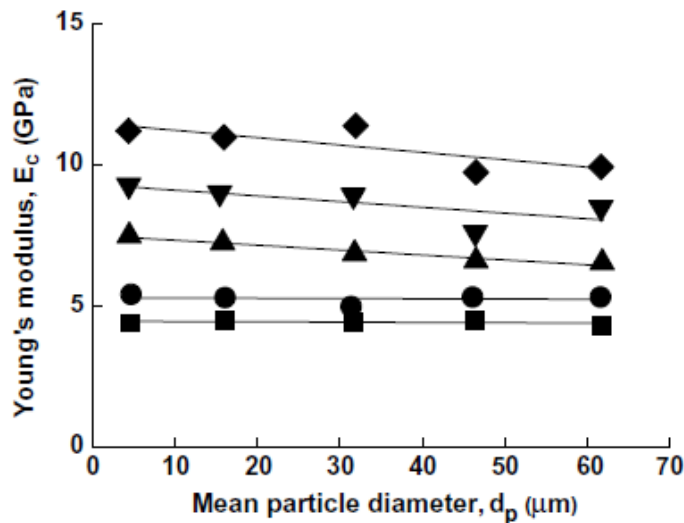


Figure 5.7 Shows the variation of young's modulus in glass filled epoxy polymer composite with particle diameter for different volume fractions of particle from 10- 46% of glass fillers [91].

For this reason, in the current design of SMA-particle reinforced SMP composite, we have modeled spherical shaped SMA particle to represent the volume fraction embedded at the center of the matrix using micro-mechanical method to model the SMA-SMP composite. This representative volume element of SMA is assumed to be in perfect bonding with the SMP matrix. In this method spherical particles are assumed to be uniformly distributed in the cube matrix in all three directions. So it is possible to consider the design of a single cell with the RVE inserted at the center of the matrix by keeping the volume fraction of the particle RVE the same as that of the entire composite structure. The advantages in using RVE in designing the composite are that:

1. When the distribution of fillers is uniform and unidirectional it is easier to obtain the global properties of the composite by considering the known properties of the constituents (matrix and the filler).
2. Additionally damage initiation and propagation can also be examined through this analysis [92].

Figure5.8 below gives a pictorial view of the RVE in the matrix for a SMA-particle reinforced SMP composite.

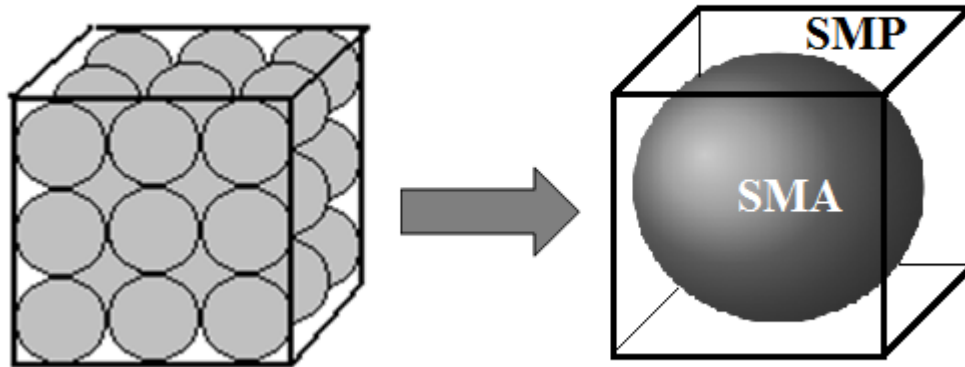


Figure 5.8 Shows the RVE of spherical SMA particle in SMP matrix.

5.4.1.2 Design of SMA Fibre-SMP Composites

- a) **Fiber form:** SMA fibers like other reinforcing fibers can be grouped into three types based on their length: short fibers (small aspect ratio), long fibers and continuous fibers (high aspect ratio). Each type of fiber imparts a certain characteristics to the composite. For example, a long continuous fiber makes the composite stronger where as a short fiber helps in better flow of the composite during processing which helps in fabrication of complex molded parts. Long fibers are used when the strength of the composite needs to be increased in a preferred direction.

Table 5.1 Increase of Young's modulus and tensile strength of a duromer matrix (polyester resin) by addition of glass fibers with a volume fraction of 65% to 70%

[93].

Type of fiber	E(GPa)	R _m (MPa)
None	3.5	90
Short fibers, irregular	20	190
Short fibers, oriented at $\pm 7^\circ$	35	520
Continuous fibers, uniaxial	38	1300

Hence based on the end application of the composite, its properties are improved by appropriate fiber form. If the primary goal is to increase the strength of a composite in one direction continuous fibers could be used and placed in the direction in which the composite has to bear the loads. Although to improve the overall performance of the composite short fibers could be used as they could be dispersed well within the matrix in different directions.

- b) **Fiber orientation:** Fiber composites are highly anisotropic, i.e. their properties are highly sensitive to fiber direction. Such as the Young's modulus of a fiber composite is determined by its elastic properties of the constituent materials and is dependent on the loading direction. The effect of carbon fiber orientation in epoxy laminate was considered by Chamis et al. [94]. When the SMA fibers are aligned parallel to the direction of application of the load (as shown in the schematic below), the modulus of the composite is higher in the fiber direction as the fiber is

stiffer than the polymer matrix. Conversely, in the transverse direction the composite is less stiff and hence has lower modulus (Figure 5.9).

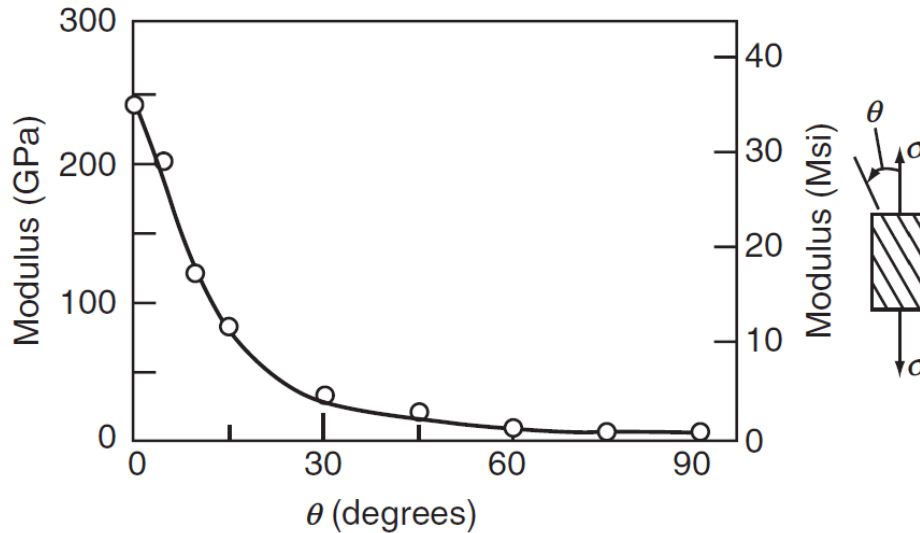


Figure 5.9 Above shows the variation of elastic modulus of carbon-epoxy laminate composite when subjected to tensile loads with orientation of the fiber[94].

c) **Fiber volume fraction:** In all systems the equations which predict the properties of a composite breakdown at high volume fractions of reinforcement because of geometric packing limitations and the necessity for the reinforcing phase to be surrounded by the matrix in order that load can be transferred to it. Usually two types of fiber packing methods are used to obtain the upper limit of the fiber volume fraction. These are a square array and a hexagonal array with circular section fiber reinforcements. From the Figure 5.10 below it is clear that the maximum volume fraction of fibers could not exceed 90% and even 78% volume fraction would be highly improbable to achieve. Hence it is a good practice to use a volume fraction of below 60% for unidirectional aligned fiber composites.

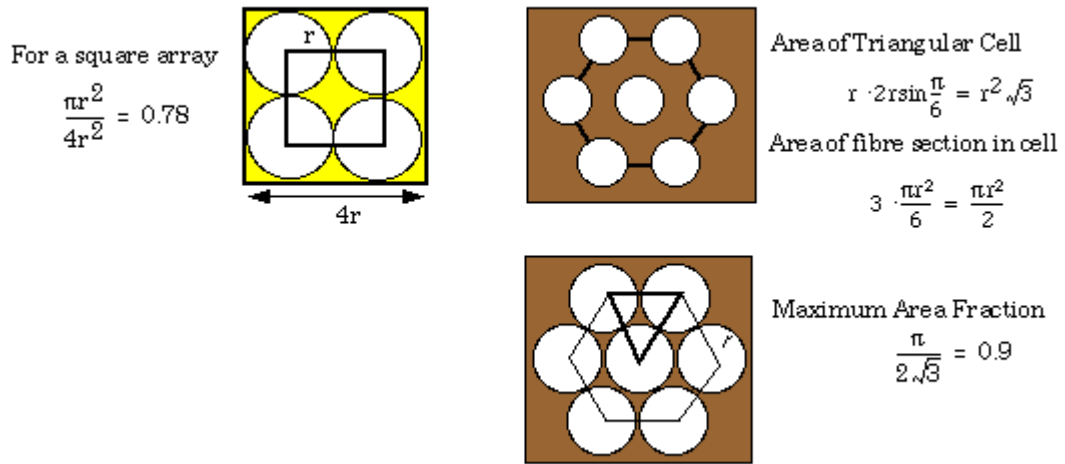


Figure 5.10 Above shows the fiber packing methods in place to obtain the maximum volume fraction of fiber that could be used in composite.

- d) Fiber size:** Lastly, it is necessary to consider an appropriate aspect ratio for SMA fiber. The strength of a composite depends on its fiber diameter, meaning fibers of smaller diameters produce composites of higher strength as they contain fewer surface defects.

Hence based on the above parameters, the design for unidirectional continuous SMA wire with loading parallel to the direction of the wire was generated in the SMP matrix using Representative Volume element method as discussed earlier for the SMA-particle SMP composite. The Figure 5.11 below shows the schematic of the model that could be used easily in the finite element analysis using RVE method. The bonding between the matrix and the wire was considered to be perfect as such the load transfer between the SMP matrix and SMA wire is possible.

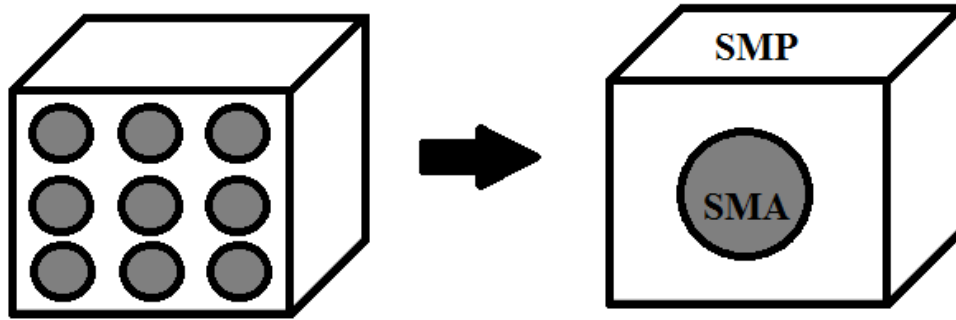


Figure 5.11 Above shows schematic of RVE of SMA-Wire in SMP composite.

Once the design of the SMA-SMP composite with both particle and fiber reinforcements were developed, the next in the modeling of the smart composite was to link these two constituent models in the finite element software (ABAQUS) to obtain the thermo-mechanical behavior of the SMA-SMP composite. In the section, the procedure to link the constitutive user subroutine that defines the complex thermo-mechanical behavior of the NiTi SMA is discussed in detail.

5.4.2 Linking SMA Model and SMP Model in ABAQUS

The user subroutine developed by Lagoudas et al. was used to in the present model to define the material properties of NiTi SMA in ABAQUS Standard: commercially available finite element software [88, 95]. ABAQUS Standard is general purpose finite element software that has a wide range of capabilities in terms of solving both linear and nonlinear problems involving the static, dynamic, thermal and electrical responses of a given material system used in conjunction with a specific component and application. Abaqus/Standard solves a system of equations implicitly at each solution “increment.” In contrast, Abaqus/Explicit marches a solution forward through time in

small time increments without solving a coupled system of equations at each increment (or even forming a global stiffness matrix).

5.4.2.1 Using User Subroutines in ABAQUS Standard

ABAQUS provides an extensive selection of user subroutines that allows the user to pick the type of subroutine based on the specific application. There are several different subroutines that are supported by ABAQUS when the user has to define a complicated nonlinear material behavior that make use of complex constitutive models that are not available in ABAQUS material models, non-uniform distributed mechanical load (pressures and body forces), to define complex ways in which friction could affect the behavior of the component, for example to describe the shear forces between the surfaces, to define the complex models for internal heat generation when a material undergoes a phase change, to define special types of elements that are not supported by ABAQUS/Standard etc.

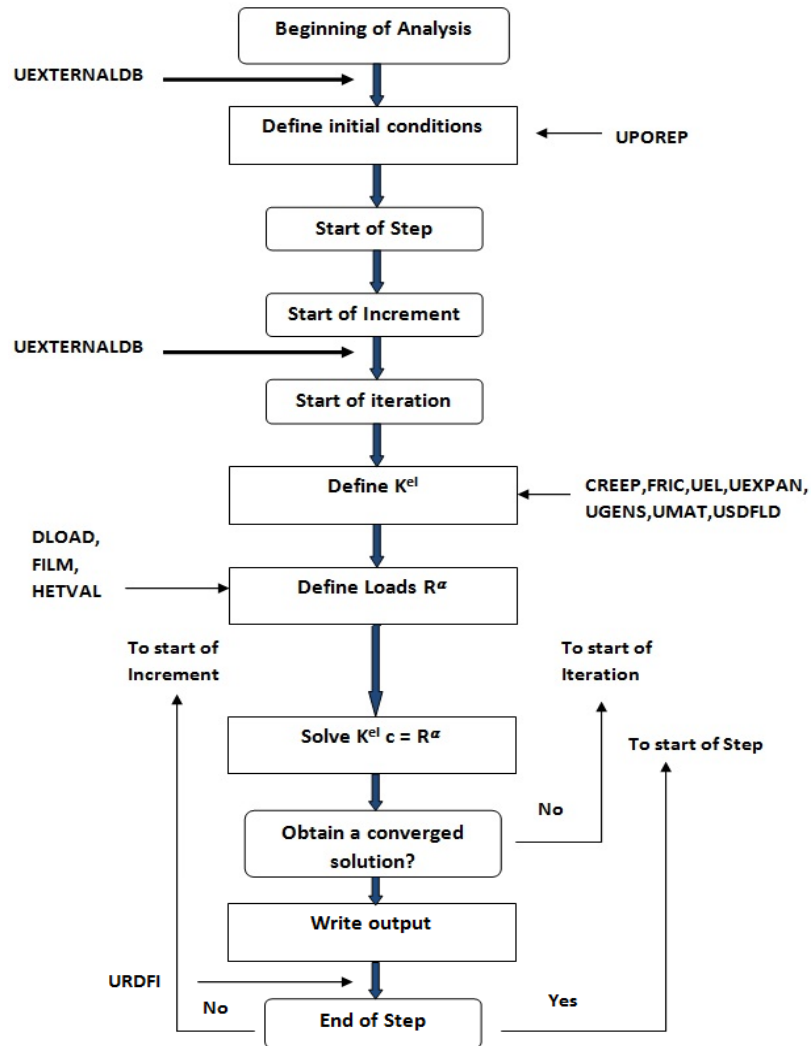


Figure 5.12 The above flow chart shows different stages at which the subroutines are called in the general analysis in ABAQUS/Standard [95].

The loads and stiffness matrices are applied and calculated in iterations and the stiffness matrix is updated at the end of each iteration. In the first iteration all of the subroutines shown in the flow chart above are called twice. In the first call the initial stiffness matrix is formed using the configuration of the model at the start of the increment. In the second call a new stiffness matrix is based on the updated stiffness from the first last iteration.

To include the user subroutines in the model, the name of the user subroutine file built by the user by an object or Fortran source code needs to be used along with the name of analysis file in ABAQUS execution command window.

5.4.3 Compiling and Linking User Subroutines with ABAQUS

It is important to use the correct compile and link commands when using a user defined subroutine. ABAQUS includes the correct compile and link commands for every platform on which it is supported in the default environment file (abaqus.env) located in the “abaqus_dir/site directory”. "abaqus_dir" is the directory in which ABAQUS was installed. Using a Fortran compiler that is compatible with those supported by the software is essential as well for proper implementation of the subroutine. The Fortran compilers that are compatible with ABAQUS are provided in their online support section. Every user subroutine in ABAQUS/Standard must include the statement: INCLUDE ‘ABA_PARAM.INC’ as the first statement after the argument list. This file is saved on the system during the installation of the software. Additionally when the variables are exchanged between the main user subroutine and subsequent subroutines, the user should specify the above include statement in all the subroutines to preserve precision.

- i. ***Subroutine argument list:*** There are three types of variables that could be given to a subroutine through an argument list. These are the variables to be defined, variable that can be defined and those that are defined for obtaining information. The variables that are used to obtain information from the analysis should not be altered as that could lead to unpredictable results.
- ii. ***Solution dependent state variables (SDVs):*** These are the variables that evolve during the analysis based on the solution of an analysis. Strain would be a

solution dependent state variable in the user subroutine UEL. Although several subroutines support the use of SDVs, the evolution of these variables needs to be specified by the user and space needs to be allocated to store the SDVs. The number of such variables that are required at the integration points or the nodes are given by the statement “*DEPVAR” with a data value specifying the number of SDVs. For example in the user subroutine for material (UMAT), the SDVs are defined as shown below:

```
*USER MATERIAL
*DEPVAR
8
```

This means there 8 solution dependent state variables that need to be defined at each node for this particular user material subroutine. And space for the evolution of these 8 SDVs is allocated accordingly.

Following steps are to be taken into consideration while writing a UMAT:

1. The constitutive equation should be defined properly by including the explicit definition of stress (Cauchy stress for large-strain applications) or definition of stress rate only
2. It could be necessary to define the internal state variables either specifically or in the rate form. Definition of dependence on time, temperature and field variables.
3. Finally, transforming the constitutive rate equation into incremental equation using suitable integration procedure.

Several variables could be defined in the UMAT subroutine such as stress, strain SDVs at the start of the increment, total and incremental values of time, temperature and user-defined filed variables, material constants, element, integration points and current step and increment numbers etc. Out of these the values of stress, SDVs and material Jacobian must be defined in the UMAT subroutine. In the current project, the already developed user subroutine by Qidwai and Lagoudas for a NiTi SMA material was used for our SMA RVE in conjunction with the hyper elastic Ogden material model for the SMP matrix. The finite element models for both SMA-particle + SMP composite and SMA-wire + SMP composite are presented in the next section.

5.5 SMA-SMP COMPOSITE

The SMA-SMP composites were designed through numerical simulations via commercial finite element program, ABAQUS. The SMP matrix was modeled with the Ogden strain energy function, by using the material coefficients shown in Table 5.2.

Table 5.2 Summary of Ogden Coefficients for the SMP.

Temperature	μ_1	α_1	μ_2	α_2
30°C	380.920	18.333	-182.824	-9.277
35°C	241.345	13.313	-117.241	-6.701
45°C	73.8194	14.690	-35.211	-7.425
50°C	16.5839	11.603	-6.782	-6.084
55°C	2.25313	2.064	-0.820	-2.152

The SMA fillers were modeled with the Lagoudas model, by using the material parameters shown in Table 5.3. The Lagoudas model was implemented in ABAQUS through a user subroutine as discuss before.

Table 5.3 Summary of Material coefficients for the SMA [88].

Material Parameter	Value
Austenite elastic modulus E^A	70 GPa
Martensite elastic modulus E^M	30 GPa
Poisson's ratio ν	0.33
Austenite coefficient of thermal expansion α^A	$22.0 \times 10^{-6}/K$
Martensite coefficient of thermal expansion α^M	$22.0 \times 10^{-6}/K$
Martensite start temperature M^{0s}	$17^\circ C$
Martensite finish temperature M^{0f}	$-3^\circ C$
Austenite start temperature A^{0s}	$21^\circ C$
Austenite finish temperature A^{0f}	$41^\circ C$
Maximum transformation strain H	0.05
Austenite stress influence coefficient $\rho\Delta s^A$	-0.35 MPa/K
Martensite stress influence coefficient $\rho\Delta s^M$	-0.35 MPa/K

Two types of composites were designed: SMA particle-SMP composite and SMA fiber-SMP composite which are presented in this section.

5.5.1 SMA Particle SMP Composite

The SMA-particle + SMP composite was built in ABAQUS using the RVE method as discussed earlier. Half of the model was used in the current analysis as it reduces the solution time as shown in the schematic below (Figure 5.13) for 50% SMA (by weight)-SMP composite. Different weight fractions of SMA were used ranging from

0 (SMP) % to 50%. The particle size was kept constant at 150 microns and the dimensions of the SMP matrix were varied according the weight fractions of the SMA particles thus resulting in SMCs with different SMA filler contents. After which the material properties were defined as discussed before using the user subroutine for SMA fillers and Ogden's strain energy functions for SMP matrix. For the next step the part composite part was then meshed using a three dimensional, reduced integrated, second order, solid elements with hybrid elements for SMP matrix (C3D8RH) where as for the SMA filler a three dimensional solid with 8 nodes was used. The bottom surface was fixed in all directions and a displacement load of 7% of the matrix height was applied on the top surface. The stress-strain curves were obtained at different temperatures ranging from RT to 55°C. From the elastic part of the loading curve, modulus values were extracted for different weight fractions of the SMA fillers. The results are presented in the next section.

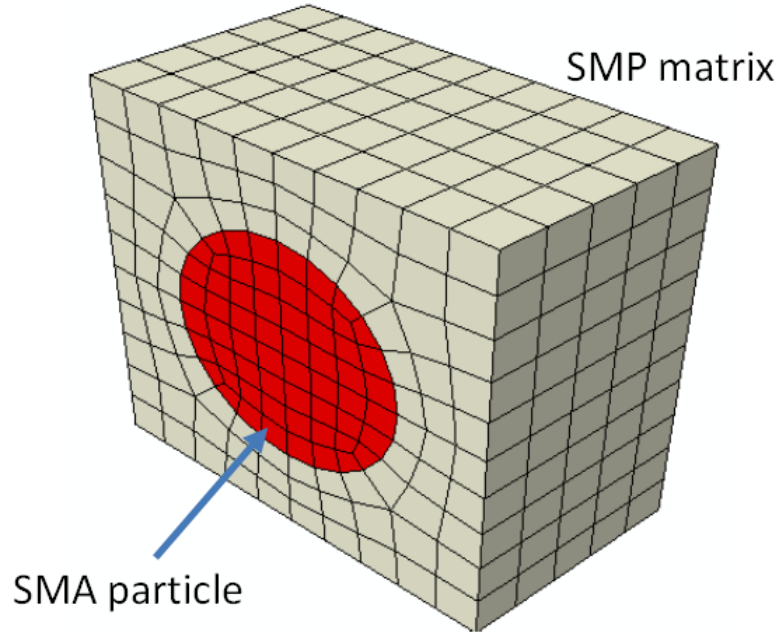


Figure 5.13 Shows the schematic of SMA (50% by weight) + SMP Particle composite FE model built in ABAQUS CAE.

5.5.2 SMA Fibre-SMP Composite

Similar to the particle composite, SMA wire was used as the reinforcing filler in the SMA-Wire + SMP composite. The FE model using the RVE of the wire was built with the SMA positioned at the center of the matrix and extending continuously throughout the length of the matrix (Figure 5.14). The diameter of the SMA wire used was 200 microns. Different weight fractions of SMA wire were generated by changing the dimensions of the SMP matrix from 0%(SMP) to 50%. Similar to the particle reinforced composite, the nodes on the bottom surface were fixed and in all directions and a uniform compressive displacement load of about 7% was applied to the nodes on the top surface. As discussed in the previous sections, the application of load based on the alignment of the SMA wires plays a crucial in improving the mechanical properties of the

composite as a whole. As the goal is to improve the modulus of the composite, the load was applied in the longitudinal direction of the wires instead of in the transverse direction. The element types used were the same as those in the particle composites.

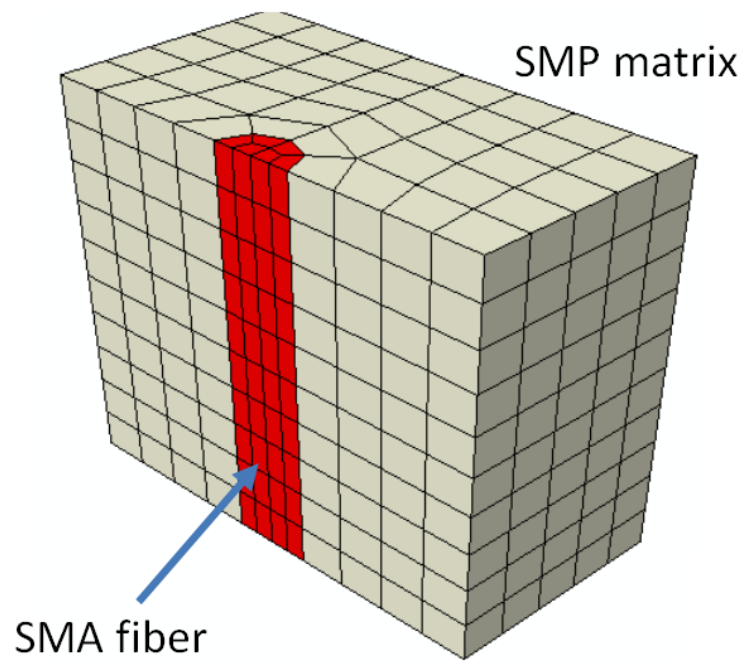
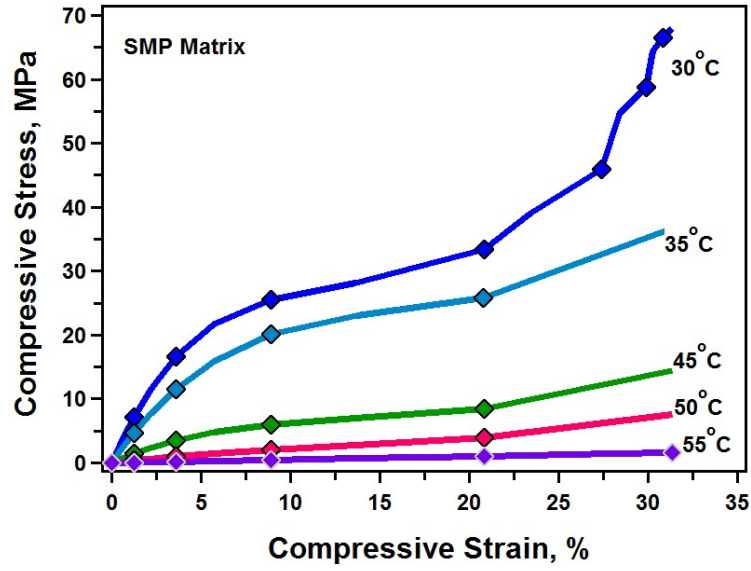


Figure 5.14 Shows the schematic of SMA (50% by weight) + SMP Wire composite FE model built in ABAQUS CAE.

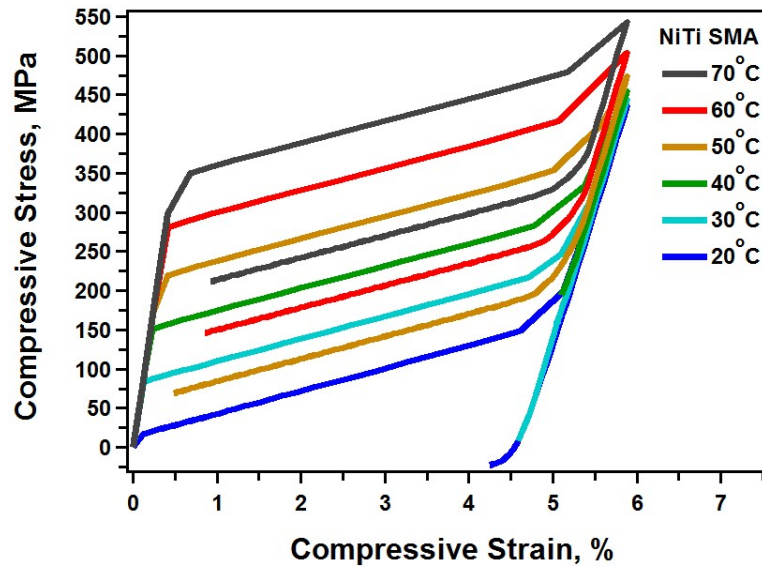
5.6 RESULTS AND DISCUSSION

5.6.1 Modeling of SMP and SMA

The mechanical responses of the SMA and SMP were simulated in compression and the stress-strain curves were obtained.



(a)



(b)

Figure 5.15 Shows the stress-strain response of (a) SMP matrix and (b) SMA reinforcement at different loading temperatures.

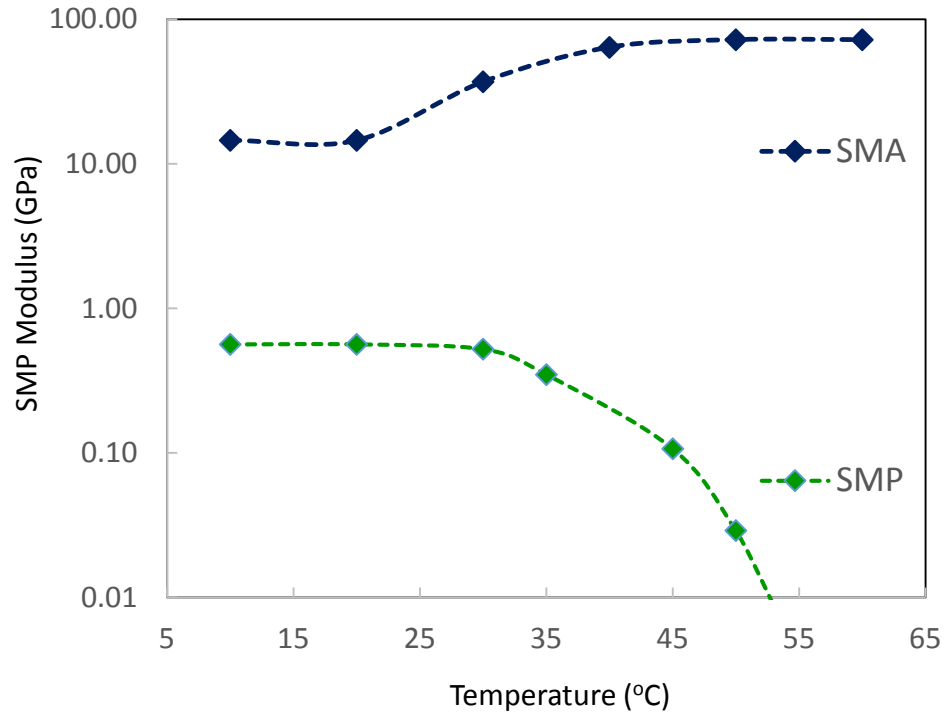


Figure 5.16 Variations of elastic modulus with temperature of the present SMA and SMP.

From the stress-strain curves shown below (Figure 5.15), the temperature dependent elastic modulus were computed, as shown in Figure 5.16.

As the temperature increases, the elastic modulus of the SMP decreases while the elastic modulus of the SMA increases. The trends are identical to the well-known schematic by Tobushi. A composite which combines the characteristics of both SMA and SMP would have appropriate mechanical strength in all temperatures.

5.6.2 SMA Particle – SMP Composites

The stress-stress responses of SMA-particle + SMP composite was modeled in ABAQUS CAE, using Lagoudas thermos-mechanical model for SMA and Ogden’s strain energy model for SMP. The Figure 5.17-Figure 5.22 below show the predicted results at

various temperatures. The stress-strain responses at different particle loading are given in this section. The typical hyper-elastic material behavior is observed in the shape memory particle composites. The composite is glassy and strong at room temperature and deforms elastically at temperatures above T_g of the SMP. Large deformations ($\sim 20\%$ strain) were observed.

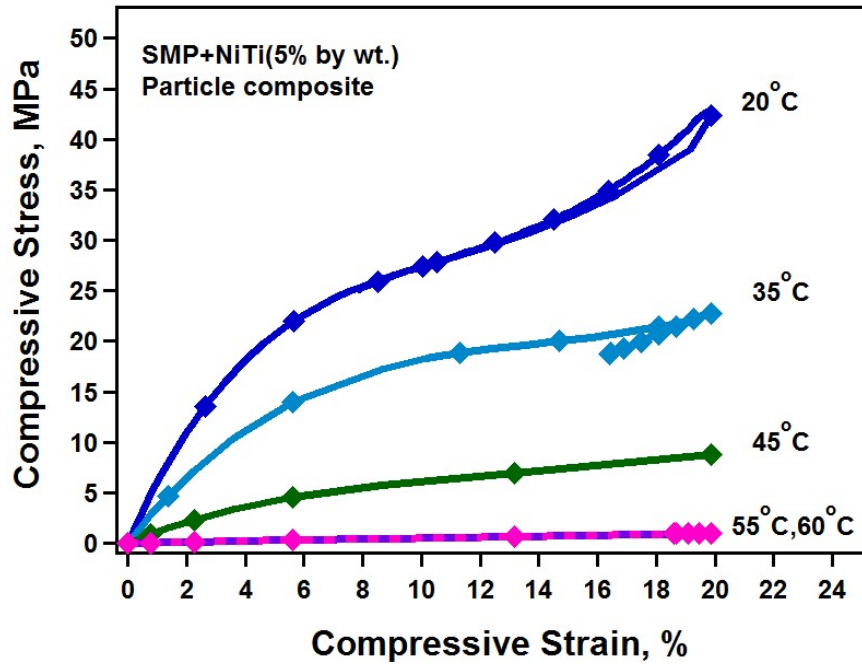


Figure 5.17 Shows the stress-strain response of NiTi 5% (by wt.) + SMP particle composite with different loading temperatures.

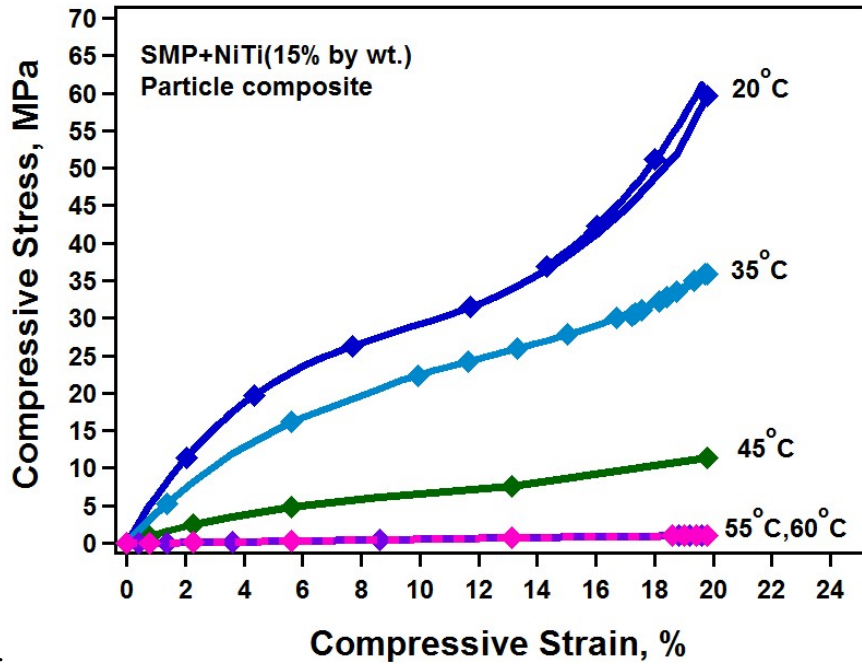


Figure 5.18 Shows the stress-strain response of NiTi 15% (by wt.) + SMP particle composite with different loading temperatures.

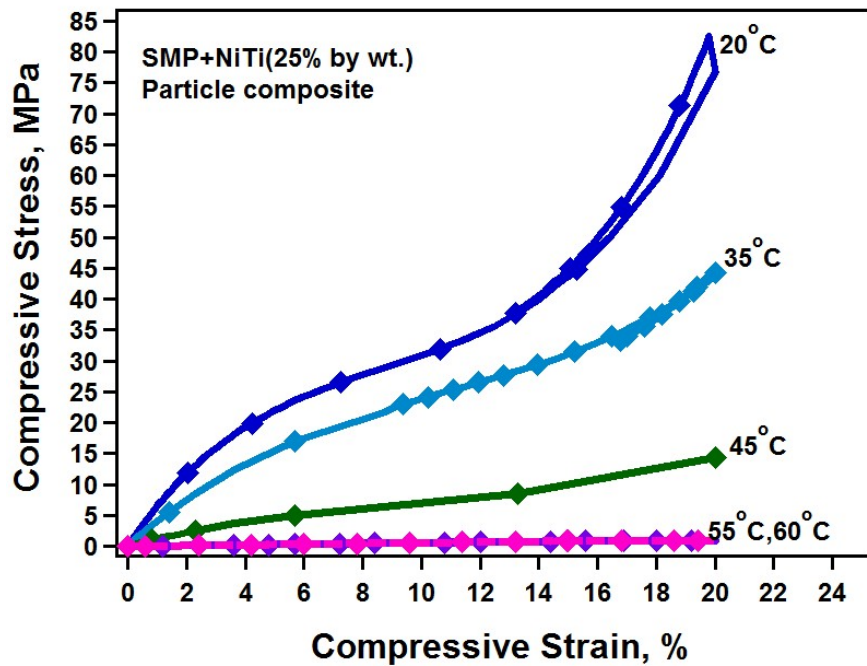


Figure 5.19 Shows the stress-strain response of NiTi 25% (by wt.) + SMP particle composite with different loading temperatures.

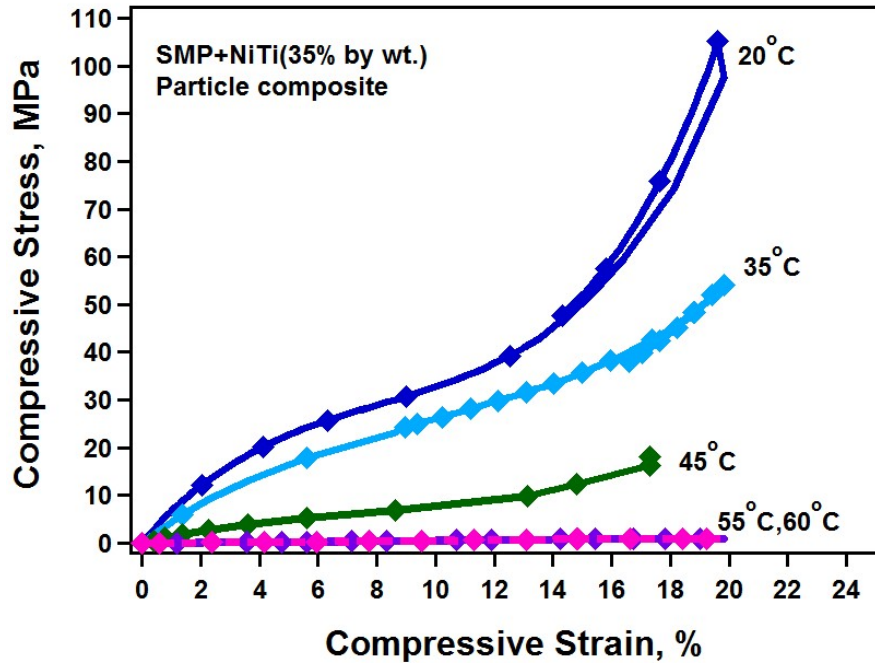


Figure 5.20 Shows the stress-strain response of NiTi 35% (by wt.) + SMP particle composite with different loading temperatures.

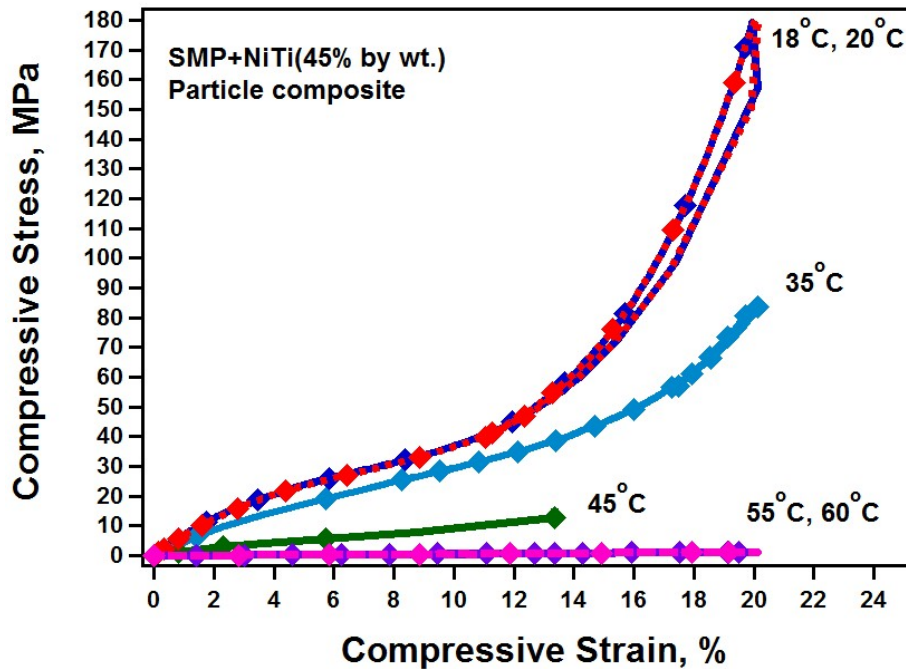


Figure 5.21 Shows the stress-strain response of NiTi 45% (by wt.) + SMP particle composite with different loading temperatures.

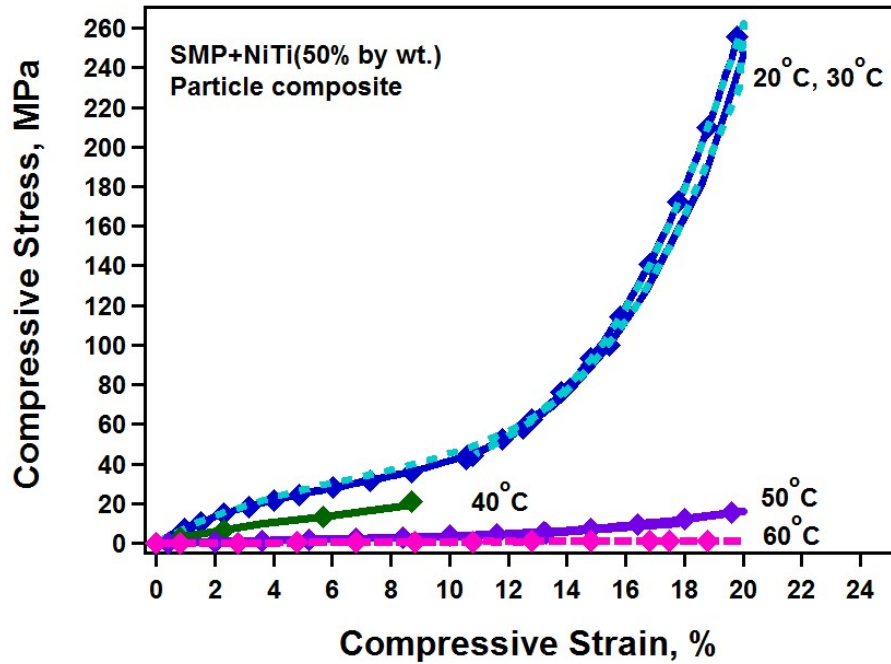


Figure 5.22 Shows the stress-strain response of NiTi 50% (by wt.) + SMP particle composite with different loading temperatures.

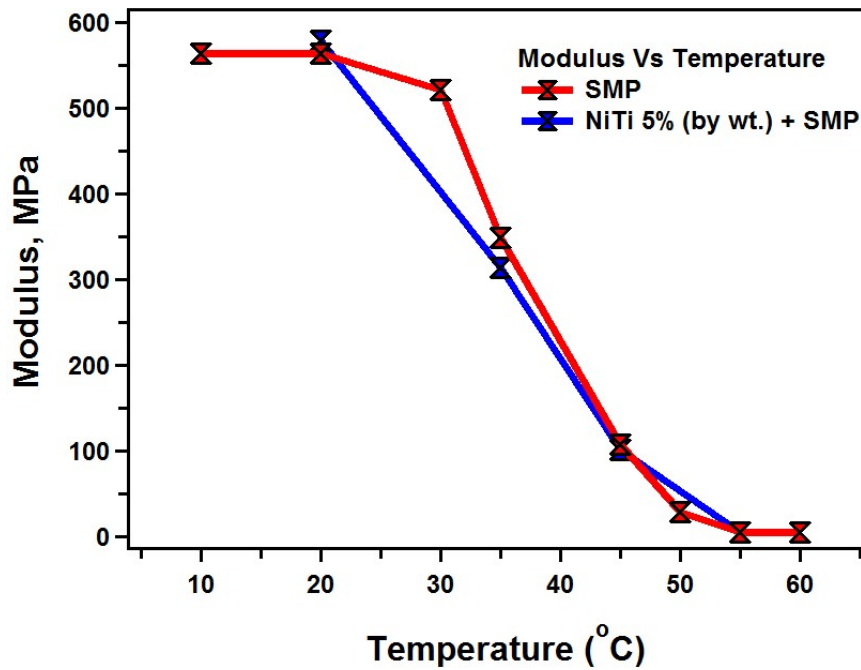


Figure 5.23 Shows the variation of modulus with temperature in NiTi 5% (by wt.) + SMP particle composite in comparison to that of SMP.

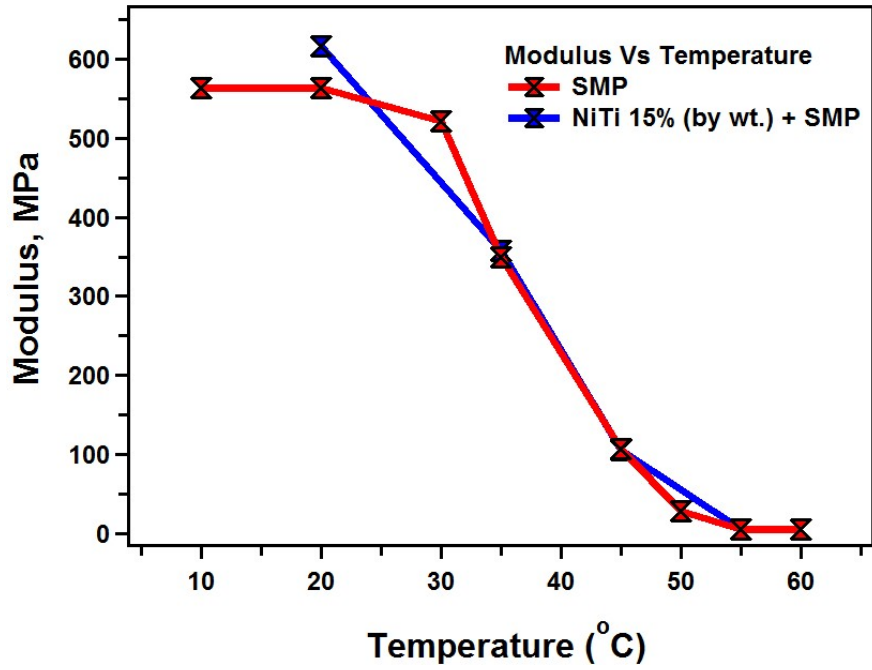


Figure 5.24 Shows the variation of modulus with temperature in NiTi 15% (by wt.) + SMP particle composite in comparison to that of SMP.

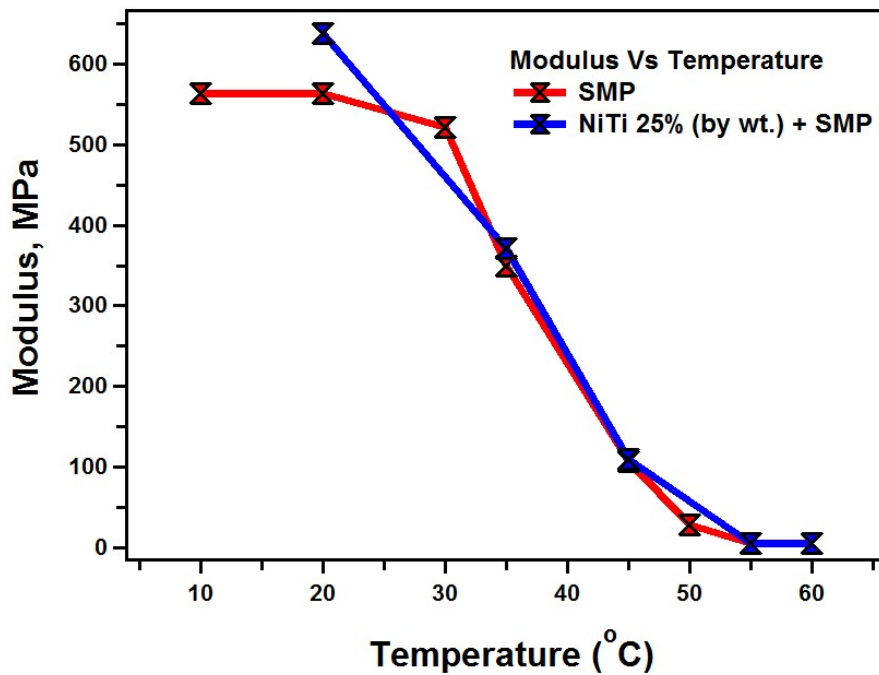


Figure 5.25 Shows the variation of modulus with temperature in NiTi 25% (by wt.) + SMP particle composite in comparison to that of SMP.

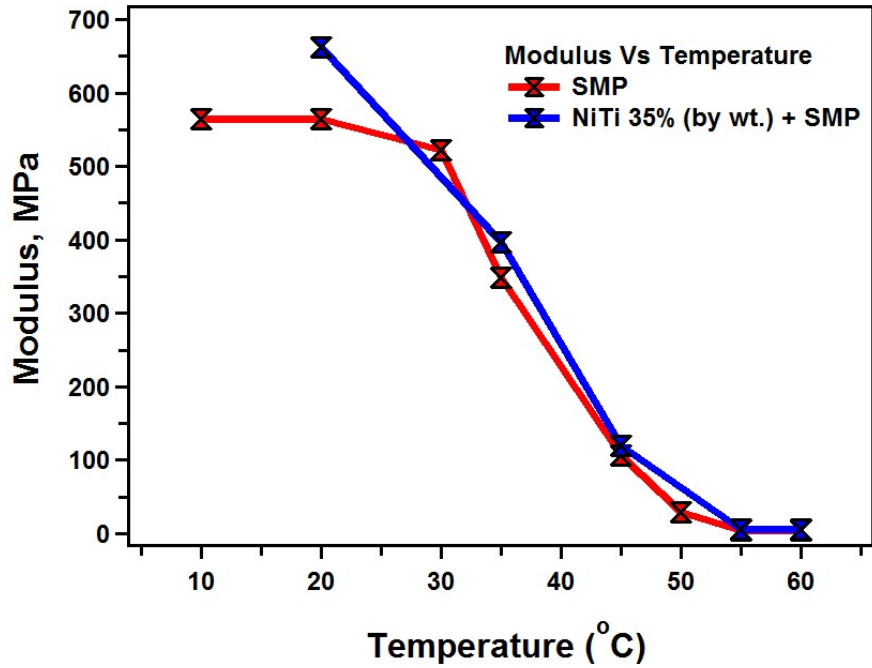


Figure 5.26 Shows the variation of modulus with temperature in NiTi 35% (by wt.) + SMP particle composite in comparison to that of SMP.

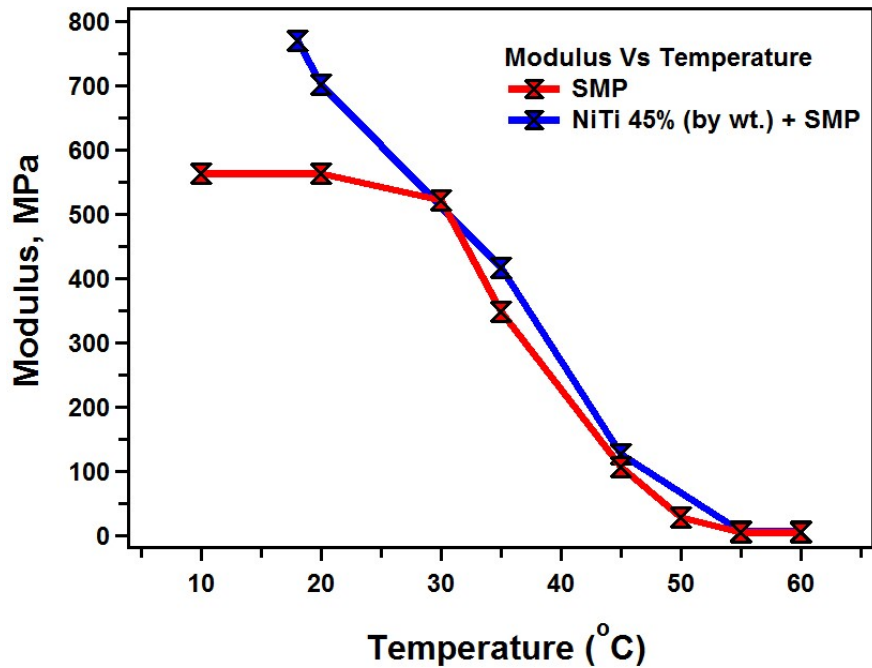


Figure 5.27 Shows the variation of modulus with temperature in NiTi 45% (by wt.) + SMP particle composite in comparison to that of SMP.

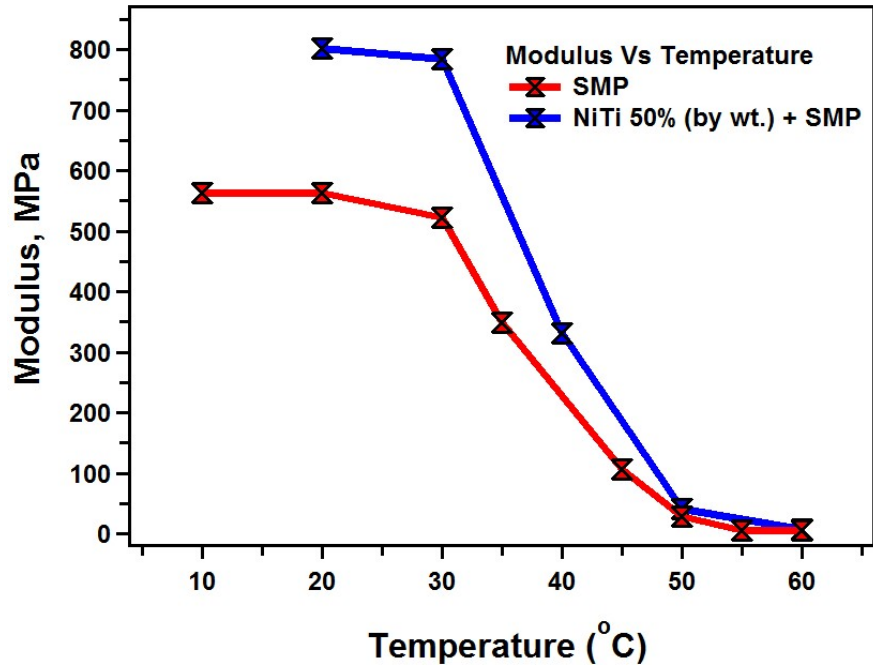


Figure 5.28 Shows the variation of modulus with temperature in NiTi 50% (by wt.) + SMP particle composite in comparison to that of SMP.

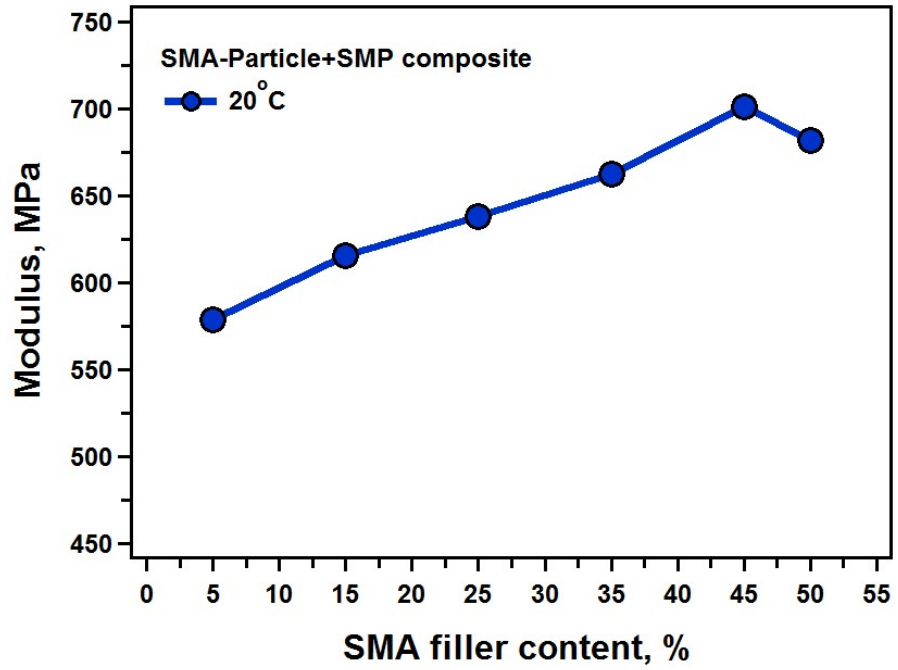


Figure 5.29 Variation of Modulus of SMA-Particle + SMP composite with SMA filler content with a loading temperature of 20°C.

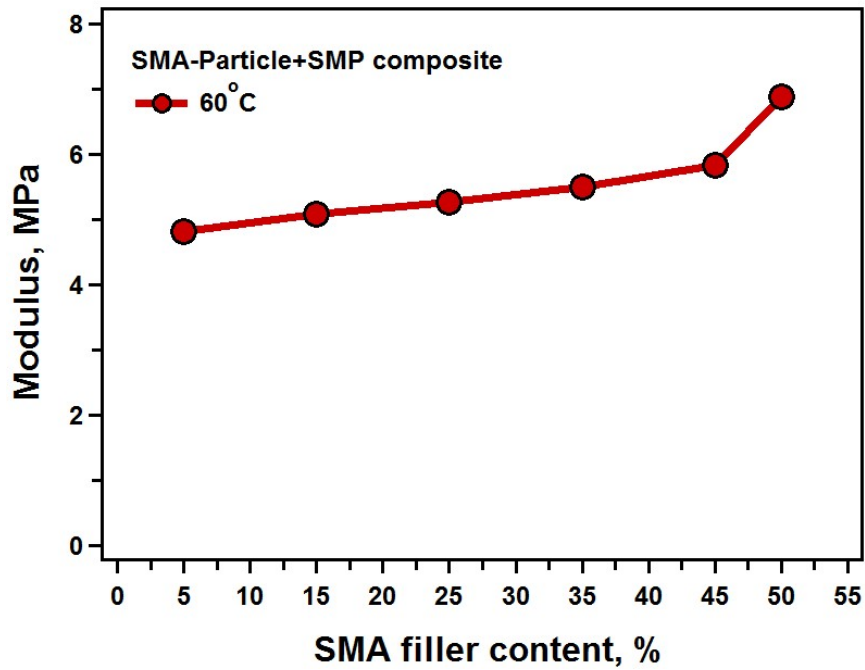


Figure 5.30 Variation of Modulus of SMA-Particle + SMP composite with SMA filler content with a loading temperature of 60°C.

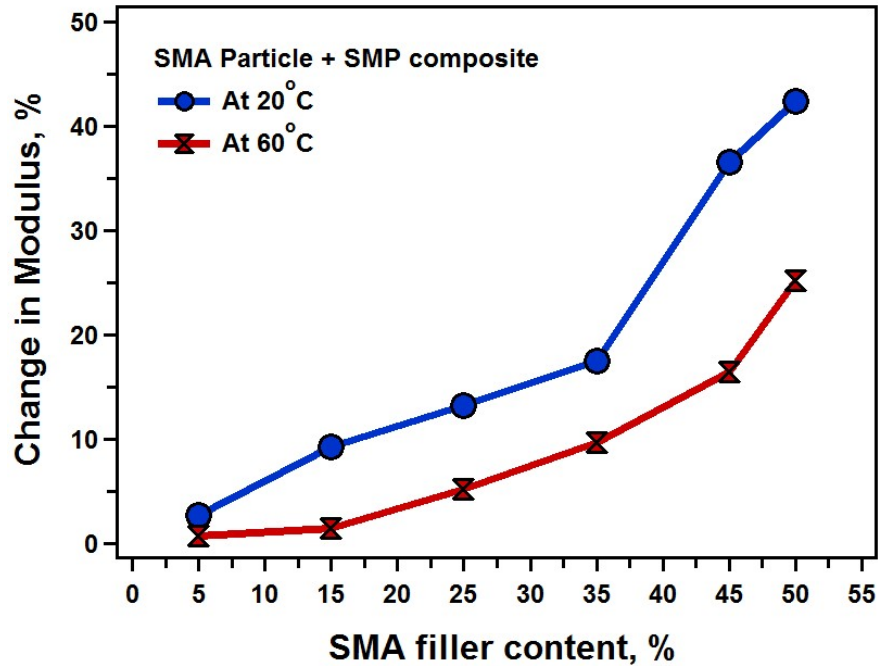


Figure 5.31 Change in Modulus of SMA+SMF particle composite with SMA filler content.

From the Figure 5.23-Figure 5.28, we can see that modulus of SMA-particle + SMF composite has increased considerably compared to that of SMF. The change in modulus at temperatures below (20°C) and above (60°C) T_g of SMF is shown in the Figure 5.31. We can see that for each filler content the increase in modulus of the composite is significant at 20°C than that at 60°C. And for both the temperatures, there is gradual increase in modulus with addition of filler content Figure 5.29-Figure 5.30. The change in modulus is significantly higher around 45% at 20C and 25% at 60C for 50% SMA filler content as expected. This is because as the filler content increases, the effective modulus of a composite material increases when there is perfect bonding between the particle fillers and the matrix enabling complete load transfer between the filler reinforcements and the matrix.

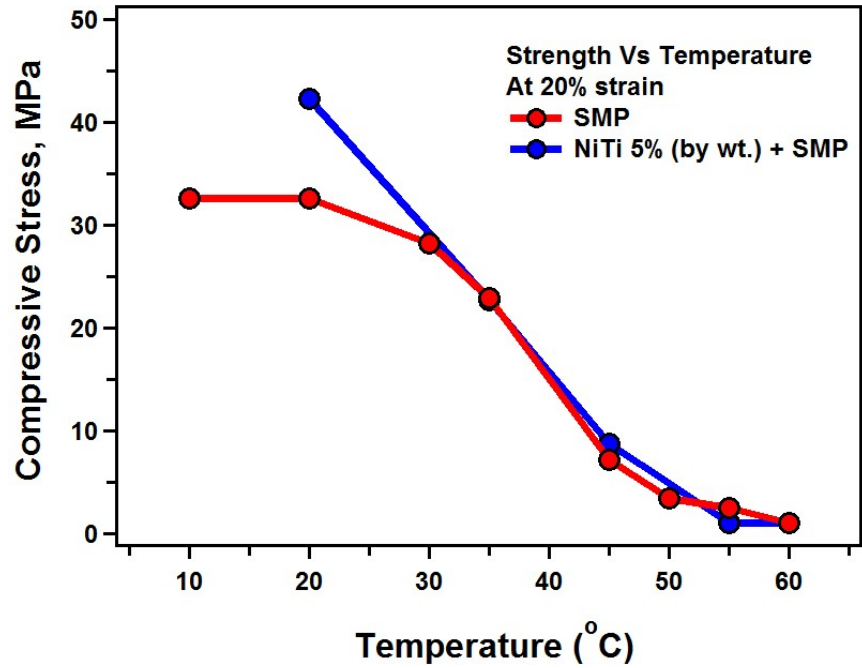


Figure 5.32 Shows the variation of strength with temperature in NiTi 5% (by wt.) + SMP particle composite in comparison to that of SMP at 20% compressive strain.

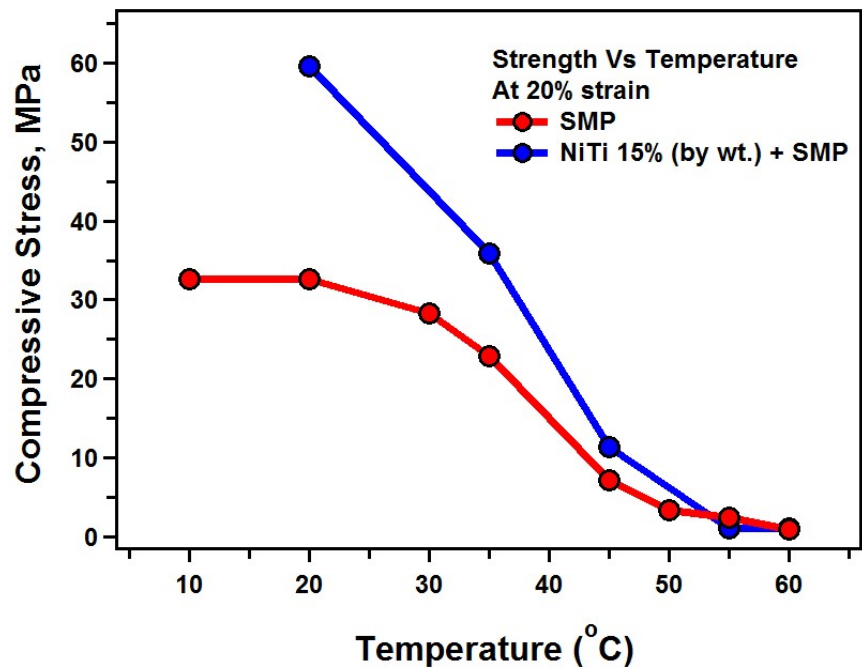


Figure 5.33 Shows the variation of strength with temperature in NiTi 15% (by wt.) + SMP particle composite in comparison to that of SMP at 20% compressive strain.

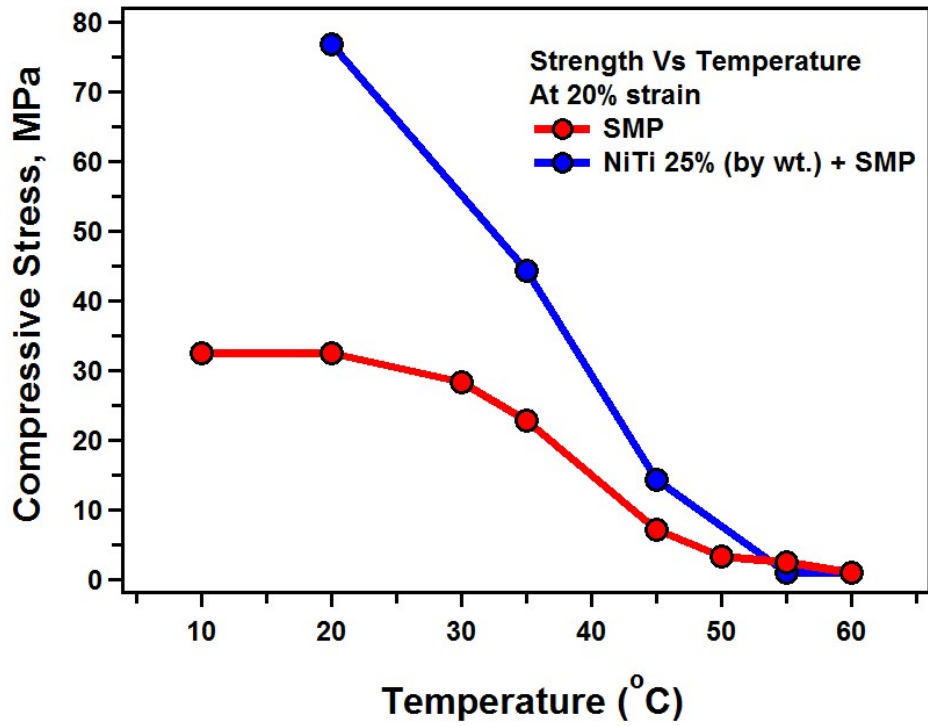


Figure 5.34 Shows the variation of strength with temperature in NiTi 25% (by wt.) + SMP particle composite in comparison to that of SMP at 20% compressive strain.

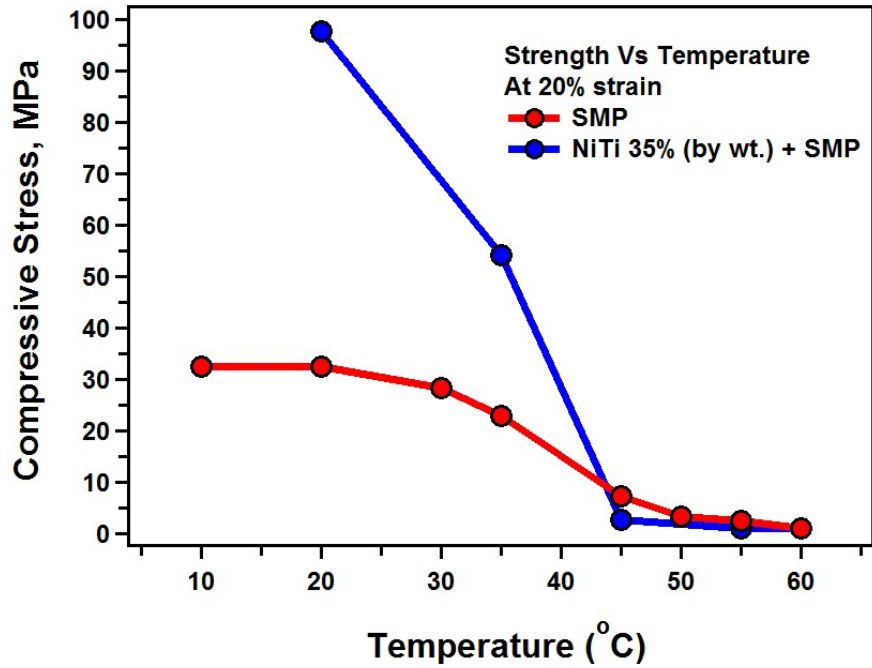


Figure 5.35 Shows the variation of strength with temperature in NiTi 35% (by wt.) + SMP particle composite in comparison to that of SMP at 20% compressive strain.

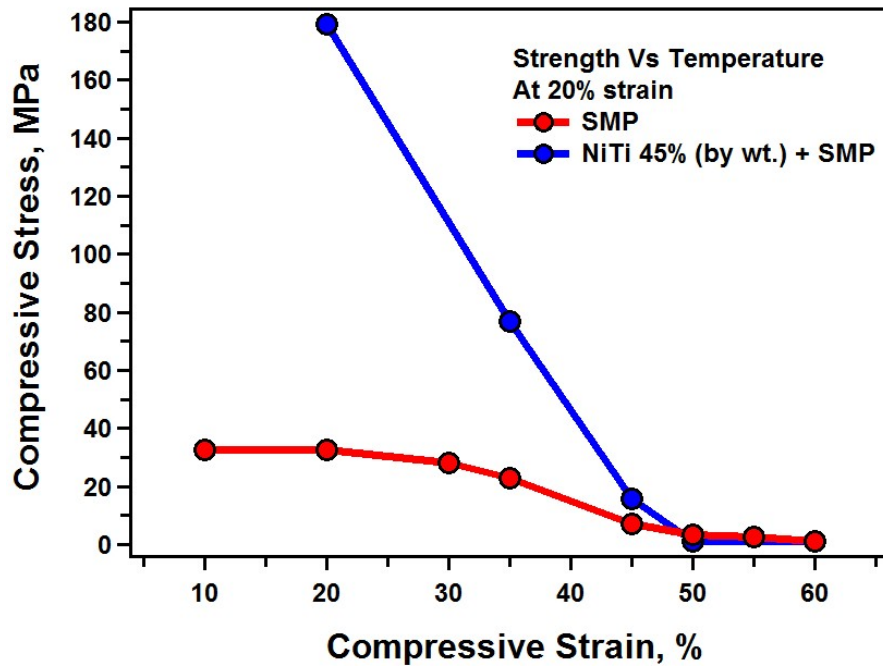


Figure 5.36 Shows the variation of strength with temperature in NiTi 45% (by wt.) + SMP particle composite in comparison to that of SMP at 20% compressive strain.

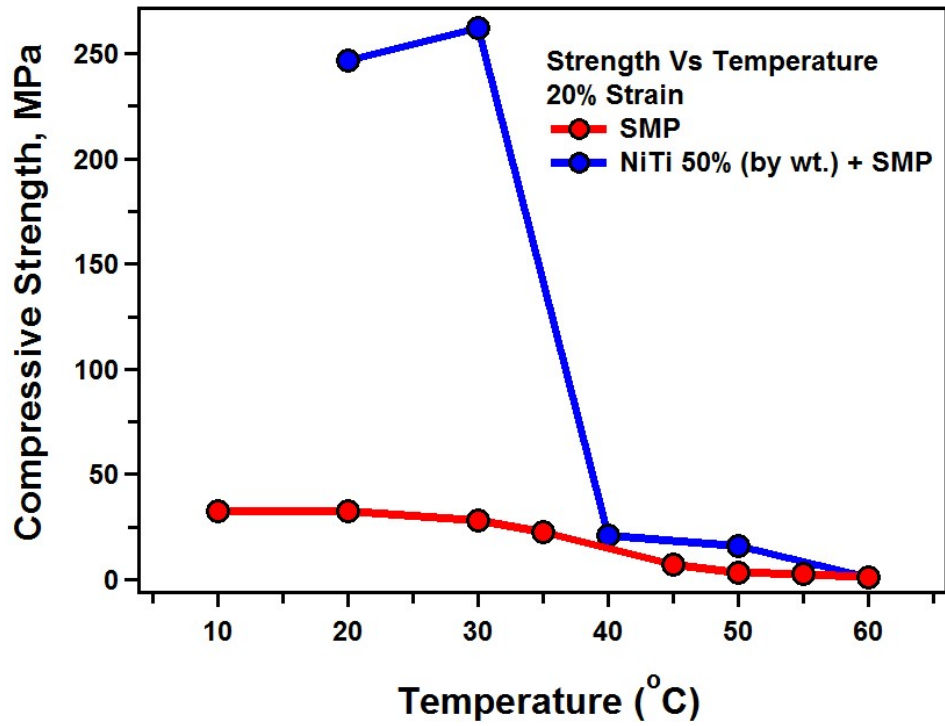


Figure 5.37 Shows the variation of strength with temperature in NiTi 50% (by wt.) + SMP particle composite in comparison to that of SMP at 20% compressive strain.

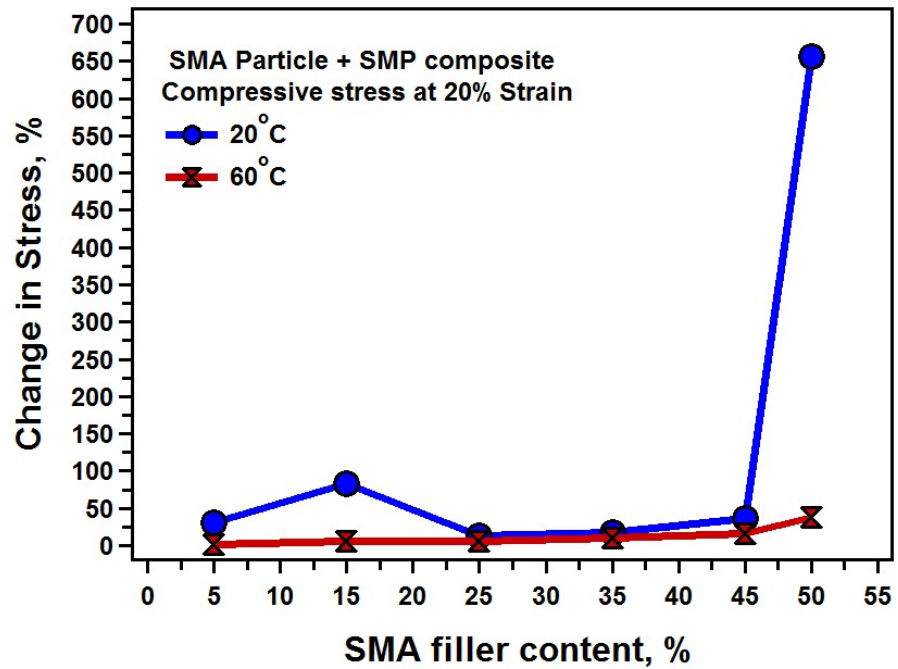


Figure 5.38 Change in Strength of SMA+SMP particle composite with SMA filler content.

From Figure 5.38 we can see that there is not much improvement in the strength of the composite with lower filler contents. But there is sudden rise in the change in strength at 20°C by approximately 660%. However, the strength drops drastically as the temperature of the composite rises above T_g . This could be due to the domination of rubber phase of the SMP at higher temperatures. When a polymer with higher T_g is chosen as a matrix for the SMA reinforcements, the resulting composite system would then have higher strength at elevated temperatures. As the polymer with higher T_g would be more stable at higher temperatures. Another reason could be that at lower filler content, there is not enough reinforcements to carry the load being applied on to the system and as the filler contents increase, load carrying capacity of the composite increases and thereby increasing the overall strength of the composite as is evident in the present case of 50% filler content.

5.6.3 SMA Fibre – SMP Composites

Hence, in order to obtain improvement in the mechanical strength and modulus, in the section, SMA-fiber + SMP composites are considered. In these composites, continuous SMA fiber is used as a reinforcing material extending throughout the matrix, aligned in the direction of application of the compressive loads. Figures 5.39 to 5.44 show the stress-strain behavior obtained from the simulation results. From the stress-strain curves, the modulus and strength of various filler contents of SMA Fiber + SMP composites were calculated. These results for modulus and strength are given in the figures 5.46 to 5.50 and in the figures 5.55 to 5.60 respectively.

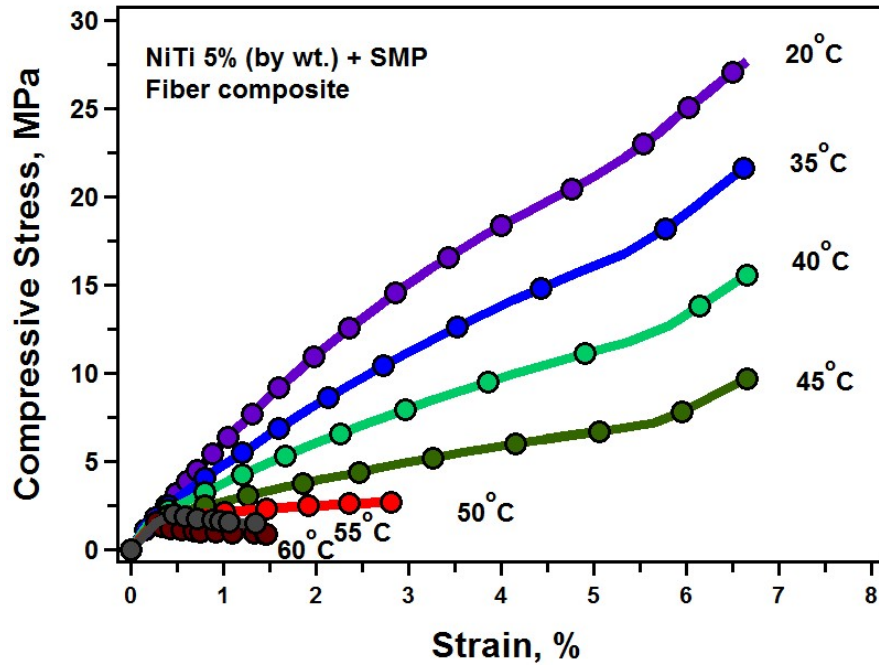


Figure 5.39 Shows the stress-strain response of NiTi 5% (by wt.) + SMP fiber composite at various temperatures.

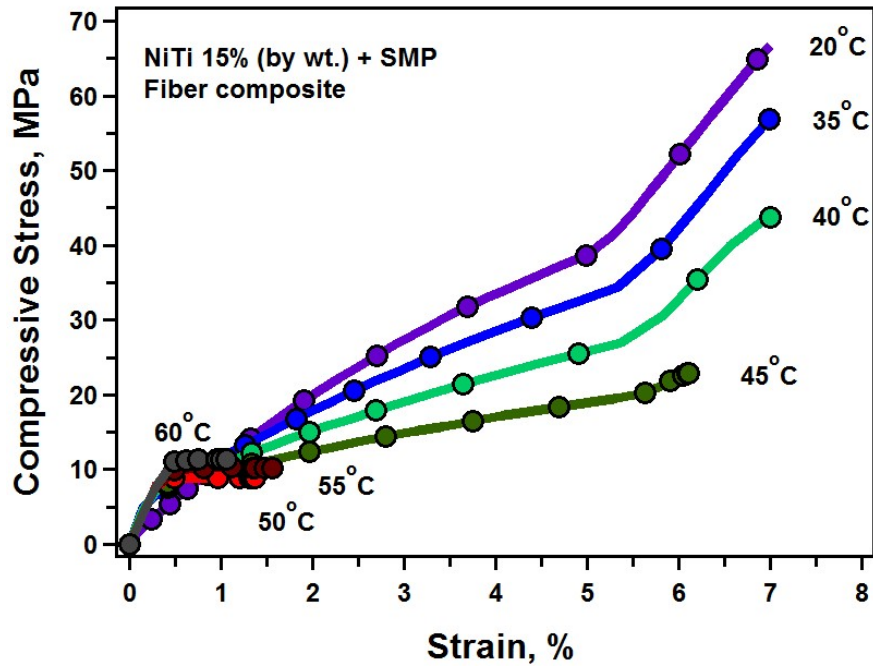


Figure 5.40 Shows the stress-strain response of NiTi 15% (by wt.) + SMP fiber composite at various temperatures.

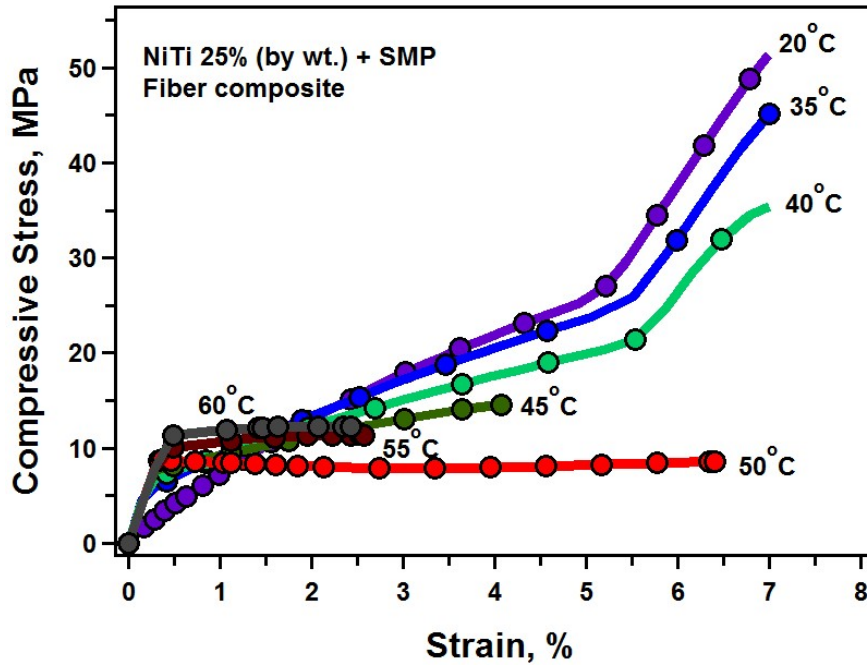


Figure 5.41 Shows the stress-strain response of NiTi 25% (by wt.) + SMP fiber composite at various temperatures.

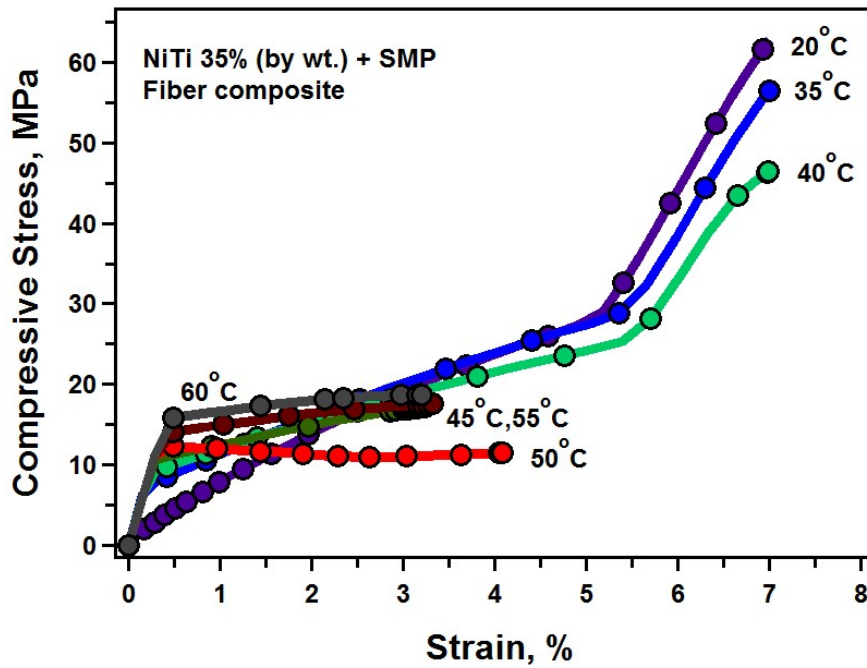


Figure 5.42 Shows the stress-strain response of NiTi 35% (by wt.) + SMP fiber composite at various temperatures.

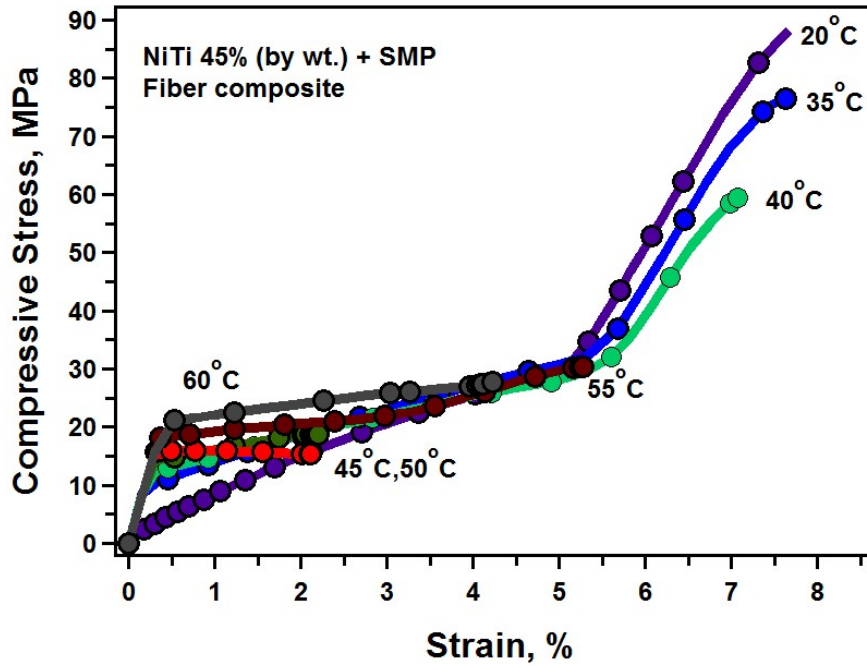


Figure 5.43 Shows the stress-strain response of NiTi 45% (by wt.) + SMP fiber composite at various temperatures.

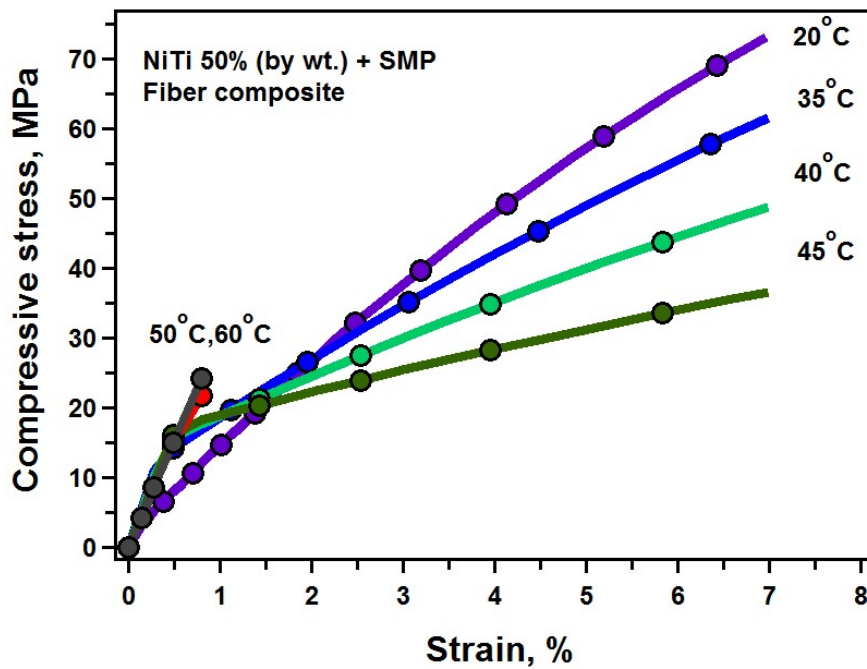


Figure 5.44 Shows the stress-strain response of NiTi 50% (by wt.) + SMP fiber composite at various temperatures.

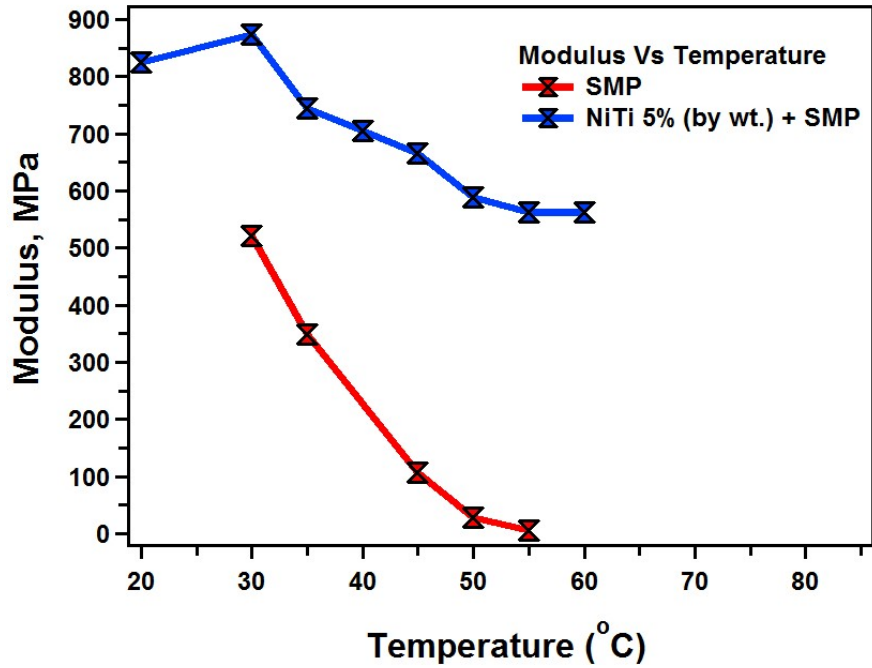


Figure 5.45 Shows the variation of modulus with temperature in NiTi 5% (by wt.) + SMP fiber composite in comparison to that of SMP.

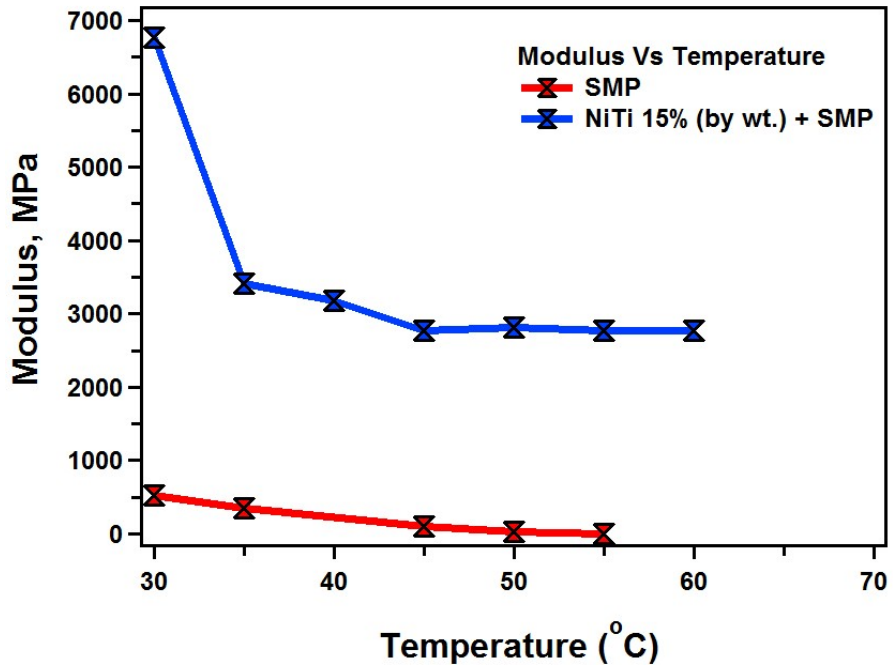


Figure 5.46 Shows the variation of modulus with temperature in NiTi 15% (by wt.) + SMP fiber composite in comparison to that of SMP.

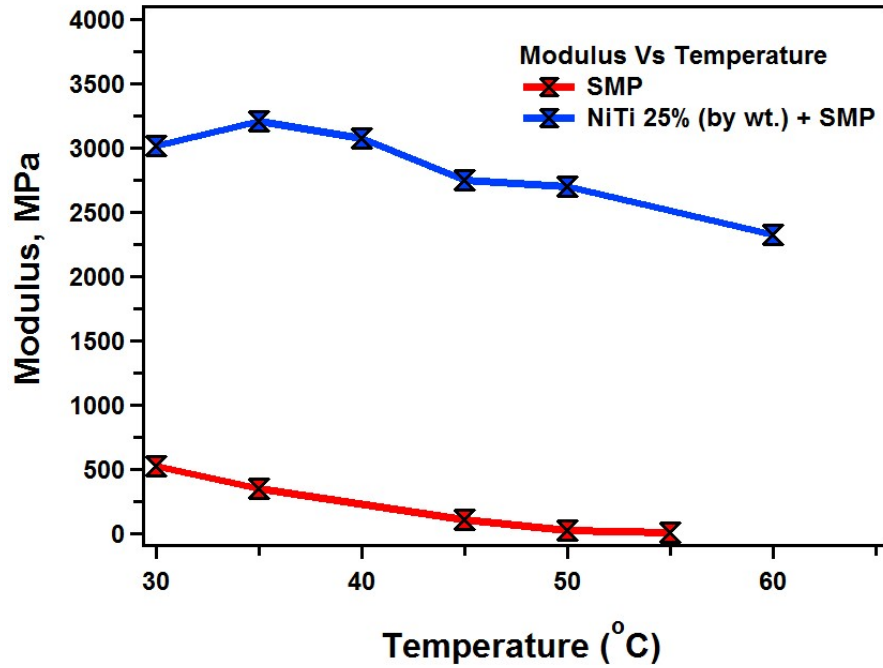


Figure 5.47 Shows the variation of modulus with temperature in NiTi 25% (by wt.) + SMP fiber composite in comparison to that of SMP.

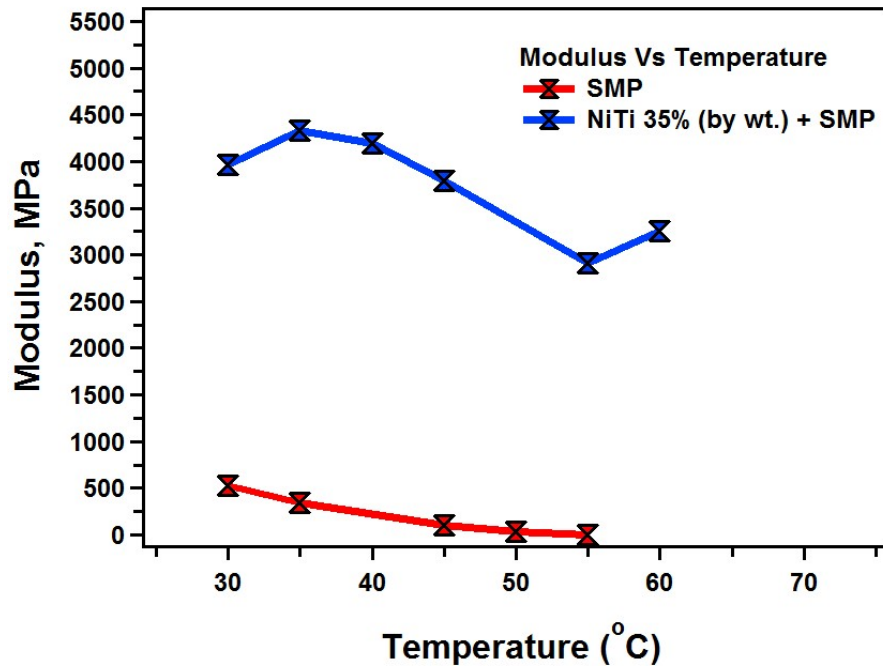


Figure 5.48 Shows the variation of modulus with temperature in NiTi 35% (by wt.) + SMP fiber composite in comparison to that of SMP.

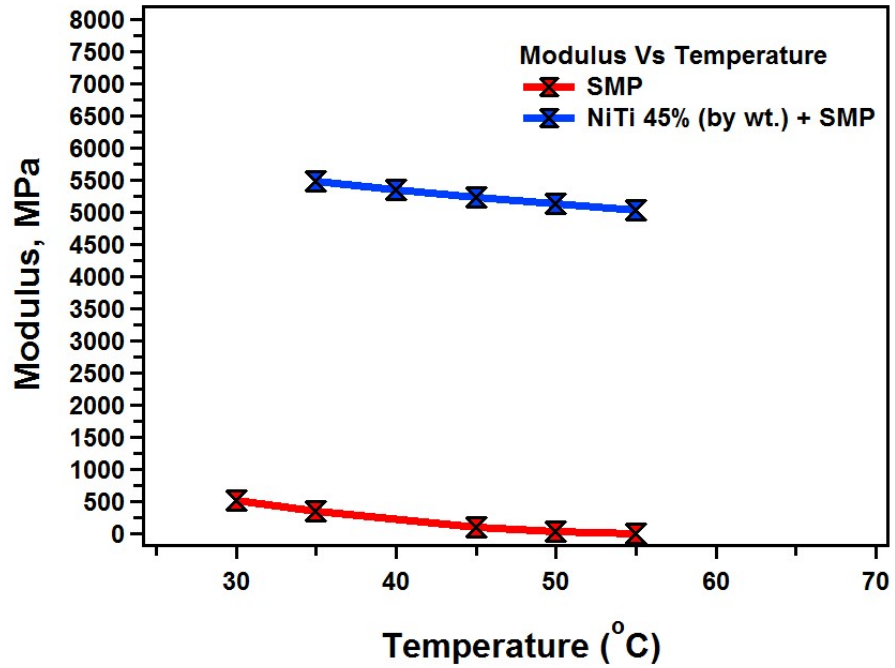


Figure 5.49 Shows the variation of modulus with temperature in NiTi 45% (by wt.) + SMP fiber composite in comparison to that of SMP.

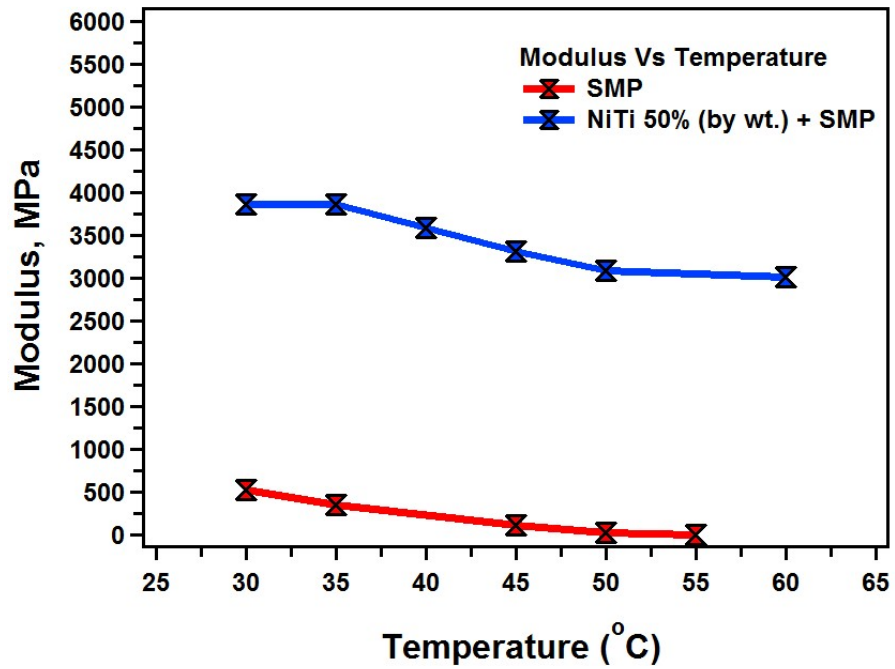


Figure 5.50 Shows the variation of modulus with temperature in NiTi 50% (by wt.) + SMP fiber composite in comparison to that of SMP.

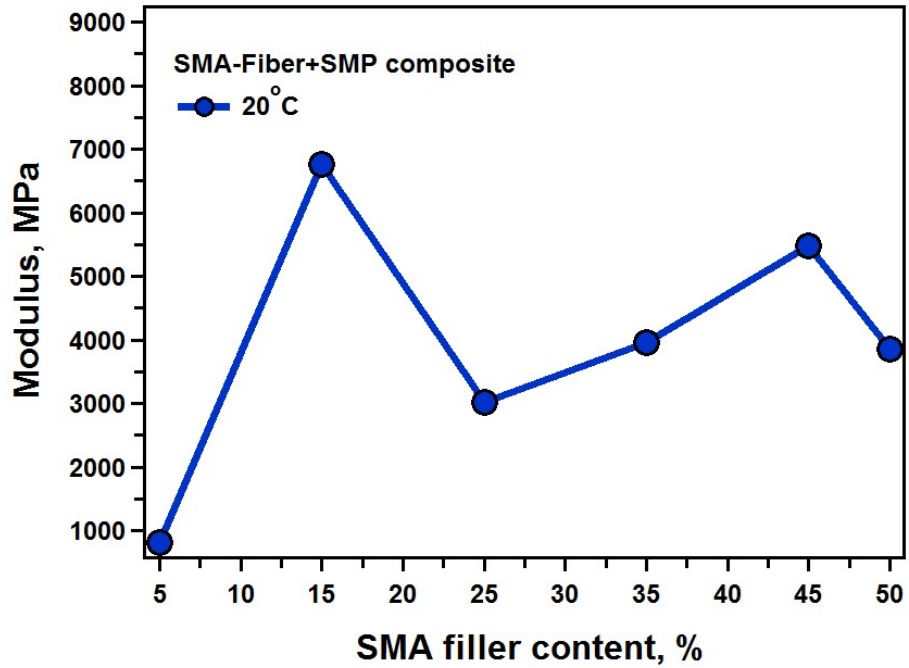


Figure 5.51 Variation of Modulus of SMA-Fiber + SMP composite with SMA filler content with a loading temperature of 20°C.

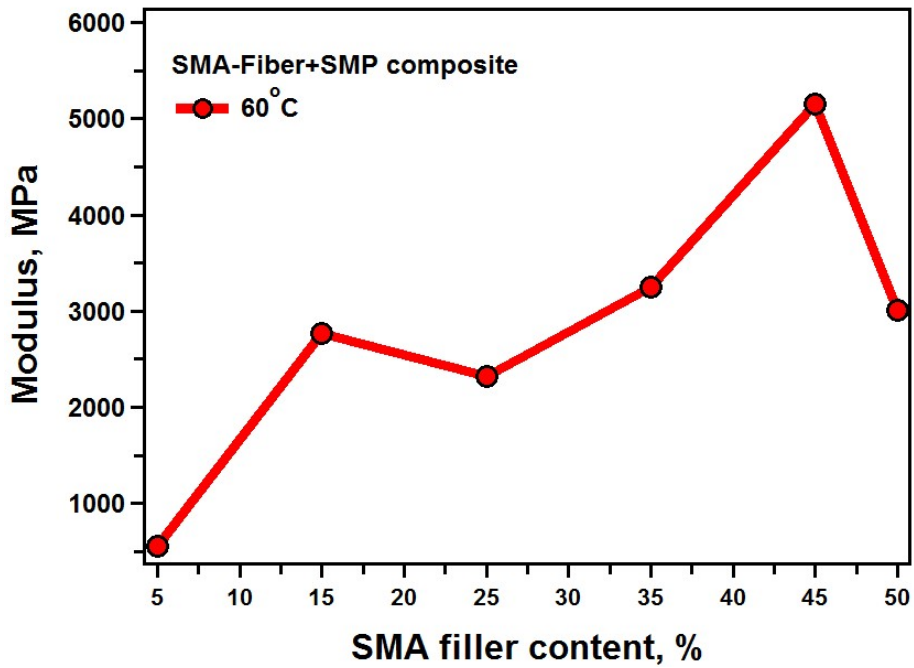


Figure 5.52 Variation of Modulus of SMA-Fiber + SMP composite with SMA filler content with a loading temperature of 60°C.

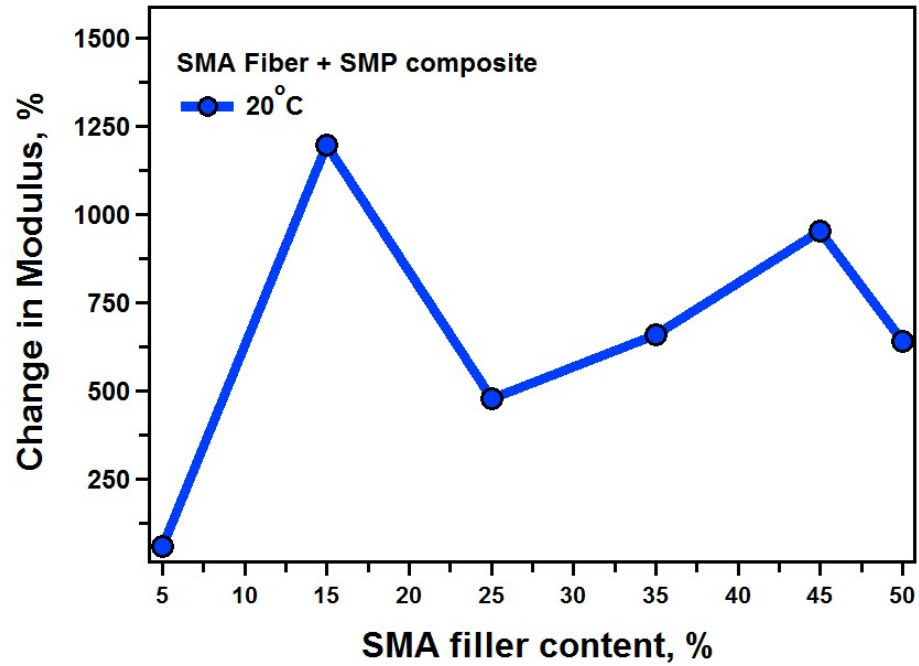


Figure 5.53 Change in Modulus of SMA+SMP fiber composite with SMA filler content at a loading temperature of 20°C.

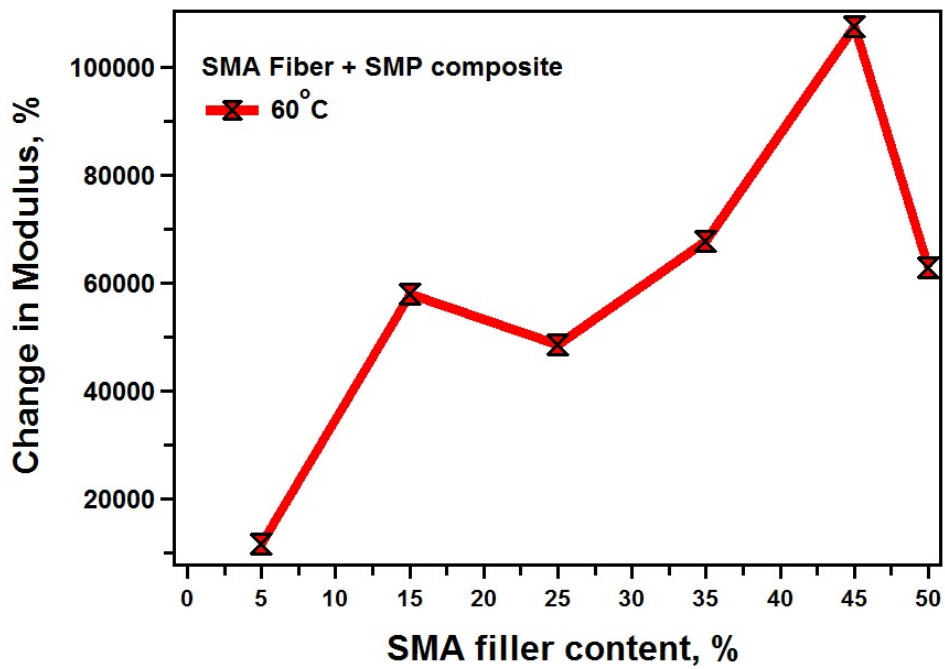


Figure 5.54 Change in Modulus of SMA+SMP fiber composite with SMA filler content at a loading temperature of 60°C.

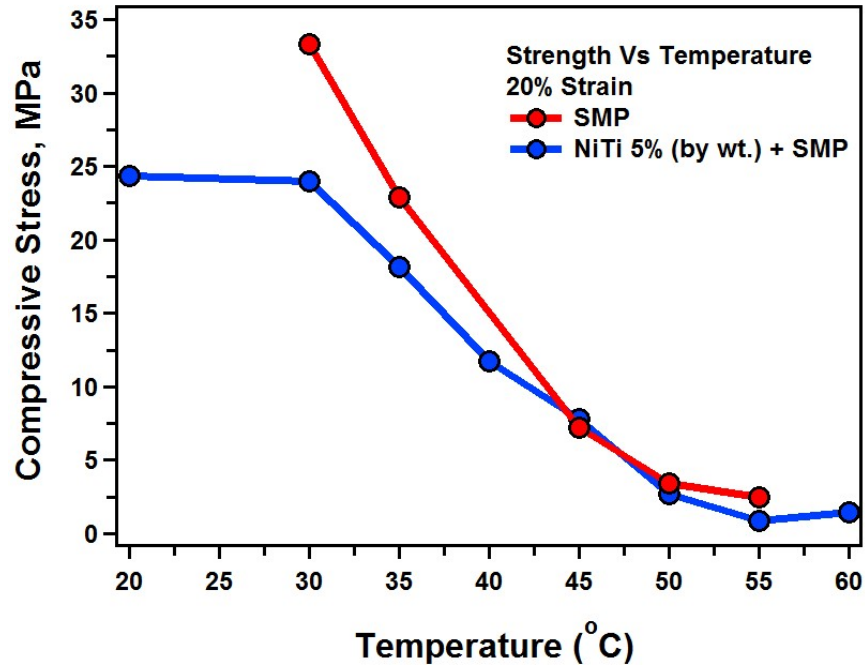


Figure 5.55 Shows the variation of strength with temperature in NiTi 5% (by wt.) + SMP fiber composite in comparison to that of SMP at 20% compressive strain.

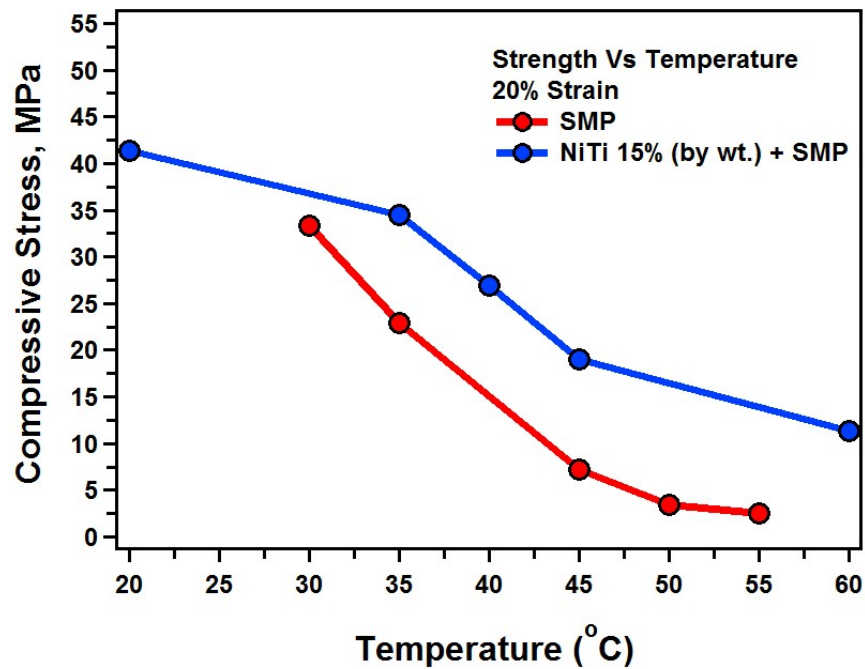


Figure 5.56 Shows the variation of strength with temperature in NiTi 15% (by wt.) + SMP fiber composite in comparison to that of SMP at 20% compressive strain.

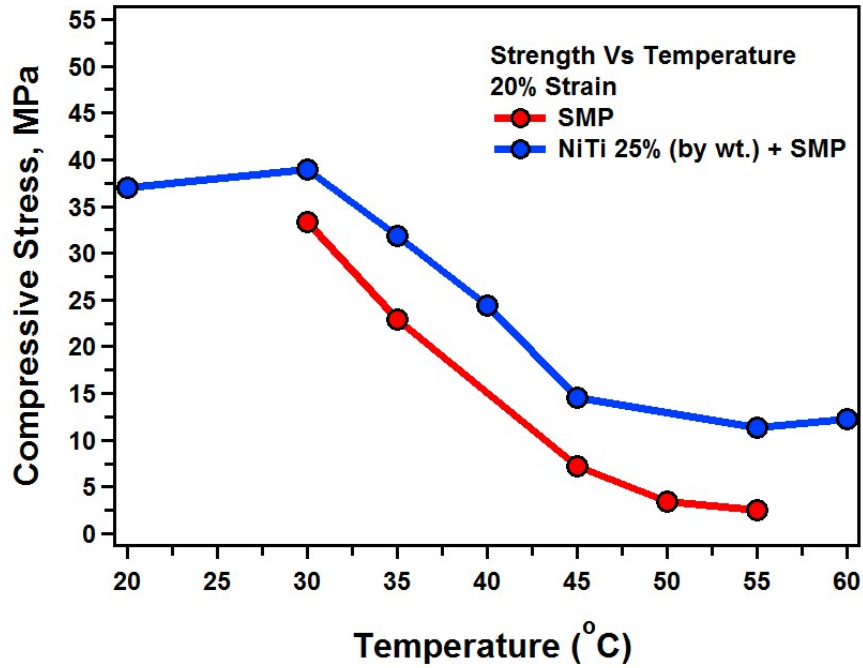


Figure 5.57 Shows the variation of strength with temperature in NiTi 25% (by wt.) + SMP fiber composite in comparison to that of SMP at 20% compressive strain.

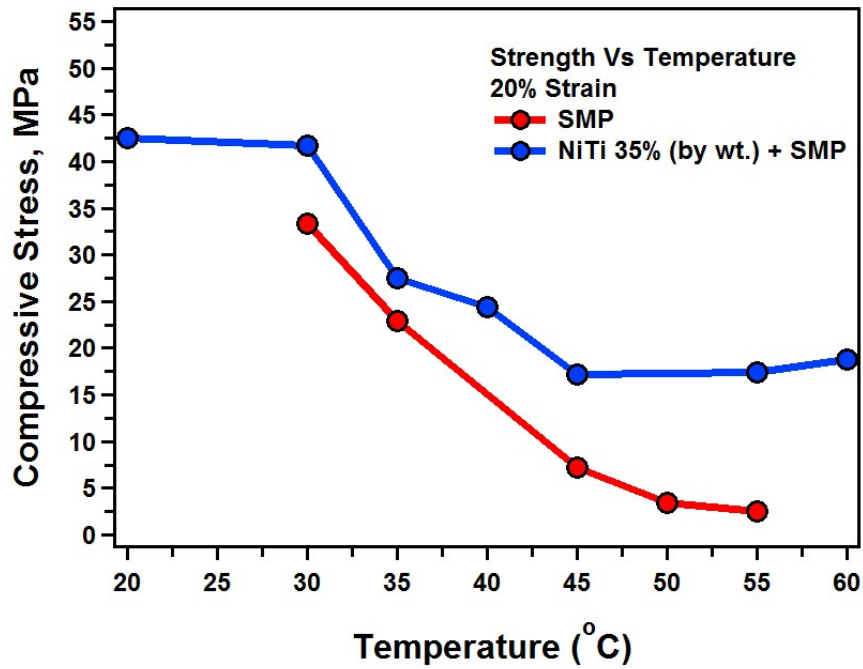


Figure 5.58 Shows the variation of strength with temperature in NiTi 35% (by wt.) + SMP fiber composite in comparison to that of SMP at 20% compressive strain.

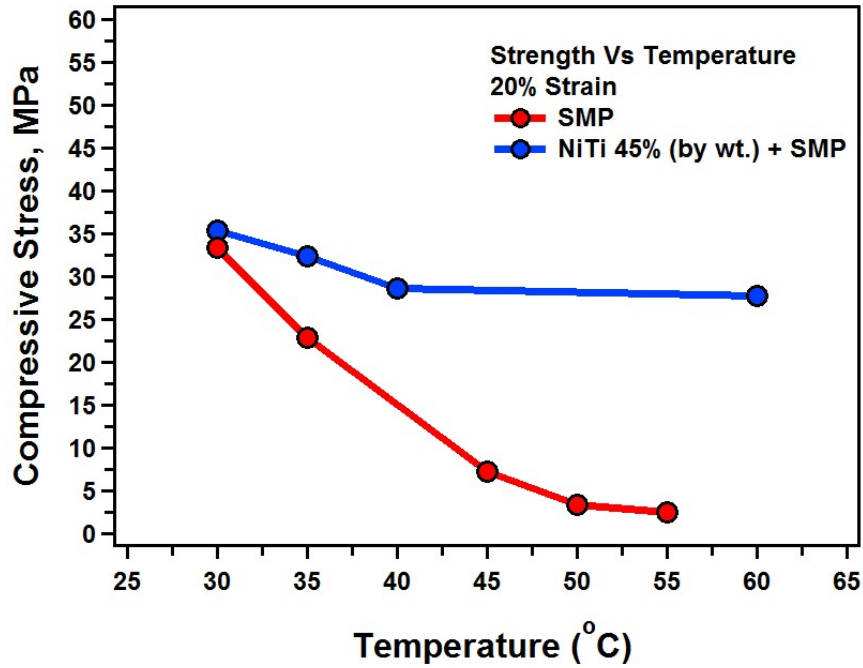


Figure 5.59 Shows the variation of strength with temperature in NiTi 45% (by wt.) + SMP fiber composite in comparison to that of SMP at 20% compressive strain.

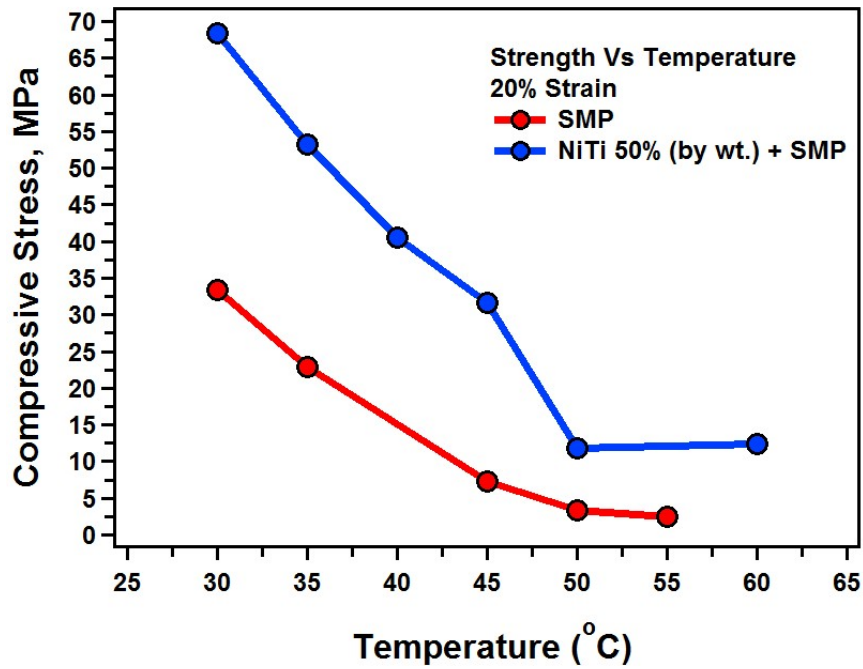


Figure 5.60 Shows the variation of strength with temperature in NiTi 50% (by wt.) + SMP fiber composite in comparison to that of SMP at 20% compressive strain.

From the figures 5.45-5.50, we can see that there is significant increase in the modulus of the shape memory composite for a range of temperatures from below T_g to above T_g . Whereas for the SMA Particle + SMP composites even at high filler contents of 50% the increase in modulus at temperatures above T_g is not as significant as that in the SMA Fiber + SMP composites. For Example, from figure 5.28, the modulus of SMA Particle (50%) + SMP composite at 60C was around 50 MPa (comparable to that of the SMP matrix). However for the same filler content of SMA Fiber + SMP composite from figure 5.50, the modulus value at 60C is close to 3000 MPa. Such a significant increase in modulus at high temperatures is possible in fiber composites. Since the SMA fiber is aligned in the direction perpendicular to the compressive loads and throughout the composite, the load carrying capacity of the composite could be increased. And as such shape memory fibers are a much suitable reinforcing materials to obtain the superior mechanical properties for multifunctional applications.

From figure 5.53, we can see that the least percent change in modulus at 20C of the SMA Fiber + SMP composite is 50% for 5% SMA filler content and the maximum is close to 1250% for 15% SMA filler content. Such a significant increase is also observed at high temperature of 60C (from Figure 5.54). In this case the least change in modulus of the SMC is seen at 10000% for 5% filler content and about 100000% for 45% filler content. Such high values of increase in mechanical properties at both temperatures below and above T_g make the SMA fiber preferred reinforcements compared to the SMA particles.

Although the strength of the SMA fiber + SMP composite did not improve as significantly as the modulus it still has shown better trend when compared with the strength of particle composite.

5.6.4 Experimental Verification of SMA Particle – SMP Composite

5.6.4.1 SMA Particle – SMP Composite Preparation

The shape memory polymer matrix used for these composites was the same Epoxy as in the other sections of the project. Hence the same procedure was used to make the SMP matrix as in section 3.2.1. However, there one major challenge with the dispersion of SMA particles in the SMP matrix. For this reason the SMP preparation method was adopted to accommodate the specific demand of homogenization of SMA particles in the matrix. To obtain a relatively uniform dispersion of SMA powders in the SMP matrix, the matrix was procured at 80°C in the furnace after mixing the three chemical constituents, namely Epoxy, Jeffamine(cross-linking agent) and NGDE3(shape recovery inducing constituent). Pre-curing of SMP increased the viscosity of the polymer mixture which in turn made the settling of the SMA NiTi powder particles to the bottom of the vial difficult. Although this would help with settling issue temporarily, as soon as the powders were mixed and furnace cured at 100°C, the crosslinks formed during pre-curing immediately broke down and the powders settled down to the bottom of the mold defeating the purpose of pre-curing. For this reason, after a several trials, a custom made setup to cure and mix the samples at room temperature after pre-curing was built. This custom setup would involve rotating the SMC composites at a constant speed of just a few tens of revolutions per minute at room temperature for 48 hours. The custom setup is shown in the Figure 5.61. This way of mixing ensured that there was uniform distribution

of NiTi SMA particles in the SMP matrix. After curing the samples at room temperature they were then furnace cured at 100°C for 90 minutes. Thus prepared samples were then cooled at room temperature and removed from the molds to be polished and tested. Several filler contents were considered to understand the behavior of SMA particle + SMP composites with the filler content of SMA particles ranging from 15% to 45% by weight.

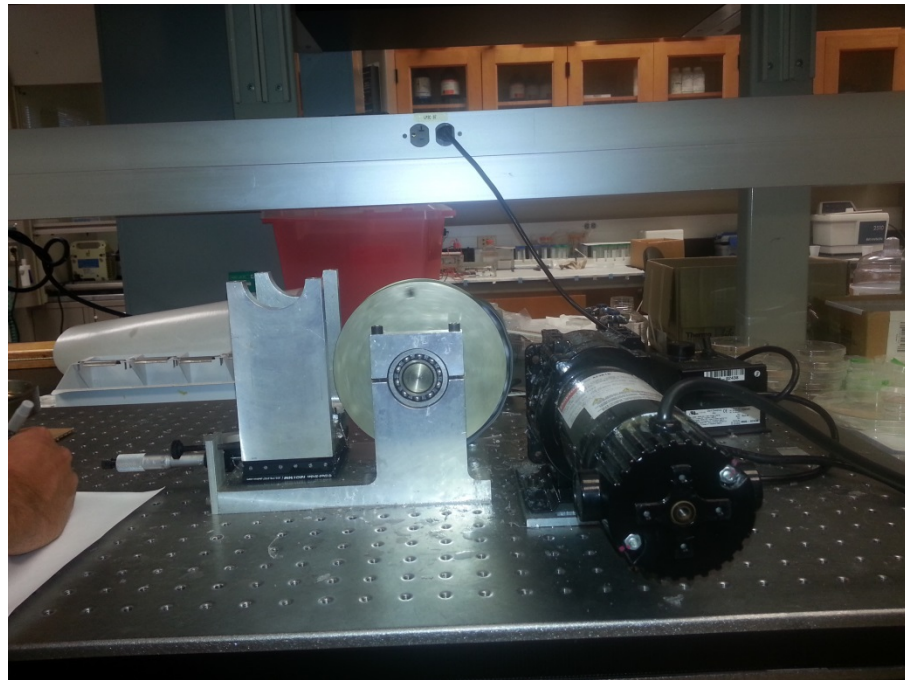


Figure 5.61 Shows the custom built mixer used to mix the NiTi SMA powder particles in the SMP matrix to obtain homogeneous dispersion of SMA particles.

5.6.4.2 Stress – Strain Behavior

The stress-strain behaviors of the SMA Particle-SMP composites were obtained through uniaxial compressive tests conducted on the BOSE ElectroForce load frame system using the force-controlled test. The cylinder samples with average size of 9.2mm × 7.46 mm were prepared to carry out the mechanical tests. The tests were performed

under the force-control mode by applying a compressive force of up to 2000 N at a rate of 0.5 N/sec at 35°C. The stress-strain curves were obtained for varying SMA filler content composites and the modulus was calculated from these results.

5.6.4.3 Results and Discussion

Figure 5.62 shows the stress-strain behavior of SMA particle + SMP composite for various SMA filler contents ranging from 15% to 45% by wt. From here we can see that the critical stress required to obtain the same strain of about 30% at a constant rate of 0.5% N/sec has increased from 15% to 45% although the critical stress value for 35% SMA filler content is higher than that of 45%. This could be due the processing technique differences in preparing and mixing of SMA fillers in the matrix. And also could be due to formation of clusters at higher SMA filler contents (45%) leading to poor load transfer between the matrix and SMA reinforcements. However, these curves could be used to obtain reliable modulus values as it is just the initial part of the loading curve.

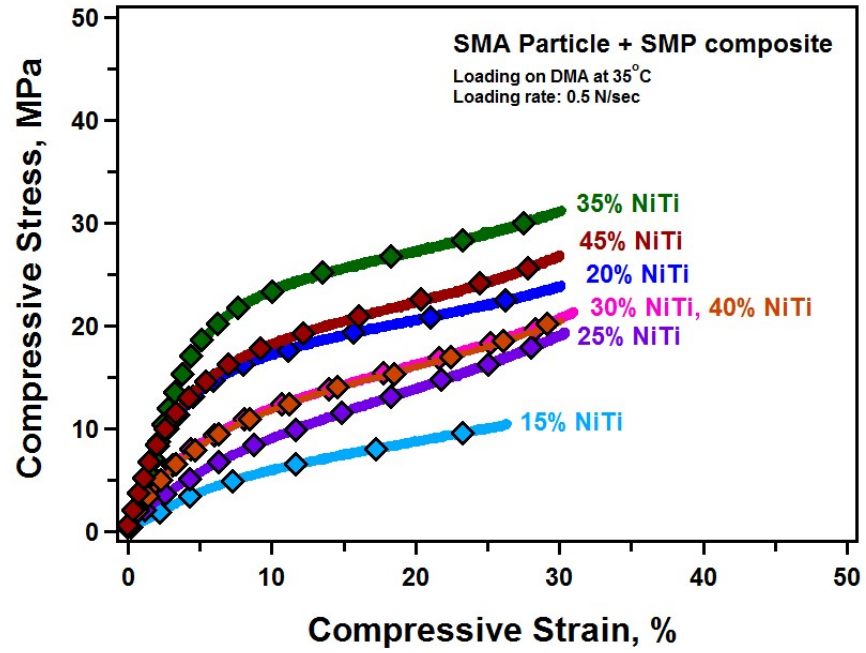


Figure 5.62 Shows the stress-strain behavior of various SMA Particle SMP composites obtained from DMA test.

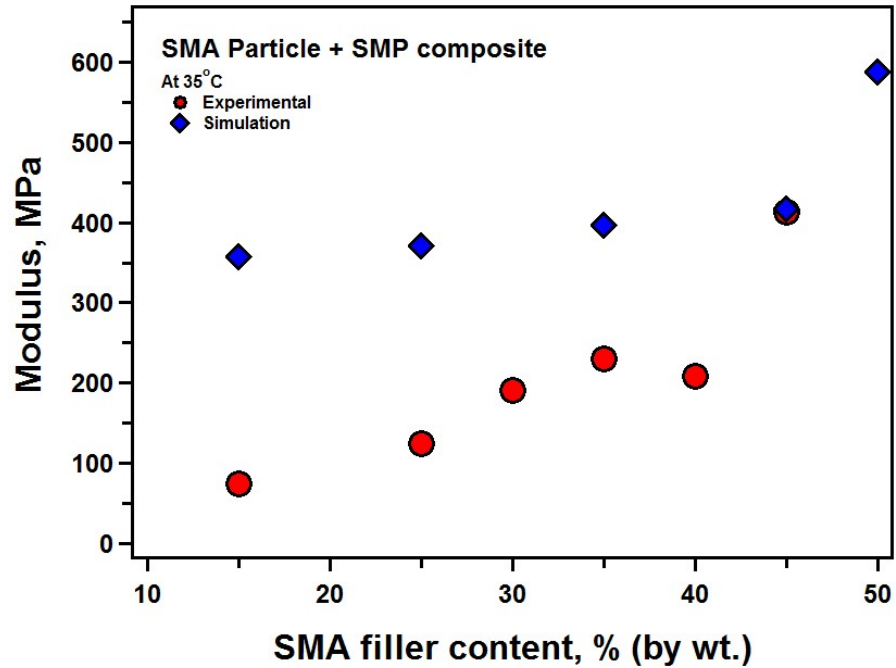


Figure 5.63 Shows the comparison of variation of modulus values obtained from experimental results and simulations for various SMA filler contents.

The modulus values for different SMA filler content composites were calculated and plotted in comparison to the modulus obtained theoretically from simulation results at 35°C as shown in the Figure 5. 63. We can see that the modulus gradually increases with the addition of SMA fillers. And there is a sudden increase in the modulus for higher SMA filler contents at around 45%. Also, the modulus obtained from simulation is comparable to that obtained from experiments as in the variation of modulus with filler content has the same trend from both the experimental and simulation results. The modulus values obtained from simulation are slightly higher for each filler content compared to the experimental results as in the simulations we assumed in ideal conditions that there is perfect bonding between the SMA particles and the SMP matrix although this may not be the case in reality.

5.7 CONCLUSIONS

The shape memory composites (SMCs) have been created by embedding SMA components (particles and fibers) into SMP matrices, which take advantage of the complementary properties of SMAs and SMPs. The epoxy-based shape memory polymer (SMP) is modeled with the Ogden strain energy model and the shape memory alloy is modeled with the Lagoudas' two-phase model. The two models are unified in a finite element program, ABAQUS, which allows the designs of shape memory composites. Two types of composites have been created: SMA-particle SMP composite and SMA-fiber SMP composites. The mechanical responses of the SMCs have been analyzed across the temperature regimes.

Additionally we could see that there is significant increase in mechanical properties when SMA fibers are used as the reinforcing material compared to the particle reinforcements. It was also observed that the modulus results obtained from the experimental stress-strain tests was in close comparison to that obtained from simulation results for various SMA fiber + SMP composites. There is a steady increase in the modulus for the fiber composites with the addition of filler contents up to 40%(by wt.) SMA fillers and after this a sudden spike in the modulus is observed for 45% and 50% (by wt.) of SMA fillers from experimental and theoretical results.

Overall, the additions of SMA fillers have significantly increased the modulus and strength of composites while maintaining the identical actuation strain to the SMP.

Chapter Six

6 DESIGN AND CHARACTERIZATION OF MULTIFUNCTIONAL SHAPE MEMORY COMPOSITES: CNT – SMP COMPOSITES

6.1 INTRODUCTION

Multifunctional materials have several applications in aero-space and automotive industry compared to single component materials. One such class of multifunctional materials are shape memory polymer composites. Reinforcing shape memory polymers with carbon nanotubes results in a stronger material and low cost to density ratio. Addition of small quantities (around 0.1%) of CNTs could prove to be cost effective as they have the capabilities to enhance the mechanical properties of the composite with such micro scale additions [96]. However to obtain additional functionality of electrically conductive polymer matrix composites by incorporating carbon nanotubes alone would prove to be a difficult task in the real engineering applications as aligning carbon nanotubes would require very high intensity of magnetic fields (7-26T) [97, 98]. For this reason conductive fillers are added that are fairly easier to align and form conductive chains. The common conductive fillers used to reduce the electrical resistivity of the polymer matrix composites include carbon black, carbon nanotubes and carbon nano fibers and Fe_2O_3 etc.[49, 99]. These powders such as carbon black form clusters and stick together making it difficult to transfer electrons between the clusters. In order to get better electrical conductivity Ni particles could be aligned in the form of chains to help the flow of electron and increase the electrical conductivity with much lower cost and lesser number of conductive fillers[100]. Since it is easier to align Ni particles in the magnetic field and also because they are less expensive than CNT fibers, they could act

as a replacement for CNT fibers alone to improve the electrical properties of the composites [101]. The objective of the present chapter is to develop multifunctional, shape memory composites, including the CNT-SMP composites and the Ni-CNT-SMP composites.

6.2 EXPERIMENTAL

6.2.1 CNT – SMP Composite Preparation

The matrix used to disperse the CNT fillers was epoxy based shape memory polymer. It mainly comprised of three substances: diglycidyl ether of bisphenol, an epoxy monomer (EPON 826, available from Hexion), (2) curing agent poly (propylene glycol) bis (2-aminopropyl) ether (Jeffamine D230, available from Huntsman), and (3) neopentyl glycol diglycidyl ether (NGDE), manufactured by TCI America. The polymer was synthesized as follow. First, all substances (epoxy monomer EPON 826, curing agent D230, and NGDE) were weighed and stored into separate glass containers. The EPON 826 was placed in the furnace and heated to 80°C for approximately 5-10 minutes to reduce its viscosity. The resultant EPON 826 was removed from the furnace and poured into the mixture of the other two ingredients. The solution was stirred for 15-30 seconds to ensure the proper mixing. To remove the bubbles that were developed during the mixing, the solution was placed under a vacuum at 20 in Hg for about 2 minutes.

CNT fillers were then dispersed in the matrix solution in measured quantities varying from 0.1% by weight to 0.75% by weight of the matrix. The dispersion characteristics are very important for the application of CNTs. It is generally very difficult to be dispersed in a polymeric matrix, since they have large surface areas and possess large van der Waals forces, which results in aggregates. For this reason mixing of

CNT fillers in the matrix was carried out using ultra-sonication. CNT-SMP mixture was suspended for 90 minutes in an ultrasonic bath of water maintained at constant temperature of 20°C in order to have low viscosity of matrix. These ultrasonic baths or cleaners have large transducer areas and tanks that produce a high-powered ultrasonic intensity throughout the entire oscillating tank. Constant power and automatic frequency control ensure optimum distribution of ultrasonic energy and reproducible results and uniform dispersion of fillers.

After thorough stirring the CNT-SMP mixture was degassed under vacuum until all gas bubbles disappeared and was poured into cylindrical Teflon molds of length 12mm and 6.25mm diameter to form CNT-SMP cylinder composites with varying CNT quantities of 0.1% to 0.75% by weight. After this step the composites were furnace cured for 90 minutes at 100°C. Then they were cooled at room temperature. The surfaces were smoothed and coated with a conductive graphite paint to obtain a proper contact with the probes of the multimeter to measure the resistance across the length and radius of the cylinder samples.

6.2.2 Ni – CNT – SMP Composite Preparation

The matrix used in the current study was epoxy based shape memory polymer. These polymers were composed of following substances: (1) diglycidyl ether of bisphenol, an epoxy monomer (EPON 826, available from Hexion), (2) curing agent poly (propylene glycol)bis(2-aminopropyl) ether (Jeffamine D230, available from Huntsman), and (3) neopentyl glycol diglycidyl ether (NGDE), manufactured by TCI America. The polymer was synthesized as follow. First, all substances (epoxy monomer EPON 826, curing agent D230, and NGDE) were weighed and stored into separate glass containers.

The EPON 826 was placed in the furnace and heated to 80°C for approximately 5-10 minutes to reduce its viscosity. The resultant EPON 826 was removed from the furnace and poured into the mixture of the other two ingredients. The solution was stirred for 15-30 seconds to ensure the proper mixing. To remove the bubbles that were developed during the mixing, the solution was placed under a vacuum at 20 in Hg for about 2 minutes.

Measured quantities of Carbon nanotubes with weight percent from 0.1% to 0.75% were added to Epoxy solution previously prepared. This mixture was then suspended in an ultrasonic bath of water and stirred for 90 minutes. The temperature of water was kept constant at 20°C to maintain the low viscosity of epoxy. After thorough stirring the CNT/Epoxy mixture was degassed under vacuum until all gas bubbles disappeared. Then the mixture was pipetted into cylindrical Teflon molds of length 12mm and 6.25mm diameter to form CNT-SMP cylinder composites with varying CNT quantities of 0.25% and 0.50% by weight. For the purpose of increasing the electrical conductivity, Ni powders were added to the prepared CNT-SMP mixture. The objective was to reduce the electrical resistivity of the multifunctional composites. For this reason, Ni particles were aligned in parallel and perpendicular to the radius of the cylindrical Teflon molds by placing them in the magnetic field for 48 hours as shown in the figure 5.1 shown below.

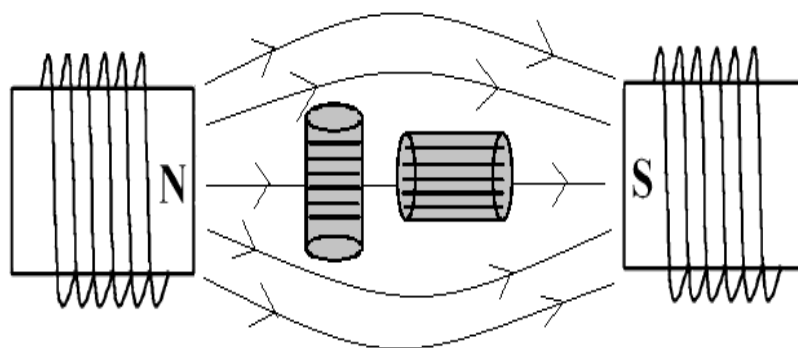


Figure 6.1 Above shows the aligned Ni chains along the radius and perpendicular to the radius of the CNT-SMP cylinder composite placed in magnetic field.

The composite samples were then removed from the magnetic field and cured in the furnace for 90 minutes at 100oC. After curing they were allowed to cool down to room temperature before they could be surface finished and desired size of the samples were cut to test the electrical resistivity. For better surface smoothness and to make the sample surfaces conductive they were coated with graphite paint and the electrical resistivity was measured.

6.2.3 Transition Temperature

The transition temperature of the CNT-SMP composites was characterized with a Perkin Elmer Pyris1 Dynamic Mechanical Analyzer (DMA). Glass transition temperature (T_g) of a material gives the temperature at which the material changes from glassy phase to a rubbery phase. DMA yields information about the mechanical properties and T_g of a specimen placed in minor, sinusoidal oscillation as a function of time and temperature by subjecting it to a small, sinusoidal, oscillating force. The CNT-SMP cylindrical specimen

of size 12 mm height by 6.25 mm diameter were placed in the DMA. They were heated to about 70°C at 2°C/min from room temperature.

6.2.4 Stress – Strain Tests

The stress-strain behaviors of the CNT-SMP composites were obtained through uniaxial compressive tests conducted on the BOSE ElectroForce load frame system using the force-controlled test. The specimens were small cylinders with the nominal height of 11 mm and nominal diameter of 6.25 mm. The tests were performed under the force-control mode by applying a compressive force of up to 2000 N at a rate of 2 N/sec at room temperature. The figure 5.2 below shows the schematics of different test setups in DMA. For our tests, compression grips were used to obtain the stress-strain behavior of CNT-SMP composite specimen.

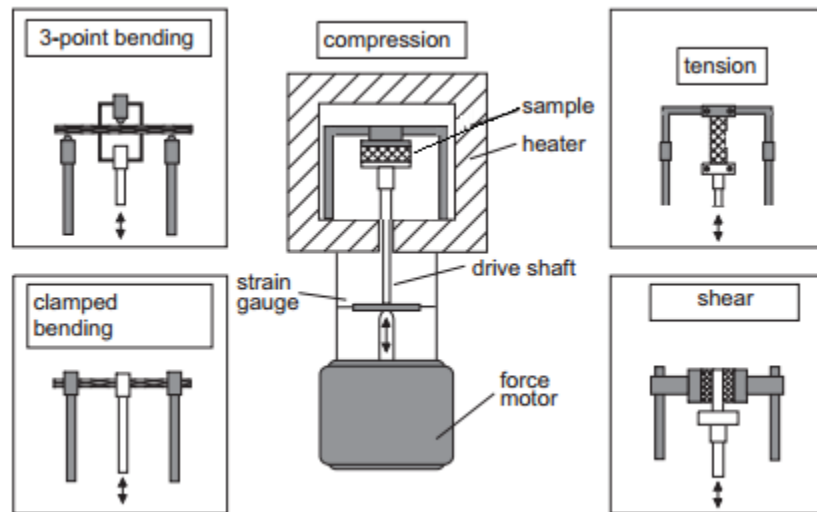


Figure 6.2 Schematic design of DMA under vertical load, showing the various possible test arrangements.

The stress-strain behaviors of the Ni-CNT-SMP composites were obtained through uniaxial compressive tests on MTS Landmark servo-hydraulic load frame shown in Figure 5.3. Cylindrical specimens with dimensions of 3.11mm(length)×3.15mm(radius) were tested. The specimens were compressed up to 100 kN with a strain rate of 10^{-4}s^{-1} . The temperature of the sample was monitored by K-type thermocouples attached on the sample and grips. The stress strain data was derived from the load-displacement curve obtained from the experiments for the composites with Ni chains aligned in both directions mentioned earlier.



Figure 6.3 Shows the MTS setup used for testing mechanical behavior of CNT-SMP composites.

6.2.5 Electrical Measurements

In order to calculate the resistivity of the composites, samples of average size: 3.11mm(length)×3.15mm(radius) were cut out and coated with graphite paint on the ends. The samples were then connected between aluminum electrodes and the resistance

was then measured using a digital multimeter as shown in the schematic below (Figure 5.4). Using the geometrical dimensions of the samples the resistivity was derived.

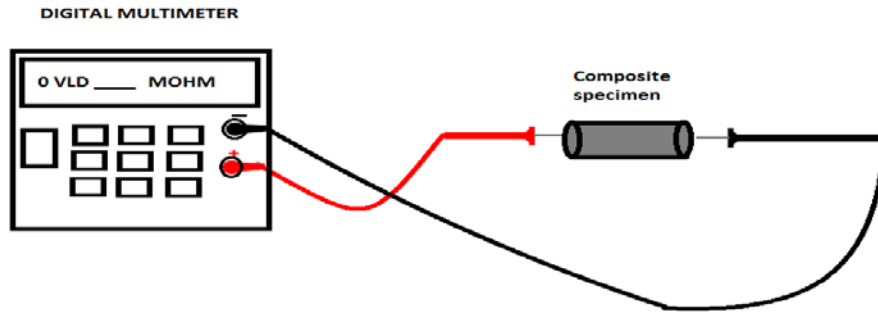


Figure 6.4 Shows the set up used to measure the electrical resistivity of CNT-Ni-SMP composites.

6.3 RESULTS AND DISCUSSION

6.3.1 Thermal Behavior of CNT – SMP Composite

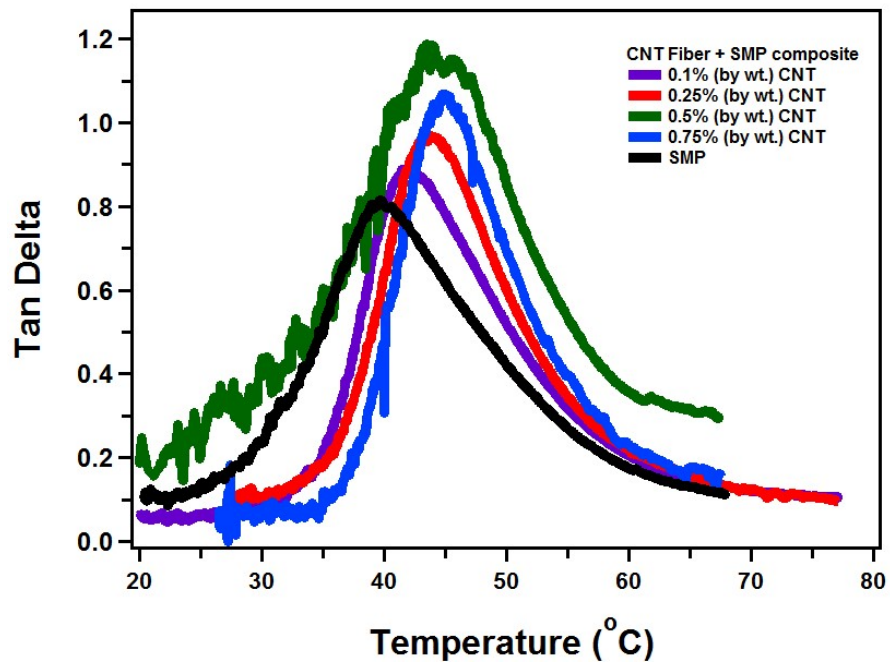


Figure 6.5 Shows the tan Delta Vs CNT filler content from thermal cycling on DMA.

We can clearly see that the T_g of the composite material increases with addition of CNT fillers. For a minor variation from 0.1% to 0.75% weight of CNT fillers there approximately an increase in T_g by 5°C as shown in the figure. This change in T_g is significant as glass transition temperature is very much dependent on the nature of material.

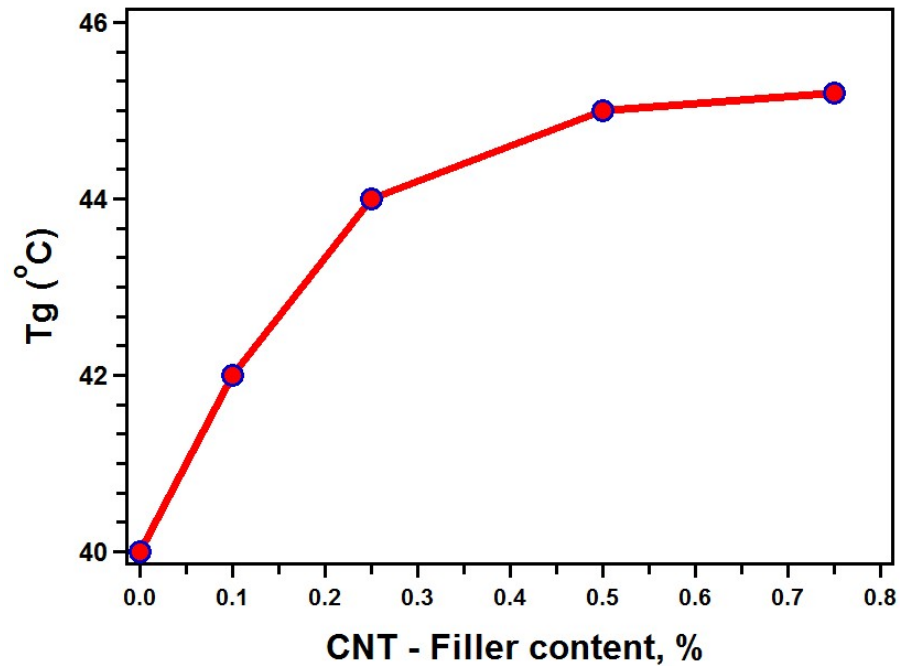


Figure 6.6 Shows the variation of T_g of CNT-SMP composites with addition of CNT fillers.

6.3.2 Mechanical Behavior of CNT – SMP Composite

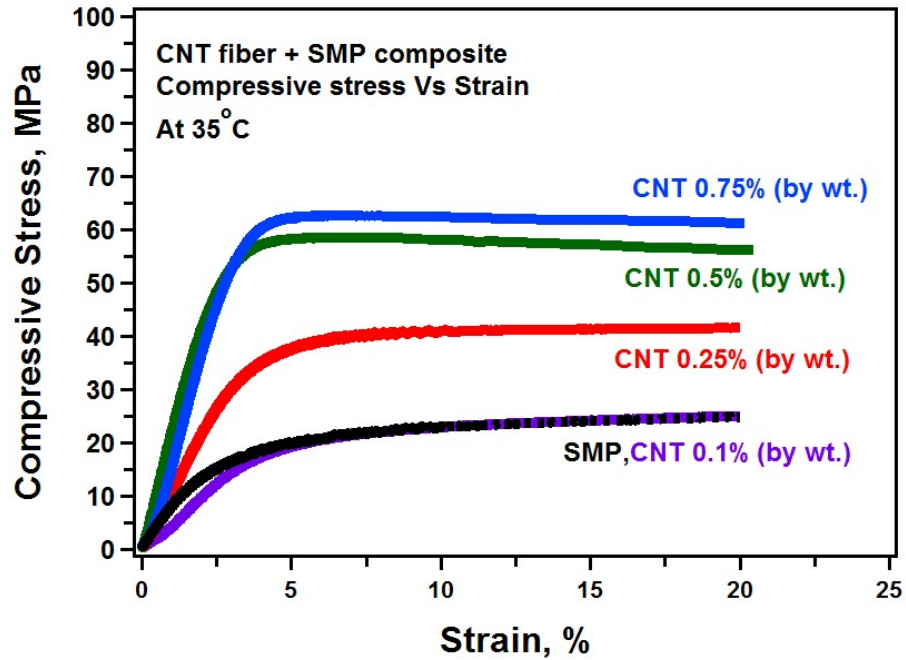


Figure 6.7 shows the mechanical behavior of CNT-SMP obtained from DMA compressive test.

From the Figure 6.7 we can see that the addition of CNT filler has significantly increased the mechanical properties of the SMP. Also with addition of small amount of fillers such as 0.25% by weight of CNT filler the compressive stress has considerably increased by about 20MPa compares to that of SMP.

From the stress-strain data obtained, the modulus of the CNT – SMP composite was calculated. We could see that there is a significant increase in the composite modulus compared to that of the polymer. The variation of modulus with CNT filler content is shown in the Figure 6.8. Similarly, the strength of the modulus was obtained from the compressive stress at 20% strain. The variation of strength with the CNT filler content is

shown in the Figure6.9. It can be seen that there is linear increase in both modulus and strength with the addition of CNT fillers up to 0.5% weight fractions. Although after this, further addition of CNTs at 0.75% (by wt.) did not result in a significant improvement of the mechanical properties. This could be due to the agglomeration of CNT fibers at higher weight fractions leading to non-homogeneous distribution of fillers.

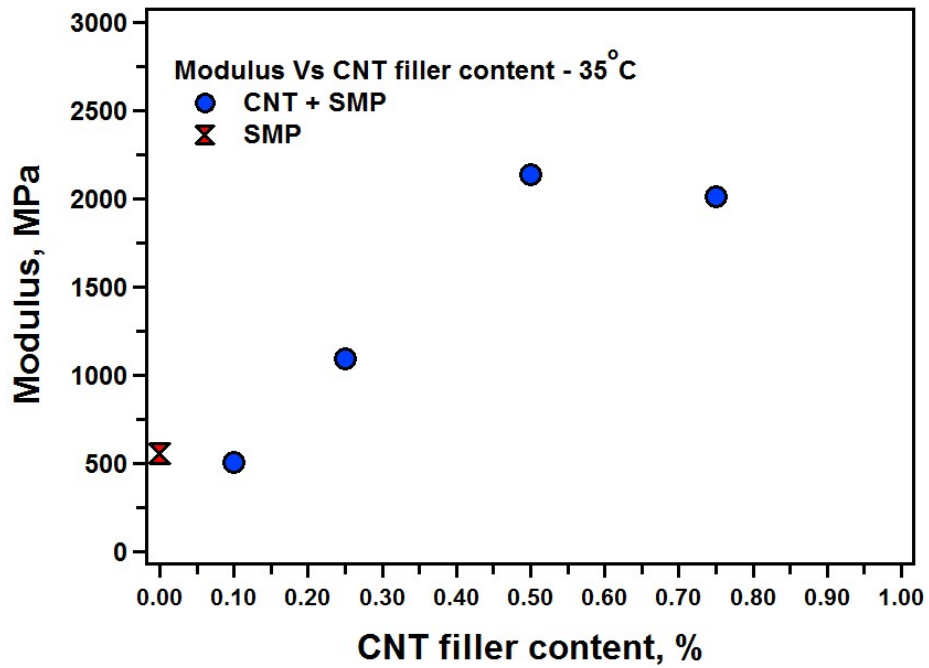


Figure 6.8 Change in Modulus of CNT+SMP particle composite with CNT filler content.

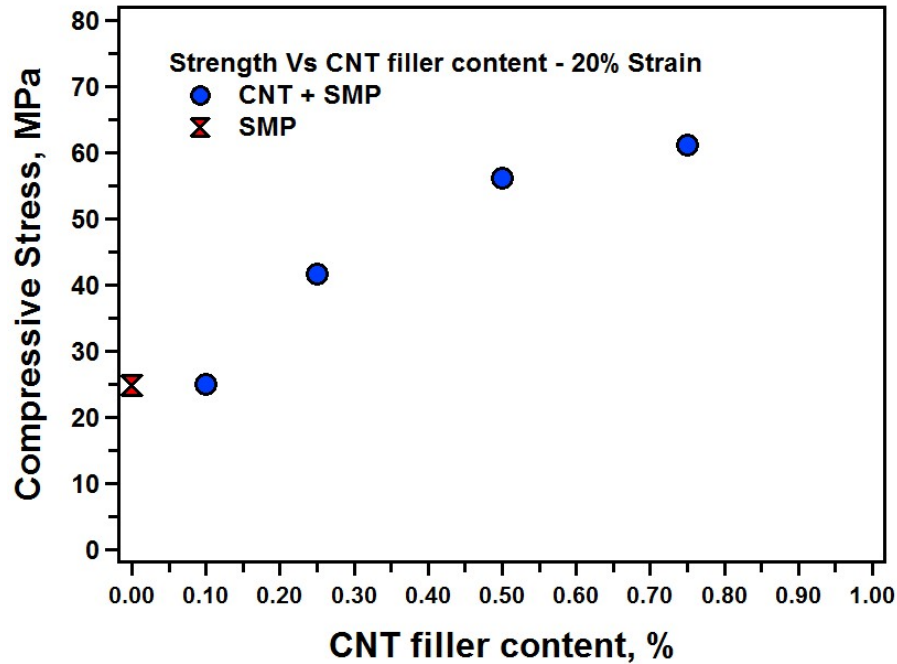


Figure 6.9 Change in strength of CNT+SMP particle composite with CNT filler content.

6.3.3 Mechanical Behavior of Ni – CNT – SMP Composite

Compression specimens with dimensions of 3.11mm (length)×3.15mm(radius) were tested by 100 kN MTS Landmark servo-hydraulic load frame with a strain rate of 10^{-4}s^{-1} . The stress strain data was derived from the load-displacement curve obtained from the experiments for the composites with Ni chains aligned in both directions mentioned earlier. From the figure 5.7 (below) we could see that there was not much change in the mechanical behavior with the addition of Ni chains in CNT-SMP composites. We can say that the addition of Ni chains has not influenced the mechanical properties of the composites.

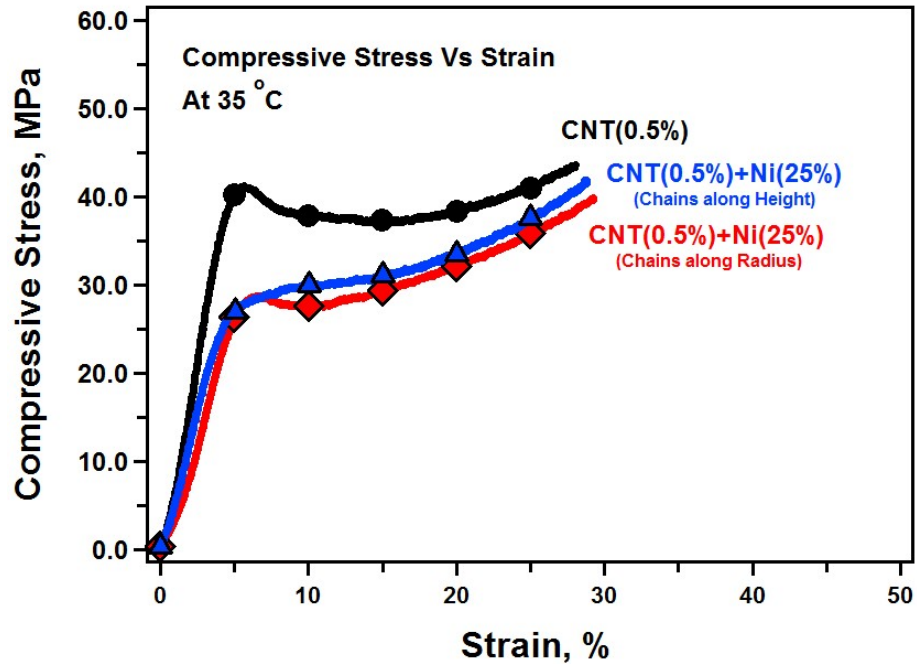


Figure 6.10 Shows the stress-strain curves of various CNT-SMP composites with Ni chains aligned in the direction parallel and perpendicular to the radius of compression specimen.

6.3.4 Electrical Behavior of CNT – SMP and Ni – CNT – SMP Composites

Electrical resistance was measured by touching the multi-meter probes to the sample surface as explained earlier in section 6.2.5. From the standard relations existing between the geometry of the sample whose electrical resistance is being measured and value of the resistance obtained from the multi-meter, the resistivity of CNT fiber + SMP composites was calculated. The figure below shows that with the addition of CNT fillers, the electrical resistivity of the composite has significantly reduced. Hence, shape memory polymer matrix composites could be reinforced with CNT fillers that improve both mechanical and electrical properties in addition to maintaining the shape recovery

behavior thereby making them multifunctional composites suitable for wider range of applications.

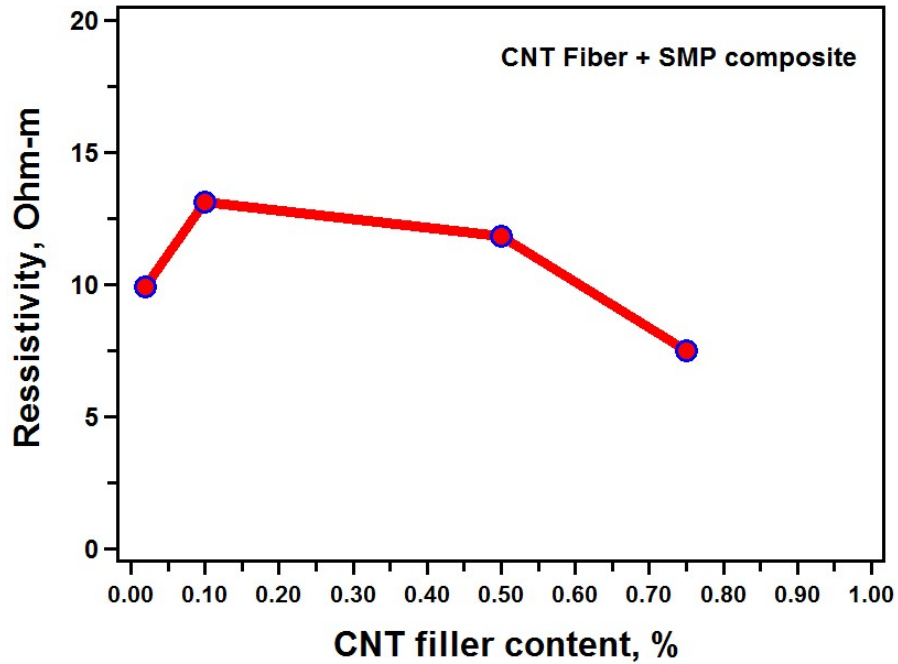


Figure 6.11 Variation of electrical resistivity of CNT fiber + SMP composites with addition of CNT filler content.

The tables 6.1 and 6.2 below give the details resistivity calculations for different composites tested. From both the tables 6.1 and 6.2 we could see that the electrical resistivity of CNT-SMP composites with no Ni powders is higher than those with Ni addition. From Table 6.1 we could see that when resistivity is measured along the direction of Ni chains the composite is more conductive than when measured perpendicular to the chain alignment. We can see that it is twice as hard to transfer the electric current in the direction perpendicular to the Ni chains.

In addition to this, the resistivity of CNT+Ni SMP composites was measured over a span of two years to observe any increase in the values. From Table 6.3 we can see that the resistivity has not changed much over the years.

Table 6.1 Resistivity of CNT (0.5% by weight)-SMP composites measured perpendicular to the radius with (a) aligned Ni(25% by weight) chains and (b) No Ni chains.


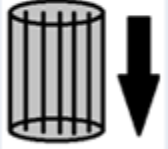
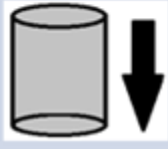
Resistivity(ohm-m)	Direction of Ni chains	Schematic
0.0640	Parallel to radius	
0.0394	Perpendicular to radius	
11.8210	No Ni chains	

Table 6.2 Resistivity of CNT (0.5% by weight)-SMP composites measured along the radius with (a) aligned Ni (25% by weight) chains and (b) No Ni chains.

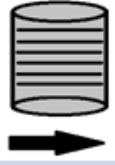
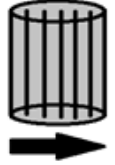
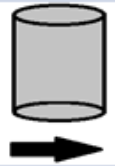
Resistivity(ohm-m)	Direction of Ni chains	Schematic
458.38	Parallel to radius	
553.16	Perpendicular to radius	
3476.48	No Ni chains	

Table 6.3 Resistivity of CNT+Ni-SMP composites measured over a span of two years.

Composite	Direction of chains	Direction of resistivity measurement	Resistivity (Ω -m)	
			Measured in 2013	Measured in 2015
CNT (0.5%) + Ni (25%) With Ni chains	Along Diameter	Normal to the chains	0.0640	0.0890
CNT (0.5%) + Ni (25%) With Ni chains	Along Height	Along the chains	0.0394	0.0665
CNT (0.5%)	No Ni	Along the height	11.82	11.82

6.4 CONCLUSIONS

From the current study it is clear that shape memory composites have higher strength and better properties with addition of reinforcement components such as carbon nanotubes and Ni powders. We could see that the addition of carbon nanotubes has significantly increased the T_g with a change of 5°C. Addition of CNT filler has significantly increased the mechanical properties of the SMP. Also with addition of small amount of fillers such as 0.25% by weight of CNT filler the compressive stress has considerably increased by about 20MPa compares to that of SMP. We could also see that the addition of small amounts of CNTs such as 0.25% by wt. to the SMP matrix, significant increase in modulus (about 500 MPa) of the SMP was observed.

Along with mechanical properties, by the addition of small amounts of Ni particles (25%) have shown improved electrical conductivity of the CNT-Ni-SMP composite. It is clear that formation of Ni chains in the polymer matrix acts as bridge between the CNT fibers and helps in improving the electrical conductivity of the composite. Additionally in the absence of Ni powders we could see a clear trend of decreasing electrical resistivity of CNT+SMP composites with the CNT filler content. This further shows that CNT are effective reinforcements to obtain multifunctional composites.

Chapter Seven

7 CONCLUSIONS AND FUTURE WORK

7.1 WORK TO DATE

Shape memory polymers (SMPs) are a special class of active materials that can recover its permanent shape from a temporarily deformed shape when exposed to an appropriate stimulus. Compared with other shape memory materials such as shape memory alloys, the SMPs can have much larger actuation strain (more than 200% recoverable elastic strain for most SMPs) and yet require relatively lower fixing forces. They also possess the advantages of low cost, low density and potential biocompatibility and biodegradability. The current study involved the processing, experimental characterizations, and numerical modelling of an epoxy-based SMP and their composites.

The epoxy-based shape memory polymer (SMP) has been fabricated as a candidate material for reconfigurable structures and devices. The material behaves as a two-phase material, exhibiting distinct mechanical behaviors at glassy and rubber states. The glass transition temperature of the present SMP was determined as: $T_g \sim 45^\circ\text{C}$, from both DSC and DMA. The coefficient of thermal expansion at the rubbery state is 2.1×10^{-4} , about twice of the CTE at glassy state. The mechanical responses of the present SMP were examined in compression mode at temperatures spanning all three regions of the polymer: glassy region (30°C , 35°C), glassy-to-rubbery transition region (45°C), and rubbery region (50°C , and 55°C). The material is seen to display typical hyperplastic behavior in the rubbery regions above T_g . At temperatures below T_g , the material shows inelastic behavior. The shape recovery behavior of the SMP has been systematically

examined and analyzed. Under unconstraint condition, the SMP has demonstrated remarkable shape recovery abilities at various fixing strains and fixing temperatures.

The shape recovery behavior of the SMP has been systematically examined and analyzed. Under unconstraint condition, the SMP has demonstrated remarkable shape recovery abilities at various fixing strains and fixing temperatures. When the constraints (loads) are applied to the fixed samples, the SMPs continue to reach the full recoveries. The SMP also has the ability of generating a high level of stress, up to 24 MPa at 50% fixed strain, which is comparable with some shape memory alloys. Under the programmed thermomechanical cycle, the material has demonstrated excellent shape fixity, i.e., the ability to hold a shape after deforming, and is able to reach full recovery upon re-heating.

The design of SMP-based structures and devices requires thorough characterization and constitutive modelling of the thermo-mechanical behavior of the materials. Several phenomenological and micromechanics based constitutive models are available for the SMPs. Some have focused on small deformations (<10% nominal strain for compression or tension), while the others have a large number of material parameters (for instance, there are up to 45 parameters in Srivastava's model). In this study, the strain energy functions, commonly used for modelling the large deformation of elastomeric materials, are used to model the stress-strain and shape recovery responses of the SMP. Among all models, the stretch-based Ogden model has provided the best fits to the stress-strain responses. The shape recovery process of the SMP has been further analyzed by using the Ogden model developed for large deformations. Each step of the thermomechanical

cycle (deforming, cooling, fixing, and recovering) has been successfully predicted, which are in good agreements with the experimental observations.

At elevated temperatures, SMP is at the rubbery state and thus exhibits high recovery strain but is lack of strength and modulus. In this study, the shape memory composites (SMCs) are created by embedding shape memory alloy (SMA) components (in the forms of particles and fibers) into SMP matrices, which take advantage of the complementary properties of SMAs and SMPs. The SMA-particle and SMA-fiber reinforced SMP composites are designed through numerical simulations. The volume fractions of the SMA fillers were varied from 0-50% wt. The SMP matrix is modeled with the Ogden strain energy model and the SMA filler is modeled with the Lagoudas' two-phase model. The two models are unified in a finite element program, ABAQUS, which allows the designs of shape memory composites. Two types of composites have been created: SMA-particle SMP composite and SMA-fiber SMP composites. The mechanical responses of the SMCs have been analyzed across the temperature regimes. Overall, the additions of SMA fillers have significantly increased the modulus and strength of composites while maintaining the identical actuation strain to the SMP.

Practical applications of the SMPs often require self-activations without the use of external stimuli, thus, it is necessary to reinforce the non-conductive shape memory polymer matrix with electrically conductive fillers. To achieve a balance of the mechanical performance and the multifunctional characteristics of shape memory polymers, new fillers were studied, including the carbon nanotubes (CNTs) and Ni

particles. Results show that the shape memory composites have higher strength and better properties with addition of multifunctional reinforcement fillers. The addition of carbon nanotubes has significantly increased the T_g with a change of 5°C . With addition of small amount of CNT fillers (0.25% wt.), the compressive stress has been increased by about 20 MPa and the modulus has been increased by about 500 MPa. In addition, by adding small amounts of Ni particles (25%) have shown improved electrical conductivity of the CNT-Ni-SMP composite. It is clear that formation of Ni chains in the polymer matrix acts as bridge between the CNT fibers and helps in improving the electrical conductivity of the composite. Additionally in the absence of Ni powders we could see a clear trend of decreasing electrical resistivity of CNT+SMP composites with the CNT filler content. This further shows that CNT are effective reinforcements to obtain multifunctional composites.

7.2 FUTURE WORK

With the current increase of interest in development of reconfigurable structures and devices, the advancement of research in the area of smart materials is paramount. In this study, an epoxy-based shape memory polymer (SMP) is synthesized and its thermomechanical properties are comprehensively characterized. In addition, numerical method to model the SMP is developed. Novel SMP-based composites have been designed, including the SMA-SMP composites and conductive CNT-SMP composites. Although the thermal, mechanical, and electrical performances of the composites are characterized, the actuation aspect of the composites have yet to be explored.

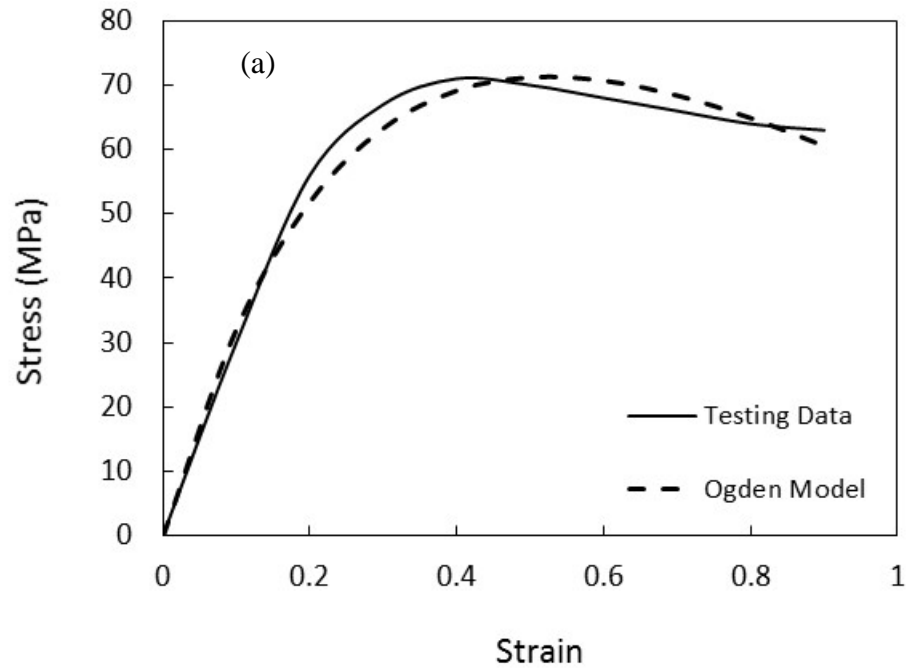
The future work may include the comprehensive examinations of the actuation abilities of the SMP composites, including shape fixing, shape recovery, stress

generation, etc. Future work also includes the development of numerical method to model the actuation behaviors of the SMP composites. The task can also include the use of commercial finite element program (which integrates the Ogden model (for SMP matrix) and -Lagoudas model (for SMA fillers)) for device designs.

Appendix A. Validation of Ogden Model with Additional SMP Material System.

The Ogden model has been further tested by using two additional SMP material systems: an epoxy based SMP (McClung, A.J.W., Tandon, G.P. and Baur, J.W. Mech Time-depend Mater, 2012, 16, 205-221.)

The epoxy based SMP has a glass transition temperature of 105°C. The stress-strain responses of the SMP have been comprehensively characterized at various regions (glassy, transitional, and rubbery regions) by tensile test. The comparisons of Ogden model and experimental measurements for the epoxy based SMP are shown in Figure A1.



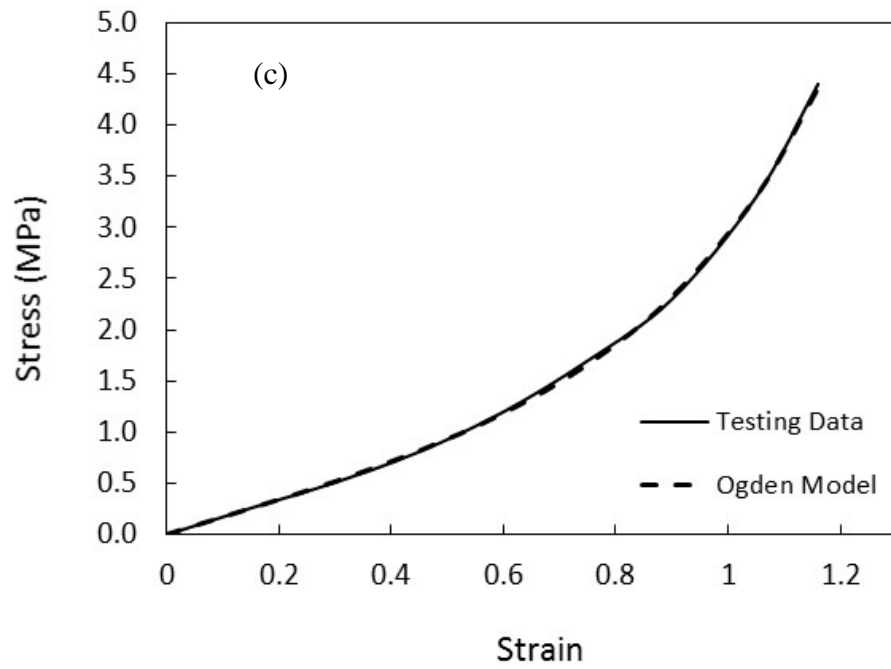
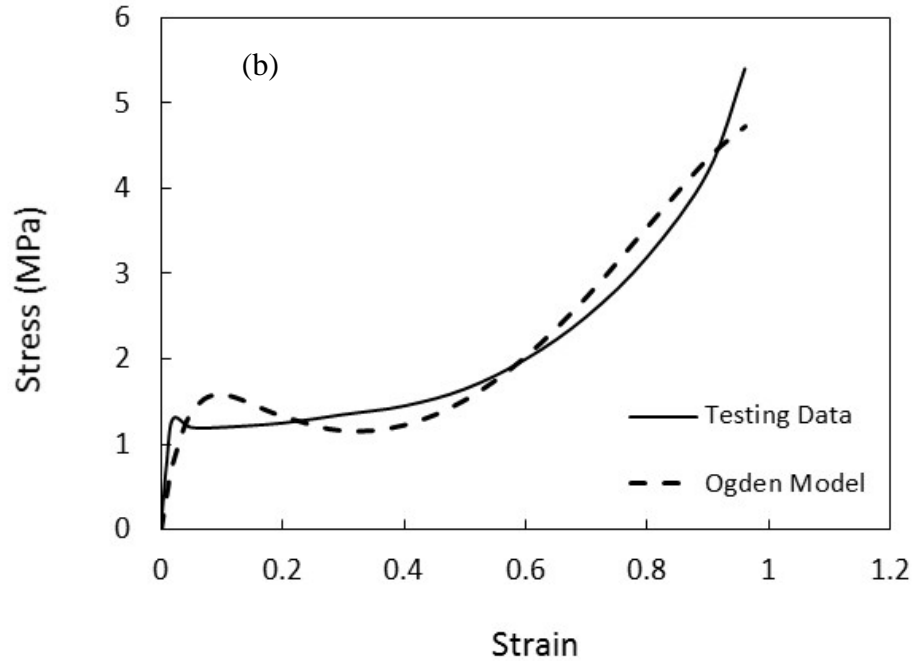


Figure A1 Predictions of stress-strain responses of an epoxy based SMP using Ogden model: (a) 25°C, (b) 90°C, and (c) 130°C.

Appendix B. Stress – Strain responses of Ni Particle – SMP Composites

Shape memory polymer was reinforced with Ni particles of average size of 4-5 μ m and placed in the magnetic field for 48 hours to form Ni particle chains.

The stress-strain behaviors of the Ni + SMP composites were obtained through uniaxial compressive tests conducted on the BOSE ElectroForce load frame system using the force-controlled test. The specimens were small cylinders with the nominal height of 11 mm and nominal diameter of 6.25 mm. The tests were performed under the force-control mode by applying a compressive force of up to 2000 N at a rate of 0.5 N/sec at 20°C.

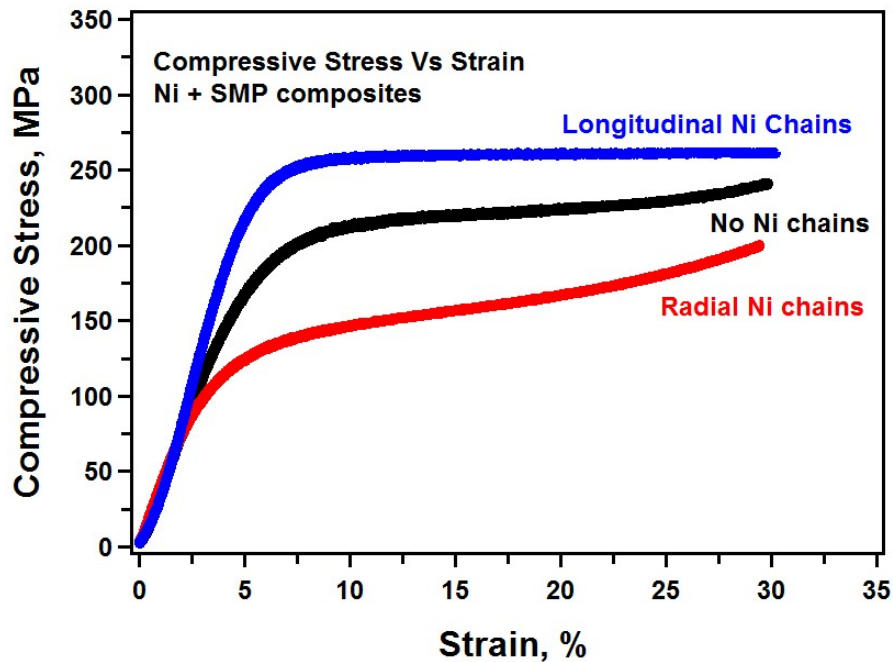


Figure B1 Shows the stress-strain response of Ni (30% by wt.) + SMP composite from DMA (Bose ElectroForce).

From Table B1 we can see that modulus of the Ni + SMP Composite is highest when the Ni chains are along the direction of the compressive loads whereas when

aligned in the direction perpendicular direction to the load they have lower modulus. This difference is much significant in strength of the composites and as expected the composite is stronger when the SMP matrix is reinforced in the direction of the load to increase its load carrying capacity.

Table B1 Shows the Mechanical properties of Ni (30%) + SMP Composites.

Ni (30%) + SMP composite	Modulus(MPa)	Strength (At 20% strain) (MPa)
No chains	38.8301	224.035
Chains along Diameter	37.0659	166.762
Chains along Height	40.2529	261.502

Appendix C. Temperature Induced Phase Transformation of SMA + SMP

Composite with Applied Stress.

The phase transformation of the SMA fiber SMP composite was modeled. The SMA fiber content was 50%. Two dimensional axisymmetric finite element model was built in Abaqus CAE using Lagoudas's user subroutine to define the non-linear shape memory alloy wire NiTi material behavior and Ogden's Strain energy density function to define the shape memory polymer. The bottom edge was fixed and displacement load was applied to the nodes on the top edge. The FE model is shown in the figure below.

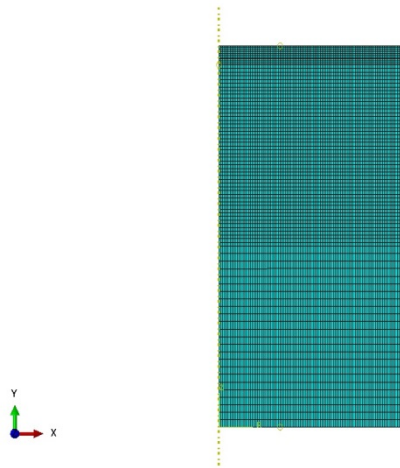


Figure C1 2D axisymmetric FE model of NiTi - Fiber + SMP composite built in Abaqus CAE.

The shape memory composite was initially at high temperature (above $A_f = 315\text{K}$) and compressed close to 4.5% of its original height. This load was maintained and the SMC was cooled below $M_f = 271\text{K}$. During cooling the SMC undergoes phase transformation resulting in large strains. These strains were then recovered when the SMC was heated to above A_f .

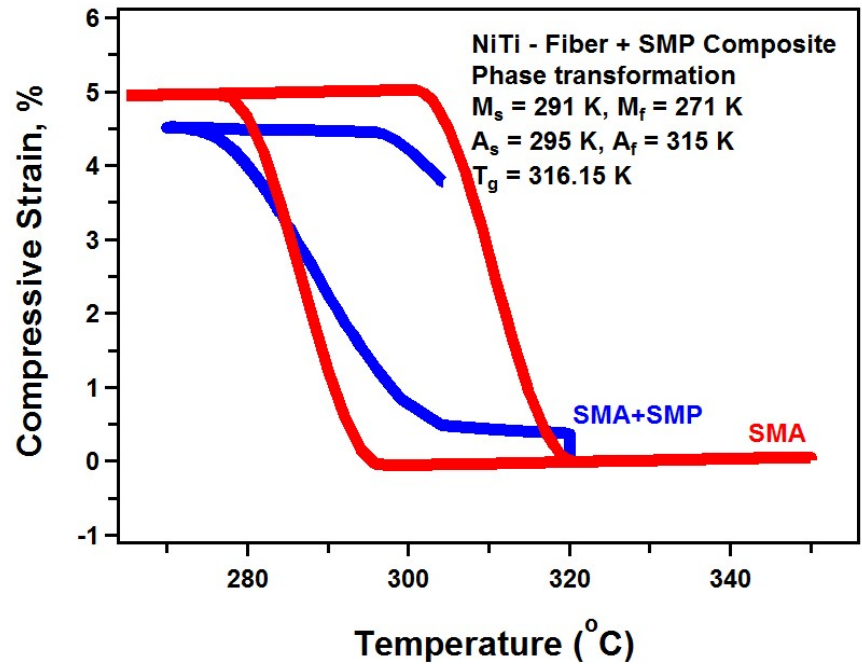


Figure C2 Shows the temperature induced phase transformations of the SMA and SMA + SMP composite.

REFERENCES

1. Thill, C.E., J.; Bond, I.; Potter, K.; Weaver, P., “*Morphing skins*”,. The Aeronautical Journal, 2008. **112**,: p. 117-139.
2. Meents, E.P.B., T.J.; Cable, K.M.; Margraf, T.W.; Havens, E. , *Self-healing reflexive composite structures for marine environments*. In Proceedings of SAMPE, 2009: p. 18-21.
3. Nelson, B.A.a.K., W.P., *Shape Recovery of Nanoindentation Imprints in a Thermoset “Shape Memory” Polymer*. Applied Physics Letters, 2005. **86**.
4. Ngan, A.H.W., Tang, B., *Viscoelastic effects during unloading in depth-sensing indentation*. Journal of Material Research, 2002. **17**(10): p. 2604-2610.
5. Ngan, *Correcting power-law viscoelastic effects in elastic modulus measurement using depth-sensing indentation*. International Journal of Solids and Structures, 2005. **42**: p. 1831–1846.
6. Oliver, W.C.a.P., G.M., *An improved technique for determining hardness and elastic modulus using load and displacement sensing indentation experiments*. Journal of Materials Research, 1992. **7**(1564).
7. Liu, C., Qin, H. and Mather, P. T, *Review of Progress in Shape-Memory Polymers*. Journal of Materials Chemistry, 2007. **17**: p. 1543-1558.
8. Lendlein, A., and Kelch, S, “*Shape-Memory Polymers,*”. Angew Chem. Int. Ed., , 2002. **41**: p. 2034-2057
9. Jinlian Hu, Yong Zhu, Huahua Huang, Jing Lu,, “*Recent advances in shape–memory polymers: Structure, mechanism, functionality, modeling and*

- applications*”,. Progress in Polymer Science,, 2012. **Volume 37**,(Issue 12,): p. 1720–1763.
10. Huang, W.M., Ding, Z., Wang, C. C., Wei, J., Zhao, Y., Purnawali, H. , “*Shape memory materials*,” Materials Today, , 2010. **13**((7-8)): p.:54-51
 11. Ratna, D.a.K.-K., J. , “*Recent Advances in Shape Memory Polymers and Composites: A Review*,” Journal of Materials Science,, 2008. **43**:: p. 254-269.
 12. Behl, M.a.L., A. , “*Shape-Memory Polymers*,”. Materials Today,, 2007. **10**(4): p.:20-28.
 13. Beloshenko, V.A., Varyukhin, V. N. and Voznyak, Y. V., “*The Shape Memory Effect in Polymers*,”. Russian Chemical Review,, 2005. **74**((3)): p. 265-283.
 14. Gall, K., Kreiner, P., Turner, D. and Hilse, M. , *Shape-Memory Polymers for Microelectromechanical Systems*, . Journal of Microelectromechanical Systems,, 2004. **13**((3,)): p. 472-483.
 15. Tobushi, H., Hara, H., Yamada, E., and Hayashi, S. , “*Thermomechanical Properties in a Thin Film of Shape Memory Polymer of Polyurethane Series*,”. Smart Materials and Structures,, 1996. **5**:: p. 483-491
 16. Tobushi, H., Hashimoto, T., Ito, N., Hayashi, S., and Yamada, E. , “*Shape Fixity and Shape Recovery in a Film of Shape Memory Polymer of Polyurethane Series*,” Journal of Intelligent Material Systems and Structures,, 1998. **9**: p.:127-136.
 17. Wei, Z.G., Sandstrom, R. and Miyazaki, S. , “*Review Shape-Memory Materials and Hybrid Composites for Smart Systems, Part I Shape-Memory Materials*,” Journal of Materials Science, , 1998. **33**:(3743-3762).

18. Atli, B., Gandhi, F. and Karst, G. , “*Thermomechanical Characterization of Shape Memory Polymers,*” *Journal of Intelligent Material Systems and Structures,*, 2009. **20**((1)): p.:87-95
19. J. Leng, X.L., Y. Liu, S. Du, , “*Shape-memory polymers and their composites: Stimulus methods and applications*”,. *Progress in Materials Science,*, 2011. **56**:: p. 1077–1135.
20. Meng, H., & Li, G., *A review of stimuli-responsive shape memory polymer composites.* *Polymer,* 2013. **54**(9): p. 2199-2221.
21. Lan, X., Liu, Y., Lv, H., Wang, X., Leng, J., & Du, S., *Fiber reinforced shape-memory polymer composite and its application in a deployable hinge.* *Smart Materials and Structures,* 2009. **18**(2): p. 024002.
22. Xu, B., Fu, Y. Q., Huang, W. M., Pei, Y. T., Chen, Z. G., De Hosson, J., ... & Reuben, R. L., *Thermal-mechanical properties of polyurethane-clay shape memory polymer nanocomposites.* *Polymers,* 2010. **2**(2): p. 31-39.
23. Gall, K., Dunn, M. L., Liu, Y., Finch, D., Lake, M., & Munshi, N. A., *Shape memory polymer nanocomposites.* *Acta Materialia,* (2002). **50**((20)): p., 5115-5126.
24. Zhang, S.Y., Z.; Govender, T.; Luo, H.; Li, B., *A novel supramolecular shape memory material based on partial α -CD-PEG inclusion complex.* . *Polymer,* 2008. **49**: p. 3205-3210.
25. Yanju Liu, H.L., Xin Lan, Jinsong Leng, Shanyi Dub, *Review of electro-active shape-memory polymer composite.* *Composites Science and Technology,* 2009. **69**: p. 2064-2068.

26. Leng, J., Lv, H., Liu, Y., & Du, S., *Electroactivate shape-memory polymer filled with nanocarbon particles and short carbon fibers*. Applied Physics Letters,, 2007. **91**((14)): p., 144105.
27. Goo NS, P.I., Yoon KJ, Jung YC, Cho JW. , *Actuation of MAV control surface using conducting shape memory polymer actuator*. In: Alison BF, editor. Proceeding of 11th international symposia on smart structures and materials. Bellingham, WA, USA: SPIE; , 2004: p. p. 194–201.
28. AM, S., *Electromagnetic activation of shape memory polymer networks containing magnetic nanoparticles*. Macromol Rapid Commun, 2006. **27**: p. 1168–72.
29. Lendlein, S.A.M.a.A., *Shape-Memory composites*. Adv Polym Sci, 2009. **226**: p. 41-95.
30. Ya-Jen Yu, S.I., 1 Keith Hearon,1,3 Jennifer N. Rodriguez,1 Chien-Chia Chu,2Thomas S. Wilson,3 Duncan J. Maitland1,3, *Thermoset Shape Memory Polyurethane Composites with Carbon Fillers*. Journal of Polymer Science Part B: Polymer Physics.
31. Kumar, P.K. and D.C. Lagoudas, *Introduction to Shape Memory Alloys*, in *Shape Memory Alloys*. 2008, Springer US. p. 1-51.
32. C. Liu, H.Q.a.P.T.M., *Review of progress in shape-memory polymers*. Journal of Materials Chemistry, March 2007. **17**((16)): p. 1543-1558.
33. Hisaaki Tobushi, S.H., Yoshiki Sugimoto and Kousuke Date, *Two-Way Bending Properties of Shape Memory Composite with SMA and SMP*. Materials, 2009. **2**: p. 1180-1192.

34. Liang C, R.C., Malafeew E., *Investigation of shape memory polymers and their hybrid composites*. J Intell Mater Syst Struct, 1997. ;**8**(:380): p. –6.
35. Van Humbeeck, J., *Non-medical applications of shape memory alloys*. Materials Science and Engineering: A, 1999. **273**: p. 134-148.
36. Humbeeck, J.V., *Non-medical applications of shape memory alloys*. Materials Science and Engineering, 1999. **A273–275**: p. 134–148.
37. Zhang RX, N.Q., Natsuki T, Iwamoto M., *Mechanical properties of composites filled with SMA particles and short fibers*. Compos Struct, 2007. **79**: p. 90-6.
38. Lee HJ, L.J., *A numerical analysis of the buckling and postbuckling behavior of laminated composite shells with embedded shape memory alloy wire actuators*. Smart Mater Struct, 2000. **9**: p. 780-7.
39. Psarras GC, P.J., Galiotis C., *Adaptive composites incorporating shape memory alloy wires Part I probing the internal stress and temperature distributions with a laser Raman sensor*. J Mater Sci, 2001. **36**(3): p. 535-46.
40. Sun SS, S.G., Han F, Wu JS., *Thermoviscoelastic analysis for a polymeric composite plate with embedded shape memory alloy wires*. Compos Struct, 2002. **58**: p. 295-302.
41. Choi YK, S.M., *Smart glass epoxy laminates with embedded Ti-based shape memory alloy*. Mater Trans, 2004. **45**(7): p. 2417-21.
42. Youssef MA, A.M., Nehdi M., *Experimental investigation on the seismic behavior of beam-column joints reinforced with superelastic shape memory alloys*. J Earthq Eng, 2008. **12**(7): p. 1205-22.

43. Li H, L.Z., Ou JP., *Experimental study of a simple reinforced concrete beam temporarily strengthened by SMA wires followed by permanent strengthening with CFRP plates*. Eng Struct, 2008. **30**(3): p. 716-23.
44. Zhang, X., Li, Q., Holesinger, T. G., Arendt, P. N., Huang, J., Kirven, P. D., ... & Zhu, Y., *Ultrastrong, Stiff, and Lightweight Carbon-Nanotube Fibers*. Advanced Materials, 2007. **19**(23): p. 4198-4201.
45. Koratkar, N.A., Wei, B., & Ajayan, P. M., *Multifunctional structural reinforcement featuring carbon nanotube films*. Composites Science and Technology, 2003. **63**(11): p. 1525-1531.
46. Breuer, O., & Sundararaj, U., *Big returns from small fibers: a review of polymer/carbon nanotube composites*. Polymer composites, 2004. **25**(6): p. 630-645.
47. Coleman, J.N., Khan, U., & Gun'ko, Y. K., *Mechanical reinforcement of polymers using carbon nanotubes*. Advanced Materials, 2006. **18**(6): p. 689-706.
48. Ajayan, P.M., and James M. Tour., *Nature 447.7148*. Materials science: nanotube composites., 2007. **1066-1068**.
49. Sahoo, N.G., Jung, Y. C., & Cho, J. W. *Electroactive shape memory effect of polyurethane composites filled with carbon nanotubes and conducting polymer*. in *Materials and manufacturing processes*,22(4). 2007.
50. Xiong, J., Zheng, Z., Qin, X., Li, M., Li, H., & Wang, X, *The thermal and mechanical properties of a polyurethane/multi-walled carbon nanotube composite*. . Carbon, 2006. **44**(13): p. 2701-2707.

51. Qing-Qing Ni, C.-s.Z., Yaqin Fu, Guangze Dai, Teruo Kimura, *Shape memory effect and mechanical properties of carbon nanotube/shape memory polymer nanocomposites*. Composite structures, 2007. **81**: p. 176–184.
52. S. R. Bakshi, D.L.a.A.A., A, *Carbon nanotube reinforced metal matrix composites – a review*. International Materials Reviews, 2010. **51**(1): p. 41-64.
53. Andrews, R., Jacques, D., Minot, M., & Rantell, T., *Fabrication of carbon multiwall nanotube/polymer composites by shear mixing*. Macromolecular Materials and Engineering, 2002. **287**(6): p. 395-403.
54. Sandler, J., Shaffer, M. S. P., Prasse, T., Bauhofer, W., Schulte, K., & Windle, A. H., *Development of a dispersion process for carbon nanotubes in an epoxy matrix and the resulting electrical properties*. Polymer composites, 1999. **40**(21): p. 5967-5971.
55. Yang, *Influence of moisture in polyurethane shape memory polymers and their electrical conductive composites*. A dissertation for the degree of doctor of philosophy. School of Mechanical and Aerospace Engineering Nanyang Technological University, Singapore;, 2005.
56. Leng, J.S., Huang, W. M., Lan, X., Liu, Y. J., & Du, S. Y., *Significantly reducing electrical resistivity by forming conductive Ni chains in a polyurethane shape-memory polymer/carbon-black composite*. Applied Physics Letters, 2008. **92**(20): p. 204101.
57. Liu, Y., Lv, H., Lan, X., Leng, J., & Du, S., *Review of electro-active shape-memory polymer composite*. Composites Science and Technology, 2009. **69**(13): p. 2064-2068.

58. Beake, B.D.a.J.F.S., *High-temperature nanoindentation testing of fused silica and other materials*,. Philosophy Magazine, , 2002. **A82**,: p. 2179.
59. Briscoe, B.J., Fiori, L., Pelillo, E., , “*Nano-indentation of polymeric surfaces*,” Journal of Physics D: Applied Physics, , 1998. **31**: p., 2395-2405.
60. Feng, G., Ngan, A.H.W., “*Effects of creep and thermal drift on modulus measurement using depth-sensing indentation*,”. Journal of Material Research,, 2002. **17**((3)): p.:660-668.
61. Fujisawa, N., Swain, M.V., , “*Effect of unloading strain rate on the elastic modulus of a viscoelastic solid determined by nanoindentation*,”. Journal of Material Research, , 2006. **21**((3)): p.:708-714.
62. Lu, Y.C., Jones, D. C., Tandon, G. P., Putthanarat, S. and Schoeppner, G. A., *High Temperature Nanoindentation of PMR-15 Polyimide*, . Experimental Mechanics,, 2009. DOI **10.1007/s11340-009-9254-5**. .
63. Y. Liu, K.G., M. Dunn, A. Greenberg, J. Diani, “*Thermomechanics of shape memory polymers: Uniaxial experiments and constitutive modeling*”. International Journal of Plasticity,, 2006. **Vol. 22**, (No. 2.): p. pp. 279-313.
64. Tandon,, J.T.F.Y.C.L.G.P., “*Thermomechanical characterization of environmentally conditioned shape memory polymer using nanoindentation*”. SPIE Proceedings, 2010. **Vol. 7644**.
65. Baer, G., Wilson, T. S., Matthews, D. L., & Maitland, D. J., “*Shape-memory behavior of thermally stimulated polyurethane for medical applications*.”. Journal of Applied Polymer Science,, 2007. **103**(6),(3882-3892.).

66. Diani, J., Gilormini, P., Frédy, C., & Rousseau, I., *"Predicting thermal shape memory of crosslinked polymer networks from linear viscoelasticity."* International Journal of Solids and Structures, 2012. **49(5)**; p. 793-799.
67. Tobushi H, H.S., Hoshio K, Ejiri Y, *Shape recovery and irrecoverable strain control in polyurethane shape-memory polymer.* Sci. Technol. Adv. Mater, 2008. **9:015009**.
68. Tanaka, K., Kobayashi, S., & Sato, Y. , *Thermomechanics of transformation pseudoelasticity and shape memory effect in alloys.* International Journal of Plasticity, 1986. **2(1)**: p. 59-72.
69. Achenbach, M., *A model for an alloy with shape memory.* International Journal of Plasticity, 1989. **5(4)**: p. 371-395.
70. Liang, C., & Rogers, C. A., *One-dimensional thermomechanical constitutive relations for shape memory materials.* Journal of intelligent material systems and structures, 1990. **1(2)**: p. 207-234.
71. Rohan Abeyaratne, J.K.K., *A continuum model of a thermoplastic solid capable of undergoing phase transitions.* Journal of Mech. Phys. Solids, 1993. **41(3)**: p. 541-571.
72. BRINSON, A.B.a.L.C., *Phase diagram based description of the hysteresis behavior of shape memory alloys.* Acta mater, 1998. **46(10)**: p. 3649-3665.
73. Sanjay Govindjee, E.R.K., *Computational aspects of one-dimensional shape memory alloy modeling with phase diagrams.* Comput. Methods Appl. Mech. Engrg, 1998. **171**: p. 309-326.

74. Auricchio F, S.E., *A temperature-dependent beam for shape-memory alloys: constitutive modelling, finite-element implementation and numerical simulations*. Comput Method Appl Mech Eng, 1999. **174**((1-2)): p. 171-90.
75. Rajagopal KR, S.A., *On the thermomechanics of the shape memory wires*. Z Angew Math Phys, 1999. **50**(3): p. 459-96.
76. Marfia S, S.E., Reddy JN, *Superelastic and shape memory effects in laminated shape-memory-alloy beams*. AIAA J, 2003. **41**(1): p. 100-9.
77. Ikeda T, N.F., Naito H, Matsuzaki Y, *Constitutive model of shape memory alloys for unidirectional loading considering inner hysteresis loops*. Smart Mater Struct, 2004. **13**(4): p. 916-25.
78. Paiva A, S.M., Braga AMB, Pacheco PMCL, *A constitutive model for shape memory alloys considering tensile-compressive asymmetry and plasticity*. Int J Solids Struct, 2005. **42**((11-12)): p. 3439-57.
79. Savi MA, P.A., *Describing internal subloops due to incomplete phase transformations in shape memory alloys*. Arch Appl Mech, 2005. **74**(9): p. 637-47.
80. Buravalla VR, K.A., *Differential and integrated form consistency in 1-D phenomenological models for shape memory alloy constitutive behavior*. Int J Solids Struct, 2007. **44**(13): p. 4369-81.
81. Evangelista V, M.S., Sacco E., *Phenomenological 3D and 1D consistent models for shape-memory alloy materials*. Comput Mech, 2009. **44**(3): p. 405-21.

82. Nallathambi AK, D.S., Chandrasekar AS, Srinivasan SM., *A 3-species model for shape memory alloys*. Int J Struct Changes Solids Mech Appl, 2009. **1**(1): p. 149-70.
83. Rizzoni R, M.M., Casari D, *Continuum mechanics and thermodynamics*, 2013. **25**(207-227).
84. Tanaka K, N.F., Hayashi T, Tobushi H, Lexcelent C, *Phenomenological analysis on subloops and cyclic behavior in shape-memory alloys under mechanical and or thermal loads*. Mech Mater, 1995. **19**(4): p. 281-92.
85. Lexcelent C, B.G., *Thermodynamical model of cyclic behaviour of Ti-Ni and Cu-Zn-Al shape memory alloys under isothermal undulated tensile tests*. Mech Mater, 1996. **24**(1): p. 59-73.
86. Bo ZH, L.D., *Thermomechanical modeling of polycrystalline SMAs under cyclic loading, part I: theoretical derivations*. Int J Eng Sci, 1999. **37**(9): p. 1089-140.
87. Petrini, F.A.a.L., *A three-dimensional model describing stress-temperature induced solid phase transformations: solution algorithm and boundary value problems*. Int. J. Numer. Meth. Engng, 2004. **64**: p. 807–836.
88. Dimitris C. Lagoudas, Z.B., Muhammad A. Qidwai and Pavlin B. Entchev, *SMA UM: User Material Subroutine for Thermomechanical Constitutive Model of Shape Memory Alloys*. 2003.
89. Tanaka, K., *A thermomechanical sketch of shape memory effect: Onedimensional tensile behavior*. Res Mechanica, 1986. **18**: p. 251–263.
90. Fu, S.Y., Feng, X. Q., Lauke, B., & Mai, Y. W., *Effects of particle size, particle/matrix interface adhesion and particle loading on mechanical properties*

- of particulate–polymer composites*. Composites Part B: Engineering, 2008. **39**(6): p. 933-961.
91. Shao-Yun Fu a, X.-Q.F., Bernd Lauke, Yiu-Wing Mai, *Effects of particle size, particle/matrix interface adhesion and particle loading on mechanical properties of particulate–polymer composites*. Composites Science and Technology, 2008. **39**: p. 933–961.
 92. Xia, Z., Zhang, Y., & Ellyin, F., *A unified periodical boundary conditions for representative volume elements of composites and applications*. International Journal of Solids and Structures, 2003. **40**(8): p. 1907-1921.
 93. Janda, R., (editor): *Kunststoffverbundsysteme*. vch Verlagsgesellschaft, Weinheim. 1990.
 94. Chamis C.C., S.J.H., *Mechanical behavior and fracture characteristics of off-axis fiber composites II —Theory and comparisons*. NASA Technical Paper, 1978. **1082**.
 95. Systemes, D., *Writing user subroutines with ABAQUS*.
 96. Rahman, A., et al. *A review of the applications of nanocarbon polymer composites*. in *Nano 6.03*. 2011.
 97. J. S. Leng, a W. M. Huang,^{2,b} X. Lan,¹ Y. J. Liu,¹ and S. Y. Du¹. *Significantly reducing electrical resistivity by forming conductive Ni chains in a polyurethane shape-memory polymer/carbon-black composite*. in *Applied Physics Letters 92*, 204101-2008. 2008. American Institute of Physics.

98. Garmestani, H., Al-Haik, M. S., Dahmen, K., Tannenbaum, R., Li, D., Sablin, S. S., & Hussaini, M. Y. *Polymer-Mediated Alignment of Carbon Nanotubes under High Magnetic Fields*. in *Advanced Materials*, 15(22). 2003.
99. Razzaq, M.Y., Anhalt, M., Frommann, L., & Weidenfeller, B. *Thermal, electrical and magnetic studies of magnetite filled polyurethane shape memory polymers*. in *Materials Science and Engineering: A*, 444(1). 2007.
100. Mamunya, Y.P., et al. *Electrical and thermal conductivity of polymers filled with metal powders*. in *European polymer journal* 38.9. 2002.
101. Sancaktar, E., & Dilsiz, N. *Anisotropic alignment of nickel particles in a magnetic field for electronically conductive adhesives applications*. in *Journal of adhesion science and technology*, 11(2). 1997.
102. T. Xie, I.A. Rousseau, Facile tailoring of thermal transition temperatures of epoxy shape memory polymers, *Polymer* 50 (2009) 1852–1856.
103. Srinivasa, A.R. and Gosh, P. A Simple, Gibbs Potential Based Multinetwork Model for Shape Memory Polymers, *AIP conference proceedings*, vol. 1029, 2008. p.58.
104. Chen, Y.C. and Lagoudas, D.C. A constitutive theory for shape memory polymers. Part I: large deformations, *Journal of the Mechanics and Physics of Solids*, 2008;56:1752.
105. Chen, Y.C. and Lagoudas, D.C. A constitutive theory for shape memory polymers. Part II: small deformations, *Journal of the Mechanics and Physics of Solids*, 2008;56:1766.

106. Qi, H.J., Nguyen, T.D., Castroa, F., Yakacki, C.M. and ShandaSa, R. Finite deformation thermo-mechanical behavior of thermally induced shape memory polymers, *Journal of the Mechanics and Physics of Solids*, 56, 2008, 1730–1751.
107. Hong, S.J., Yu, W.R. and Youk, J.H. Thermomechanical deformation analysis of shape memory polymers using viscoelasticity, *AIP Conference Proceedings*, vol. 907, 2007. p.853.
108. McClung, A.J.W., Tandon, G.P. and Baur, J.W., Strain Rate- and Temperature-Dependent Tensile Properties of an Epoxy-Based, Thermosetting, Shape Memory Polymer (Veriflex-E), *Mech Time-depend Mater*, 2012, 16, 205-221.
109. Lendlein, A., Jiang, H., Jünger, O., & Langer, R., Light-induced shape-memory polymers, *Nature*, 434(7035), 879-882.

VITA

Sesha Spandana Pulla was born in Visakhapatnam, India. She got her bachelor degree from GITAM University, Andhra Pradesh, India. In August, 2009 she was admitted to graduate school at the University of Kentucky. She received her degree of Master of Science from University of Kentucky, USA in December, 2011. She then enrolled for PhD Program at University of Kentucky in January 2012. She has published 3 journal articles during her graduate tenure.